

Archives file

3121

UM-HSRI-77-7

A FOUNDATION FOR SYSTEMS ANTHROPOMETRY

Phase I

Herbert M. Reynolds, Ph.D.

CONTRACT F44620-76-C-0115

AIR FORCE OFFICE OF SCIENTIFIC RESEARCH
BOLLING AFB, D.C. 20332

Interim Report
January 31, 1977



THE UNIVERSITY OF MICHIGAN
HIGHWAY SAFETY RESEARCH INSTITUTE

REPORT DOCUMENTATION PAGE		READ INSTRUCTIONS BEFORE COMPLETING FORM
1. REPORT NUMBER	2. GOVT ACCESSION NO.	3. RECIPIENT'S CATALOG NUMBER
4. TITLE (and Subtitle) A FOUNDATION FOR SYSTEMS ANTHROPOMETRY Phase I		5. TYPE OF REPORT & PERIOD COVERED Interim Scientific 1 June 76 - 30 Nov 76
7. AUTHOR(s) Herbert M. Reynolds, PhD		6. PERFORMING ORG. REPORT NUMBER UM-HSRI 77-7
9. PERFORMING ORGANIZATION NAME AND ADDRESS Highway Safety Research Institute The University of Michigan Ann Arbor, Michigan 48109		8. CONTRACT OR GRANT NUMBER(s) F44620-76-C-0115
11. CONTROLLING OFFICE NAME AND ADDRESS Air Force Office of Scientific Research (NL) Bolling AFB DC 20332		10. PROGRAM ELEMENT, PROJECT, TASK AREA & WORK UNIT NUMBERS 61102F 2313/A4
14. MONITORING AGENCY NAME & ADDRESS (if different from Controlling Office)		12. REPORT DATE 31 January 1977
		13. NUMBER OF PAGES 129
		15. SECURITY CLASS. (of this report) Unclassified
		15a. DECLASSIFICATION/DOWNGRADING SCHEDULE
16. DISTRIBUTION STATEMENT (of this Report) Approved for public release; distribution unlimited.		
17. DISTRIBUTION STATEMENT (of the abstract entered in Block 20, if different from Report)		
18. SUPPLEMENTARY NOTES		
19. KEY WORDS (Continue on reverse side if necessary and identify by block number) Anthropometry, Biomechanics, Kinematics, Human Engineering, Links, Joint Centers of Mobility, Anatomical Axes Systems, Anthropometric Landmarks		
20. ABSTRACT (Continue on reverse side if necessary and identify by block number) The purpose of the present program is to conduct basic research into the properties and requirements of three-dimensional dynamic anthropometry. In essence, the research has the expressed goal of inductively describing the linkage of the whole body for predicting body motion in three-dimensional dynamic computer simulations. This effort may be divided into three subsidiary tasks dealing with 1) the identification, location, and relationship of externally and internally "stable" landmarks; 2) the definition		

An Interim Report To

UNITED STATES AIR FORCE
OFFICE OF SCIENTIFIC RESEARCH
Bolling AFB, D.C. 20332

A FOUNDATION FOR SYSTEMS ANTHROPOMETRY
Phase I

AN INTERIM REPORT FOR PHASE I OF CONTRACT #F44620-76-C-0115

HERBERT M. REYNOLDS, Ph.D.
PRINCIPAL INVESTIGATOR

January 31, 1977

Prepared by

Highway Safety Research Institute
The University of Michigan
Ann Arbor 48109

TABLE OF CONTENTS

Section	Page
1.0. Introduction.....	1
2.0. Perspectives on Systems Anthropometry.....	2
3.0. Methodological Considerations for Systems Anthropometry....	14
3.1. Landmark Definitions.....	15
3.2. Three-Dimensional Geometry: Axes Systems.....	18
3.3. Kinematical Problems for Systems Anthropometry.....	23
4.0. Task Reports for Phase I.....	27
4.1. Errors in Definition of an Anatomically-Based Co-ordinate System Using Anthropometric Data (D. H. Robbins).....	29
4.1.1. Introduction.....	29
4.1.2. Analysis.....	31
4.1.3. Examples.....	32
4.1.4. Conclusions.....	34
4.2. Radiographic Methodology for Systems Anthropometry Measurement (M. Bender).....	35
4.2.1. Origin Calibration and Image Distance Calibration.....	37
4.2.2. Quantitative Stereoradiography.....	43
4.2.3. Sources of Error.....	50
4.3. Body Sizing Scheme for Systems Anthropometry (H. M. Reynolds and D. H. Golomb).....	53
4.4. Three-Dimensional Geometry of the Adult Pelvis (H. M. Reynolds).....	56
4.5. Statistical and Probabilistic Properties of Three-Dimensional Anthropometric Data (D. H. Golomb). 4.5.1. Discussion of a Linkage Model.....	69
4.5.2. Analysis of Stewardess Data.....	71
4.6. Geometric Model Estimates of Inertial Properties of Body Segments (B. Bowman).....	103
4.6.1. Analytical Determination of the Inertial Properties of a Cored Frustum of a Right Elliptical Cone.....	103

	Page
4.6.1.1. Definition of a Mathematical Operator.....	108
4.6.1.2. Constants.....	108
4.6.1.3. Mass Properties.....	109
4.6.1.4. Moments of Inertia.....	110
4.6.1.5. Use of the Formulae.....	111
4.6.2. Computer Evaluation of Inertial Properties...	111
4.7. Measurement of Striated Muscle Density for Geometric Model Input (J. Freeman).....	113
4.7.1. Procedure.....	114
4.7.2. Discussion.....	118
4.7.3. Summary.....	119
5.0. Summary, Conclusions and Recommendations.....	120
6.0. Bibliography.....	122

LIST OF FIGURES

<u>Number</u>		Page
1.	Systems Analysis of "a Priori" Design Approach Utilizing Systems Anthropometry.....	5
2.	Stick Figure "Linkage" Model.....	8
3.	Body Segmentation Scheme of Dempster (1955) to arrive at 27 Segments.....	10
4.	Body Segmentation Scheme used on Cadavers by (a) Clauser, et al. (1969) and Chandler, et al. (1975) and on Living Subjects (b).....	11
5.	Comparison of Parametric Characteristics of Workspace and Impact Models.....	13
6.	Radiograph of Right Innominate Bone with Targeting Device Placed on Boney Surfaces.....	16
7.	Diagram of Primary, Secondary and Tertiary Axis Systems.....	19
8.	Pelvic Data and Coordinate System.....	30
9.	Basic Configurations for Producing Stereoradiographs.....	36
10.	Photograph of X-ray Image Distance and Origin Calibration Device.....	38
11.	X-ray Radiograph of Calibration Device.....	40
12.	Image Distance Calibration Geometry.....	41
13.	Origin Calibration Geometry.....	44
14.	Stereoradiography Geometry for Determining Elevation of a Point from a Reference Point on a Surface.....	45
15.	Diagram of Coordinates of Two Stereopair Points.....	47
16.	Equivalent Composite of the Stereopair.....	49
17.	X-ray Stereopair of Calibration Device.....	52
18.	Sizing Scheme for Male and Female Specimens from the Hamann-Todd Skeletal Collection.....	57
19.	Sample Hamann-Todd Data Collection Sheet and Translation from the German.....	61

Number		Page
20	Photograph of Subject in Standard Seated Position.....	72
21	Correlation of Surface Landmarks with Vertex.....	80
22	Correlation of Surface Landmarks with Iliocristale.....	89
23	Projection of Least Volume Ellipsoid Axes, Scaled to Explained Variance, on to XZ Plane.....	95
24	Y-Component of Variance along the Axes of the Least Volume Ellipsoids.....	101
25	A Cored Frustum of a Right Elliptical Cone.....	105
26	Sample Cadaver Examination Sheet.....	115
27	Sample Data and Calculation Sheet used in Tissue Density Determination Process.....	117

LIST OF TABLES

Number		Page
1	Potential Coordinate System Locations using Anthropometric Data.....	33
2	Comparison by Sizing Cells of 1960-62 Health Examination Survey and Hamann-Todd Collection for Males and Females.....	58
3	Correlations of Z-Coordinate of Landmarks with Standard Anthropometry.....	74
4	Correlations of X-Coordinate of Landmarks with Standard Anthropometry.....	75
5	Correlations of Y-Coordinate of Landmarks with Standard Anthropometry.....	77
6	Landmark Coordinate Correlations.....	81
7	Covariance Matrices of Landmarks.....	90
8	Principle Components Analysis of Three-Dimensional Stewardess Data.....	93
9	Inertial Property Parameters.....	106
10	Example Output from Computer Program which Evaluates Inertial Properties of Segments.....	112

1.0 Introduction

This interim report has been prepared to describe progress in the first six month's effort of a research program sponsored by the Air Force Office of Scientific Research contract # F44620-76-C0115. The results of our current research activities have contributed primarily to a philosophical and analytical understanding of future directions for systems anthropometry. This suggested frame of research is discussed in sections that follow as argumentative propositions from which profitable research hypotheses will result. Our results to date are based upon discussions, readings from the literature, and analysis of available data.

2.0 Perspective on Systems Anthropometry

Progress in dynamic systems anthropometry for the past 20 years has been dominated by the reports and papers of Wilfrid Taylor Dempster. His Air Force-sponsored research as an anatomist led to a significant advance in our understanding of the dynamic properties of the human body. In essence, he successfully illustrated the complexity of the open-chain link system of the human body but decided that only an approximation of the linkage system geometry was possible (Dempster, 1960). He assumed that a "...link...must change its length, of course, from moment-to-moment in an unpredictable way" (p. 571, 1960). Thus, Dempster conceived body measurements as practical point-to-point lengths similar to those made by traditional anthropometrists for a hundred years or more. His landmarks for anthropometric lengths improved estimates of the possible kinematic range of body activity, but they are, at best, two-dimensional approximations.

A recent AMRL-sponsored investigation conducted by Snyder, Chaffin and Schutz (1974) continued the work of Dempster into the torso. Linkage concepts were again utilized as points on and in the body, but this investigation presented evidence to contradict Dempster's unpredictable link assumption. The results of this investigation point out that the dynamic body does behave in a statistically predictable manner. The variation associated with the predicted results, however, must be carefully considered in a model of the open-chain link system of the human body.

For our purposes, there are three fundamental sources of variation - measurement errors, sampling errors and population differences. An

analogy of measuring the distance between two chalk points on a blackboard demonstrates these errors. First, two points are made on the blackboard and never erased. Measurement error is the difference between lengths measured in successive trials. The second major error - sampling - occurs when the chalk points are erased and put on the blackboard at the time of each successive measurement. Thus, the points at each time of measurement represent two points from the infinite population of points. The third major source of variation - population differences - occurs in chalkboard and chalk which are not manufactured uniformly. These differences are often referred to as problems in quality control and/or tolerance in machines and adaptive variation in biological populations. All three of these sources of variation interact and each contains part of the other in a hierarchy going from measurement and sampling error to population differences.

There are possible strategies available to minimize the effects of this variation on the predictive results (Churchill and McConville, 1976).

Strategy 1. Sample size may be decreased as measurement accuracy increases. Thus, the level of confidence is based upon measurement accuracy and precision rather than a large sample size.

Strategy 2. Experimental variation due to sampling errors and population differences may be reduced by appropriate subject selection.

To summarize what has been said thus far - Systems Anthropometry and Dempster's Dynamic Anthropometry have the same goals but different methodologies. Dempster did not develop either a set of data or a methodology which would be capable of treating the human body as a

three-dimensional dynamic system. Dempster primarily refined the landmarks used in traditional anthropometric studies by demonstrating relationships between a complex open-chain linkage model of the body limbs and certain bony landmarks on those limbs.

The research task at present is to lay the foundation for an anthropometric description of the body that will be suitable for three-dimensional predictive models (e.g. manikins, mathematical, statistical) of dynamic behavior of the body. Figure 1 presents a systems analysis of how and where this systems anthropometry will be used to solve dynamic man-machine interface problems. This approach presumes that if the geometry and the forces in an environment can be specified, the results of dynamic interaction between man and machine can be predicted. As a consequence, insight into possible risks and benefits can be obtained from modeling results prior to hardware implementation and experimental testing. For example, the effect of a change in the design of a restraint system could be simulated in a dynamic model to obtain information on the possible benefits or risks of such changes for the population. Empirical quantitative descriptions of the environment are more available than equivalent descriptions of the human body. This is particularly evident in our knowledge of body geometry and the probabilistic distribution of these geometrics in the population. Once the methodology is formulated and appropriate data collected, the more traditional experimental approach using the actual physical environment can be used to validate the predicted results rather than to evaluate the man/machine system.

The characteristics of this systems anthropometry that differentiate it from other efforts is the unique combination of deterministic parameters with probabilistic functions that describe the fundamental properties of

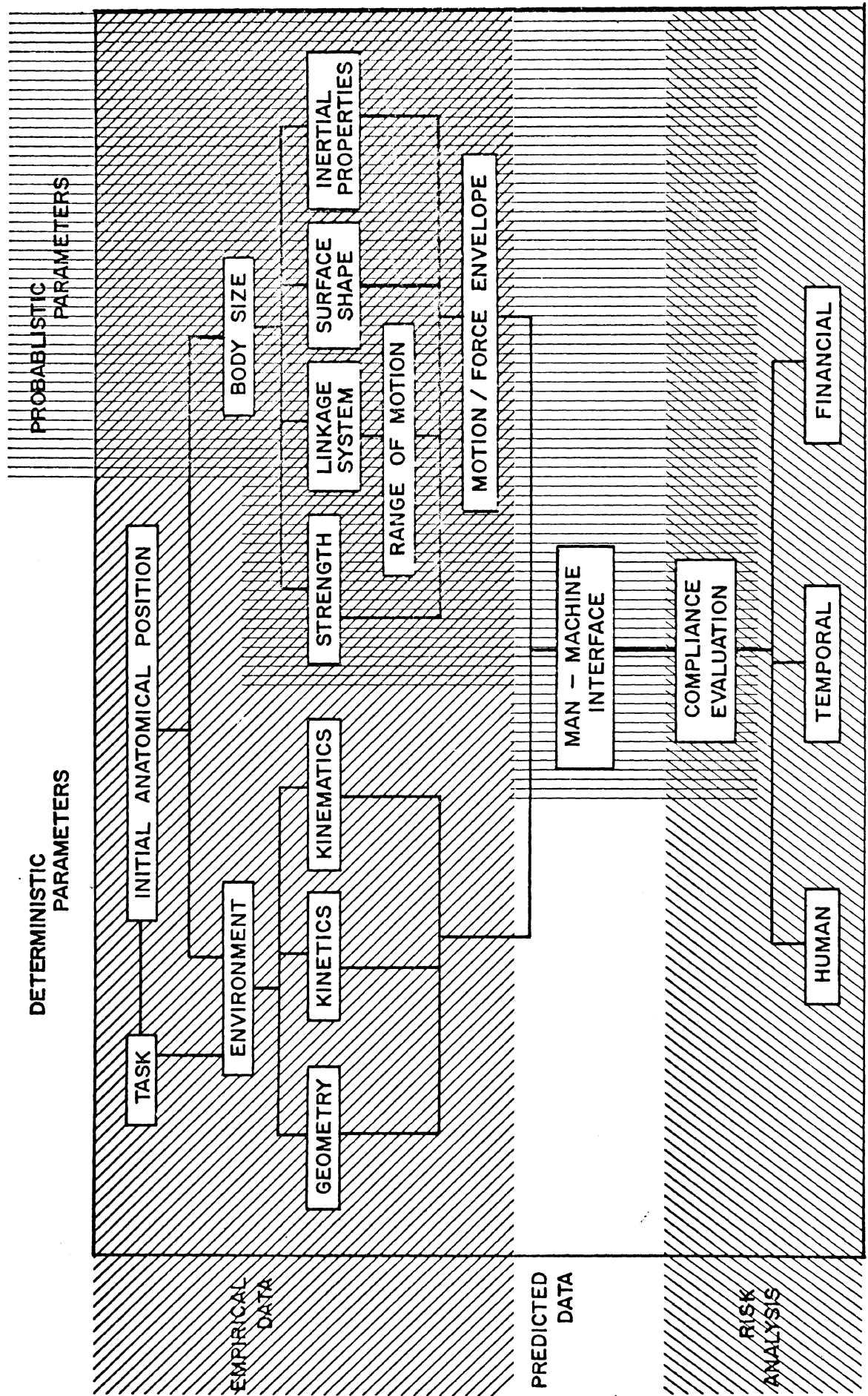


Figure 1. Systems Analysis of "a Priori" Design Approach Utilizing Systems Anthropometry.

the dynamic human body. The fundamental deterministic parameters of links, mass, shape, and strength have probabilistic properties. It is also recognized that the deterministic force-displacement parameters have probabilistic properties, but they are confounded by unique dynamic-task-environments. Presently, for lack of the needed empirical data on all of these parameters in the population, every instance in which a variable in a specified task-environment is modified or changed, new empirical data are needed to determine the response characteristics of the dynamic body. In some instances, the task-environment-body relationships may be assumed to be collinear in a simulation. This simplifies the problem but brings in a major risk factor in the assessment of the results. Therefore, it appears that with more empirical data describing the fundamental properties of the human body that have probability distributions, the risk factors in assessing the simulation results may be reduced. Figure 1 attempts to present a systems overview of how the major parameters in a simulation would be utilized relative to the type of parameters and type of data.

Recent modeling and experimental efforts at the University of Illinois at Chicago Circle by Andriacchi, Schultz, Belytschko and others sharply illustrates the paucity of empirical data on the dynamic geometry of the human body. These investigators have attempted to study the human spine in a geometrical configuration model (Schultz and Galante, 1970). They used planar radiographic data from Bakke (1931) for range of motion (in vivo), and in a more recent study (Andriacchi, et al, 1974), they used data on osteological specimens from Lanier (1939) and anthropometric information on embalmed cadavers from Clauser, McConville and Young (1969) for spinal geometry. It is remarkable that these sources are available

and that the investigators in Chicago were capable of synthesizing data with such unique differences. This sort of examination of the basic data set in models leads only to questions of validation and application. Others have approached their modeling efforts from the same basis - in essence, educated guesses of the body linkage geometry.

Our current description of the human body linkage system is derived from a series of interconnected fixed surface landmarks. Lengths between these surface landmarks are measured on the body by various techniques and incorporated into models. For example, Figure 2 presents a stick-man model based on two studies (Dempster, 1964; Snyder, Chaffin and Schultz, 1972) that relied primarily on the surface expression of the skeletal landmarks suitable for a linkage model of the human body. While this approach can present basic generalized body linkage configuration information, it relies on only one physical dimension--point-to-point lengths.

The addition of other physical dimensions--time and mass--increases the complexity of the problem but still requires a basic understanding of the human linkage system. A recent kinematic study of paths of movement of the upper extremity (Ayoub, Deivanayagam, and Kennedy, 1976) demonstrates the complexity and magnitude of the problem when the linkage system is studied by measurements of length and time. These paths of motion were measured in a limb composed of several joints each of which has several degrees of freedom. A major source of variation in their results is apparently observed in the paths of extension and return of the arm to the initial position. Variation observed in the two total paths may be ascribed to an interaction between the musculo-skeletal system and the laws of physics (e.g. the effect of gravity might have accentuated this variation).

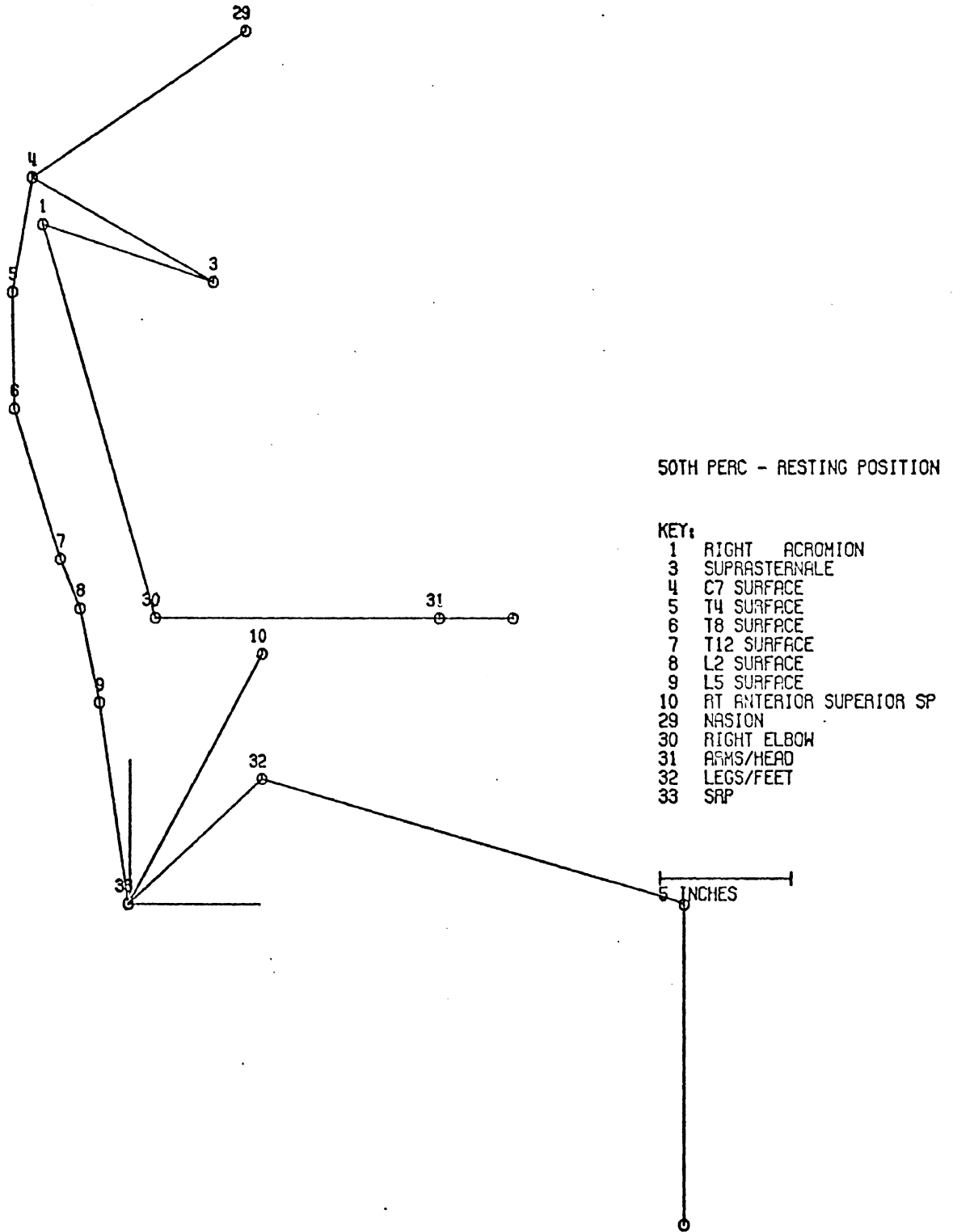


Figure 2. Stick Figure "Linkage" Model

In my opinion, their results point out that there may be more reproducibility associated with the initial and final body position geometry than in the paths of motion between the two configurations. That is to say, variation in the static geometry of the initial and final positions is primarily a function of anatomical differences in body size whereas variation in the paths of motion is possibly a function of several independent external and internal parameters that have unique relationships to these paths of motion.

Other studies have concentrated on the length and mass dimensions of the body (Clauser, et al., 1969; Chandler, et al., 1975). These investigations have continued research in the mass distribution of the body relative to a fixed-length linkage system. They have measured each segment in the appendages--arms, legs, and head--as a fixed-length link with inertial properties. These segments have been treated as rigid bodies connected at hinge points in the joints.

However, the torso does not apparently behave as a unit or as a series of discrete segments in regard to the relationship between its links and mass distribution. Past efforts at segmenting the body, and in particular, the torso, are depicted in Figure 3 (Dempster, 1955) and Figure 4a (Clauser, et al., 1969; Chandler, et al., 1975) and 4b (studies on the living). Only Dempster attempted to deal with the complex relationship between mass distribution and the linkage system of the torso. His segmentation plan was based upon musculature associated with his linkage system concept in the shoulder and a functional anatomical division of upper and lower torso (See Figure 3).

Thus, the addition of a second physical dimension produces immediate methodological consequences. The present investigation is systematically

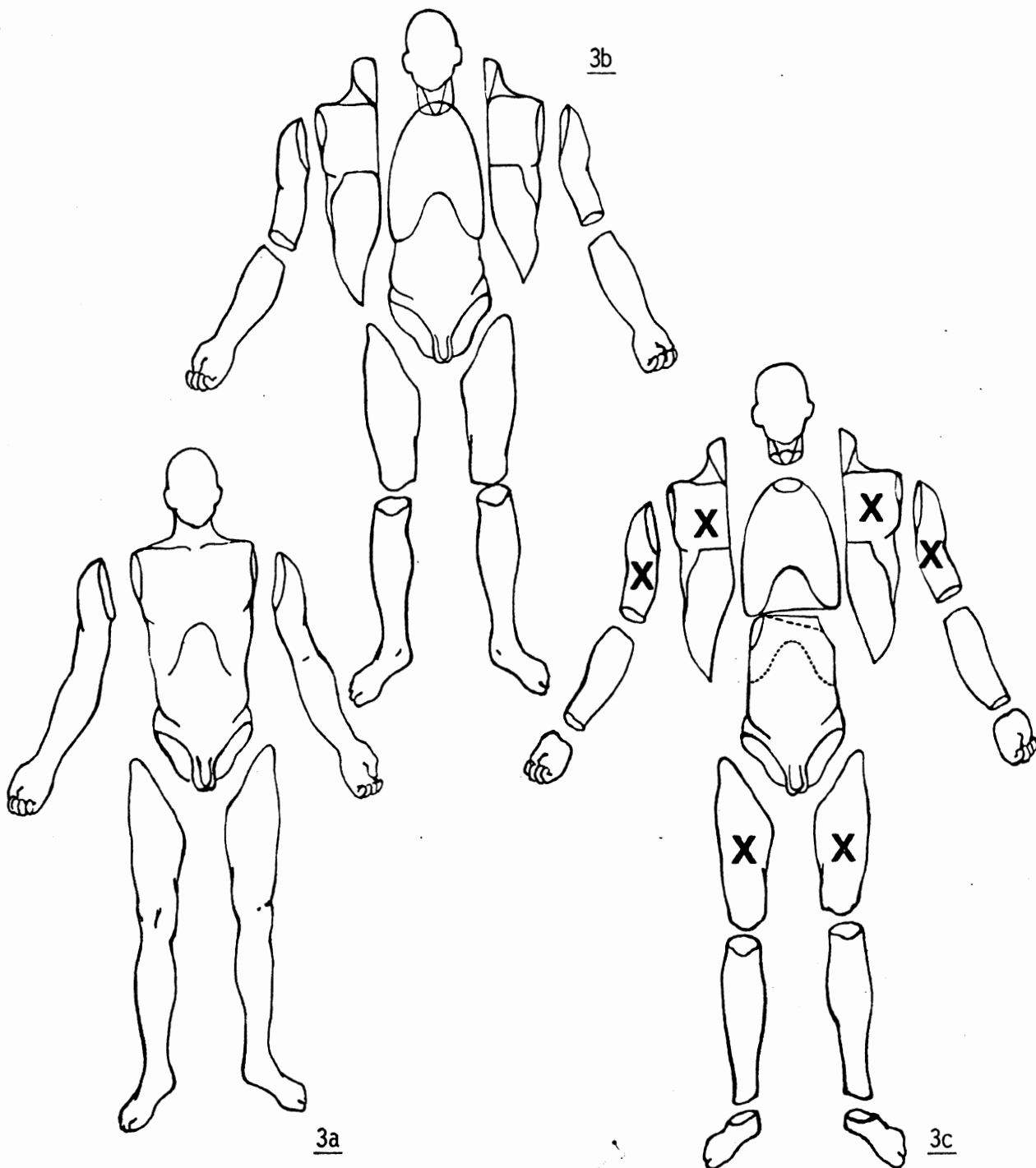


Figure 3. Segmentation Scheme Used by Dempster (1955) to Arrive at 27 Segments by Starting at a, Proceeding Through b, and c Cuts.

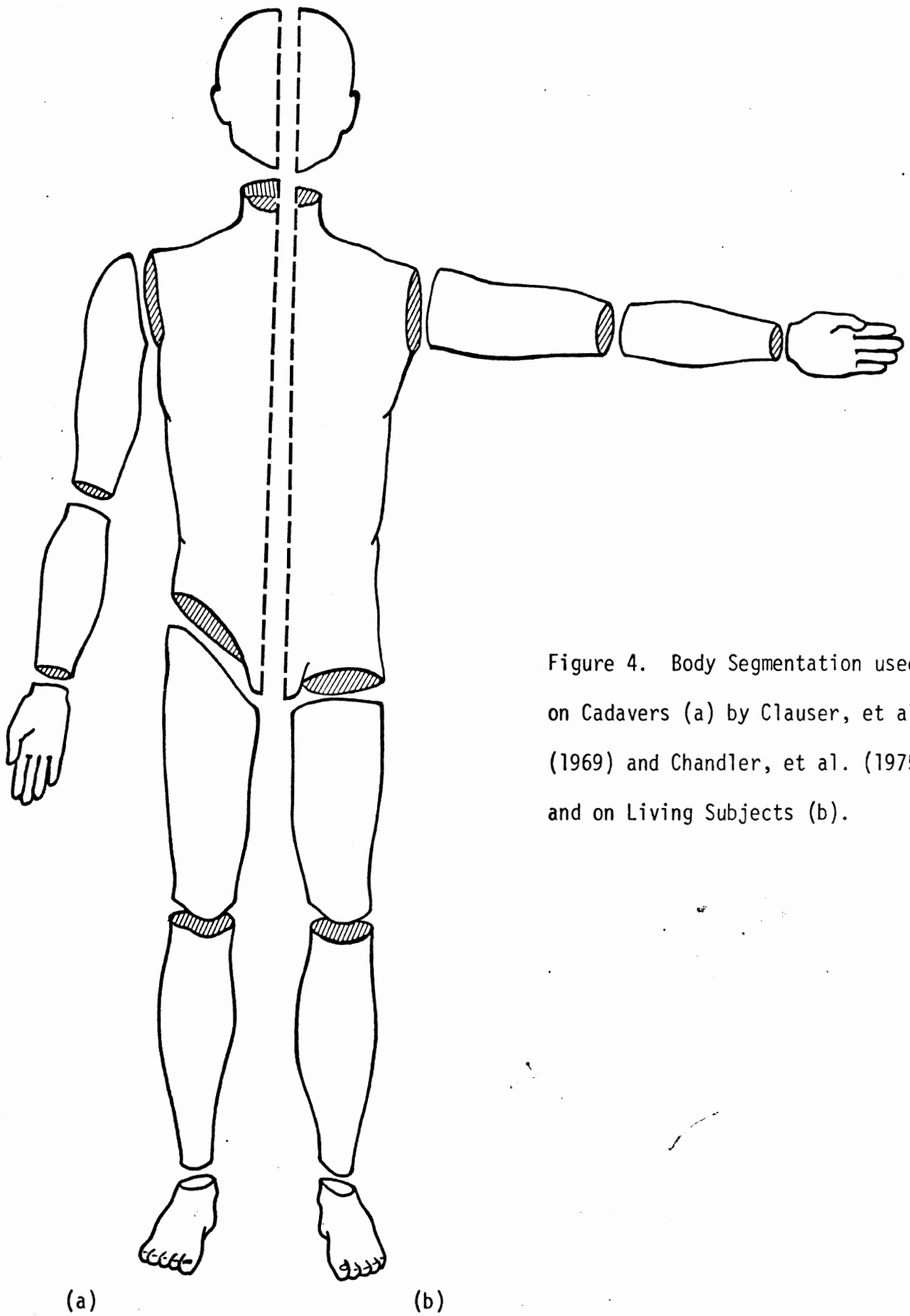


Figure 4. Body Segmentation used on Cadavers (a) by Clauser, et al. (1969) and Chandler, et al. (1975) and on Living Subjects (b).

approaching the study of man in a dynamic mode that requires measurements of length and mass in the context of time. The foundation of a new systems anthropometry will lie in a methodology that can treat the human body as a dynamic system. As a result, a unique synthesis of several fields of investigation is occurring and new words are forming and old words are taking on a new meaning.

The study of the link, shape, mass and strength of the human body as a system may be called "anthropomechanics" - a cumbersome word, but it conveys the desired meaning. The data generated in this field of investigation are ultimately used in simulations that study the activity or response of a body within a given dynamic environment. There has been a division in the data, personnel and models that treat the activity of the body in workspace problems separately from the response of the body in impact and acceleration problems. It is felt that this division is perhaps more artificial than real. Figure 4 presents a comparison of the two types of models with respect to some general parametric characteristics of each. For three-dimensional models, the anthropomechanical data input appears to be more different in semantics than in substance. The real differences appear in the deterministic environments represented in both models. These differences probably will require analytically different approaches until mathematical and computer techniques are sufficiently advanced to handle the real-time and display differences. Despite these differences, the effect upon anthropomechanical data required is negligible. The environmental requirements of three-dimensional analysis makes the two problems even more comparable in their anthropomechanical data input.

PARAMETERS		DYNAMIC MODELS	
		WORKSPACE	IMPACT
Environment	Time	Long -----	Short
	Geometry	Three-Dimensional	
	Kinetics	Internal -----	External
	Kinematics	Reach Envelope -----	Response Envelope
Anthropomechanics	Linkage	Joint Centers of Mobility	
	Range of Motion	Voluntary (Active) -----	Involuntary (Passive)
	Surface Shape	Clearance -----	Contact Surface
	Inertial Properties	Mass, Center of Mass, and Momental Ellipsoid of Inertia	
	Strength	Active -----	Passive

Figure 5. Comparison of parametric characteristics of Workspace and Impact Models.

3.0 Methodological Considerations for Systems Anthropometry.

The preceding section attempted to place Systems Anthropometry within the perspective of past, present, and future research utilization. Actual implementation of a methodology that will lay the foundation for Systems Anthropometry is in the developmental stage. As a result, some of the elements required in a Systems Anthropometry will be discussed in the following subsections. These elements are, in general, landmark definition, three-dimensional geometric measurements, and kinematical problems of Systems Anthropometry.

3.1. Landmark Definitions

Landmark definition is perhaps one of the most critical problems confronting advances in three-dimensional systems anthropometry. Analysis of errors arising from presently available identification techniques of landmarks is discussed in a following section by D. Hurley Robbins. The errors are significant problems for both accuracy and precision of the results, and efforts to reduce the error by a significant amount may require an independent research investigation.

At present, we have devised a targeting technique which has solved some of the problems. Radiographic tests of the technique revealed that the target is visible on radiographs of osteological specimens (Figure 6). The target is made of four small wires of tungsten arrayed in a pattern that defines a point on the surface of any irregularly shaped body. A malleable target of minimal depth is necessary due to the three-dimensional requirement of observing the same point in two separate views. This targeting procedure should meet the geometric requirements of landmark definition but we may encounter imaging problems when the targets are applied and radiographs are taken of cadaver subjects. Accurate identification of the anatomical landmark may remain basically a perceptive quality of the investigator but perhaps the precision with which the landmarks are targeted will be increased through the use of the previously described targeting device.

A major barrier for dynamic anthropometry for many years has been found in the landmarks. Basically, without a discrete point, uniquely defined, measurements only approximate a fixed body geometry. Traditional definitions have primarily relied upon the surface expression of skeletal

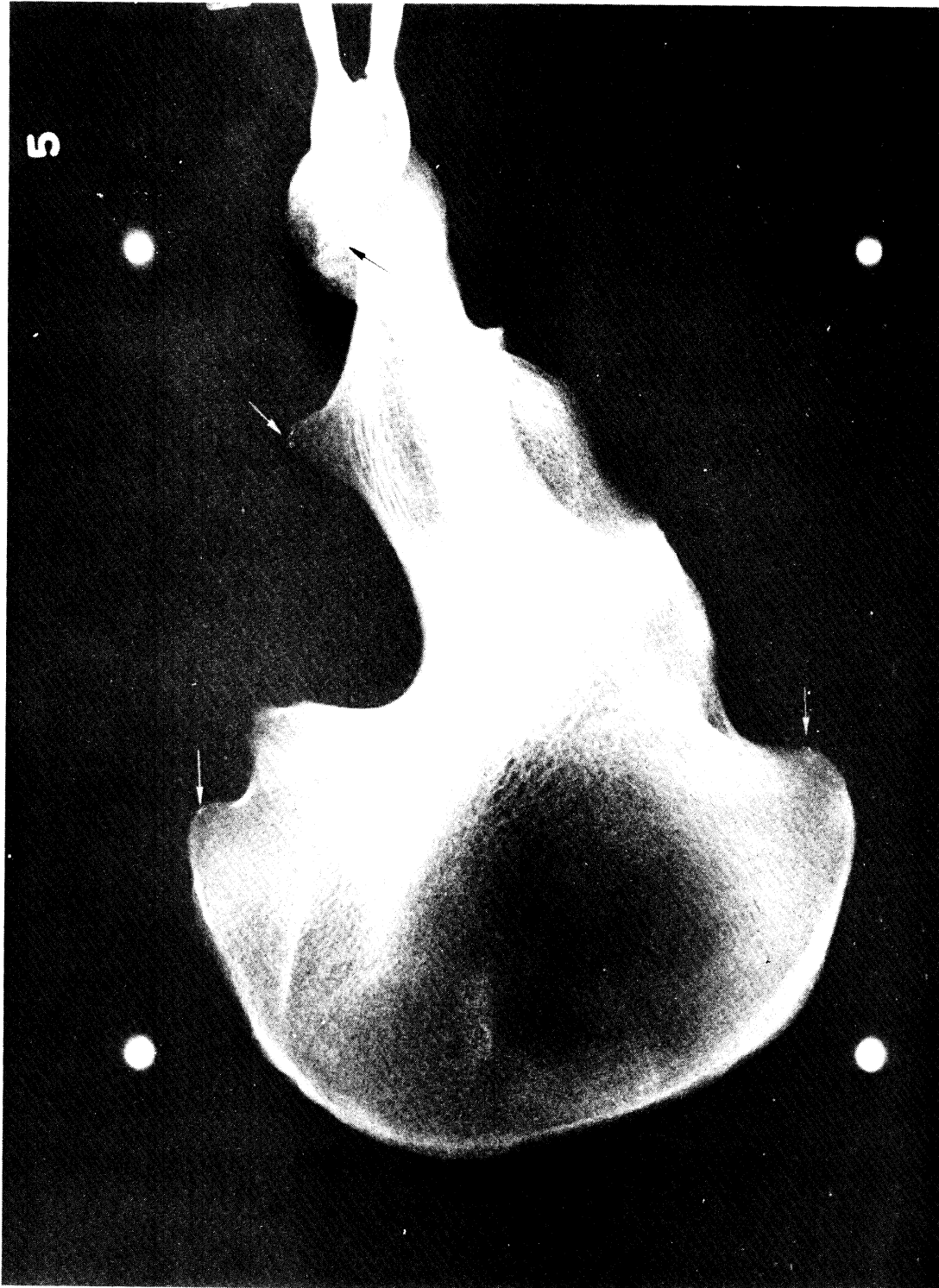


Figure 6

Radiographs of Right Innominate Bone with Targeting Device Placed on Bony Surfaces, not Necessarily Representing an Anthropometric Landmark

or muscular landmarks. For the purposes of three-dimensional systems anthropometry, landmarks will be projected onto the skeleton as vectors from the body surface. The targeting device aids in the solution to the immediately asked question of "how do you define a point on the surface of the skin?" In essence, the targeting device defines the point and the anthropometrist defines the area. The problem changes from defining a finite point in a large surface area to defining a finite area and measuring a point defined by the target. Thus, the accuracy of point definition is determined by the accuracy of the targeting device, and the precision of point definition is determined by the area boundary definition.

In conclusion, landmarks must be selected and defined initially on osteological material. They must be palpable from the surface of the skin, as well as targetable for a radiograph. The experimental procedure will be to study the skeleton to define landmarks and then measure the location of a surface target relative to those skeletally-defined landmark locations. Since this investigation is using fresh cadavers, the program will consist first of x-raying the body in a fixed position with the appropriate surface targets in place. Next, the skeleton will be exposed immediately under the surface ("external") landmark and another set of radiographs made for the same unaltered body position to measure the location of skeletal ("internal") landmarks. The results will provide a correlation of three-dimensional cartesian coordinate locations of the two target locations (external and internal). The remaining investigative activities will be devoted to the mathematical functions of those landmarks relative to the joint centers of mobility.

3.2 Three-dimensional Geometry: Axes Systems.

Three-dimensional geometric data requires the use of frames of reference (Figure 7). There are two probable origins for the primary, inertial frame of reference that are dependent upon the initial anatomical position. At present, the origin for the seated position should be the the Seat Reference Point (SRP) and the Floor Reference Point (FRP) for the standing position. In both instances the principal axes will have the same orientation. The z-axis will be aligned with the vertical gravity vector, the x- and y-axes will be in the horizontal plane. Their orientation will be determined by the anatomical orientation of the body such that posterior to anterior defines the + x direction, right lateral to left lateral defines the + y direction, and inferior to superior defines the + z direction. Only in the initial anatomical position will it be necessary to establish these directions, thereafter, they will remain fixed and immutable. In summary, the primary frame of reference will be a right-handed orthogonal axis system relatively aligned with the gravity vector and fixed to the environmental geometry.

The secondary reference system will be defined by anatomical landmarks measured with cartesian coordinates in the primary axis system. This secondary axis system will, however, have statistical properties that will not be observed in the primary axis system. That is, it will reflect variation in the population and therefore have a probable error associated with it. The secondary axis system defined in the pelvis by the right and left anterior superior iliac spines and symphysis reflects measurement error, sampling error and population differences whereas the primary axis system only contains measurement error. This pelvis axis system has been proposed for use at NAMRL in their human volunteer sled tests (Thomas, personal communication).

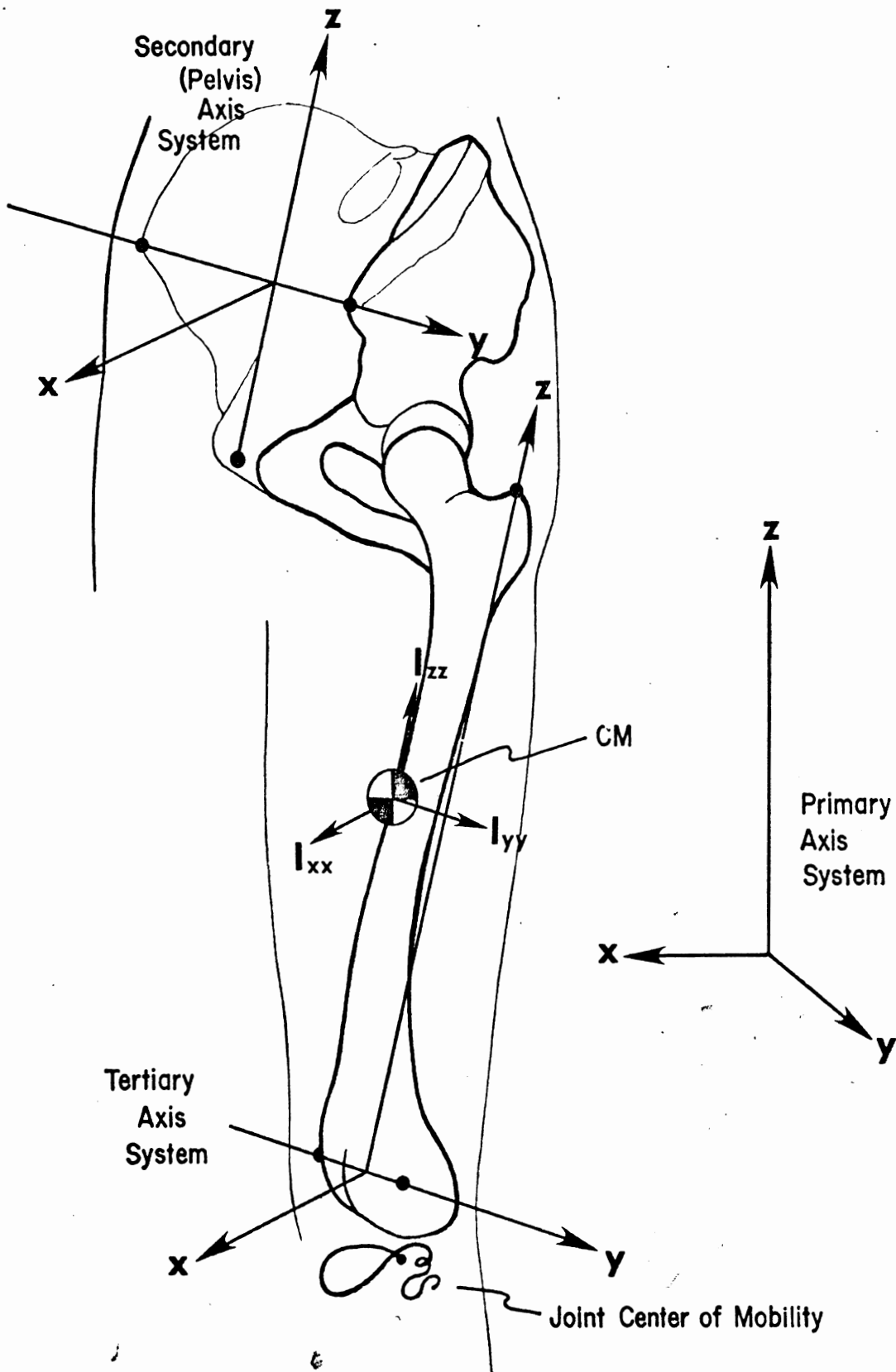


Figure 7. Diagram of Primary, Secondary and tertiary axis systems.

At least one other axis system is needed to define completely the geometry for simulating motion of a multi-segment body. This tertiary axis system defines the spatial orientation of each segment, the location of the joint centers of mobility, the location of segment centers of mass, and a reference frame for the momental ellipsoid of inertia. Each tertiary axis system, however, must be carefully defined so that there is no motion between landmarks used in its definition. Thus, the axis system will be "stable" and always reflect motion of the segment relative to the secondary axis system.

Traditional simulation concepts have considered the body as a series of interconnected rigid geometrical bodies that simulate the segments of the body. Hanavan (1964) defined such a model for estimating the mass distribution properties of the whole body in various fixed positions. In Hanavan's model, as well as succeeding more sophisticated models, segment axes systems have been defined by the principal axes of inertia located at the segment's center of mass. Dynamic simulations, founded in a deterministic philosophy from which mechanistic analogues of the human body have been devised, treat each segment as pivoting "mass-links." Thus, each link has a fixed pivot point, fixed mass, and the geometry of the mass is partially defined by its fixed-length link. This analytical treatment is mathematically "clean" since it uses intrinsic properties of the geometric bodies to simulate anatomical segments of the human body.

The linkage system has thus become an engineering concept superimposed upon the human anatomy. It cannot supplant the musculo-skeletal system since the link is a conceptual parameter for describing body motion and does not incorporate any of the random properties of the human dynamic system. Links have been defined as straight-line distances between proximal

and distal pivot points which represent joint centers of rotation. However, these joint centers of rotation are in reality probabilistic paths of instantaneous centers of joint rotation which can and do apparently change the link length as a function of movement in adjacent segments (Dempster, 1960). Thus, the fixed-length link is not a fundamental anatomical unit but an analytical engineering tool with which the skeleton and joints have been modeled.

The present research is therefore developing different analytical concepts of the linkage system utilizing joint centers of mobility and changing link lengths which affect the choice of landmarks of segment axis system definition. Systems anthropometry will perhaps not change the use of some of these geometric shape simulations to estimate the mass distribution properties of segments, but it will provide three-dimensional data on the location of anatomical landmarks used to define segment axes systems. Therefore, landmarks used in defining axes systems must be chosen such that they are "stable" and always remain fixed between adjacent joint centers of mobility that define the segment.

In addition, as illustrated in Figure 7, the center of mass and momental ellipsoid of inertia of each segment can also be located relative to the tertiary axis system. These mass distribution properties could then be based upon empirically predicted data rather than the current estimates based upon geometric models. To date, empirical information on the direction and location of the principal axes of inertia have been measured only once on six embalmed male cadavers (Chandler, et al., 1975). An investigative effort is presently in progress sponsored jointly by AMRL and NHTSA to quantify these parameters on a sample of thirty living men. This new study will investigate only the mass distribution properties of these subjects and not

the kinematic properties necessary for a complete description of the human dynamic system. In order to relate these new results with the results of the present investigation, comparable segment axes systems based upon anatomical landmarks are necessary. Each segment axis system, therefore, is defined by three surface landmarks. Within this axis system, the principal axes of inertia will be located at the segment center of mass. The present investigation has proposed a similar procedure to locate the joint center of mobility for each major joint. As a result, the inertial and kinematical geometries may be described comparably within the same set of axes systems. However, the axes systems must be defined and described carefully since some of the landmarks currently being used for their definition may need to be re-defined as research progresses in the present investigation.

3.3. Kinematical Problems for Systems Anthropometry

The kinematical problem focuses on joint centers of mobility. Previous efforts have simulated body motion using hinge points that introduce errors in some link length estimates of as much as 5 cm. (Dempster, 1955). Since the body is an open-chain link system of many biomechanically significant joints, the difference in geometric body motion configuration between predicted and real could become substantial.

In order to reconcile these geometric differences, a three-dimensional anthropometry is required that quantitatively defines joint kinematics. Link length, therefore, can be considered to be the result of three-dimensional body position at a fixed point in time. It would not be a measured quantity but a parameter derived from an analysis of body geometry. This is perhaps the most radical implication of three-dimensional systems anthropometry. That is, the linkage system may be defined by centers of joint mobility located within anatomical axes systems.

Phase II will investigate the thigh, pelvic, and lumbar segments that provide contrasts in the problems encountered in joint centers of mobility and axes systems definition in the body. For example, the thigh has three landmarks on the femur at Trochanterion and the right and left femoral condyles whereas the lumbar region contains 4 to 6 vertebrae that are difficult to identify with palpation and also have some relative motion among them (Snyder, et al., 1974). The pelvis is perhaps best-suited for defining an anatomically-based axis system, because it has several reasonably well-defined skeletal landmarks that are commensurately distant from one another.

Geometric description of joint centers of mobility can be resolved

into experimental hypotheses. First, what is the size, or volume, of each joint center of mobility boundary? Thus, can the joint centers be adequately modeled as points or are probabilistic paths of instantaneous joint centers of rotation necessary? These questions must be posed for each significant joint which in the present investigation would be initially the hip joint centers and the L5/S1 joint centers of mobility.

For example, the hip has a ball-and-socket joint whose center of rotation has been traditionally defined by Trochanterion on the femur in anthropometric surveys. Dempster (1955) proposed however, that the hip joint center could only be located within a "...1.2- to 1.5-inch ellipse" (p. 117) when measured as a point halfway between the seat surface and the anterior-superior iliac spine with the body in a seated position. Thus, the location of the hip joint center has a certain amount of error which according to Dempster could be substantial. It would appear that a point may not be sufficient to describe the geometry of joint mobility found in the hip. Since the L5/S1 joint center of mobility has not been equally studied, any conclusions regarding it would be premature except to say that its skeletal geometry restrict motion to a larger degree than found in the hip joint. Thus, the lumbar/pelvic joint center of mobility may be less complex than the pelvic/femur center.

Other hypotheses can be posed for experiments that test the degree to which differing amounts of motion of one segment relative to an adjacent fixed segment affects the geometry of the joint center of mobility. For example, the femur is a rigid bone whose path of motion in the sagittal plane relative to a fixed pelvis axis system can be plotted. The geometry of the joint center of mobility must be studied in the hip joint relative to the total time elapsed for the motion. Thus, is the description of the

hip joint center of mobility from a time-lapse stereo-radiographic series of measurements applicable to a "high-speed" environment? Tests of a rate-dependency hypothesis require time-lapse and high-speed (over 100 frames per second) radiographic capability both of which are available at HSRI.

The actual test configuration has not been decided, but the possibility of using non-human primates is being discussed. Non-human primates would be desirable in order to determine the amount of information needed by type of joint and associated degrees of freedom, and also to test the relationship between in vivo and fresh primate cadaver kinematic results. Furthermore, the non-human primates have a very real advantage over fresh cadavers in regard to their body size and physical maneuverability. The use of non-human primates, however, would not provide quantitative data applicable to the human body but would make dynamic research hypotheses more feasible to test. Thus, based upon the results obtained from a very limited number of non-human primates, the types of data required to describe and predict the kinematic behavior of the joint center of mobility could be prescribed.

Subsequent studies would then be undertaken to determine the most probable paths of motion for each major joint center of mobility. For example, for each degree of freedom in a joint, one equation describing the most probable path of motion would be defined. The hip joint has three degrees of freedom defined by extension-flexion in a para-sagittal plane, abduction-adduction in the frontal plane, and rotation in the transverse plane. As a result, each plane would contain a most probable path of motion which would be empirically described relative to the pelvic axis system. A generalized form of the data will be necessary since they must

describe the joint center of mobility geometry for a specified sample of individuals within the population.

In conclusion, this section has significant implications for Phase II and following research in Phase III. In postulating the methodological implications of systems anthropometry, several research problems have been discussed. Solution of these problems will represent significant progress in our knowledge of the dynamic human body. Specifically, these results will eventually provide the basis for a complete geometric description of the dynamic human body based on empirical data.

4.0. Task Reports for Phase I

The following subsections have been written by members of the research team. Each section summarizes the results of specific tasks identified by the project director to accomplish the goals of Phase I. The goals and appropriate sections are as follows:

a) Establish the data collection methodology for the new system anthropometry, including development of a means of spatially identifying anatomical and anthropometric landmarks suitable for a three-dimensional coordinate description.

Subsection 4.1 D. H. Robbins

4.2 M. Bender

b) Develop a data analysis methodology, and determine utility of the data in present or future models, such as AMRL's COMBIMAN Model.

Subsection 4.3 H. M. Reynolds and D. H. Golomb

4.5 D. H. Golomb

c) Coordinate data collection and analysis in mutually complementary formats.

Subsection 4.4 H. M. Reynolds

4.6 B. Bowman

4.7 J. Freeman

d) Examine and analyze three-dimensional cartesian coordinate data already collected on 280 individuals for the development of suitable statistical summarization and presentation techniques.

Subsection 4.5 D. H. Golomb

Some of these sections will serve as the basis for papers to be presented at scientific meetings as well as publications in scientific

journals. In particular, Subsections 4.1 and 4.3 will be used for oral presentations and 4.5 will be used as the basis for two written publications. The overall results of Phase I research will be discussed in Section 5.0 with the addition of specific recommendations for Phases II and III.

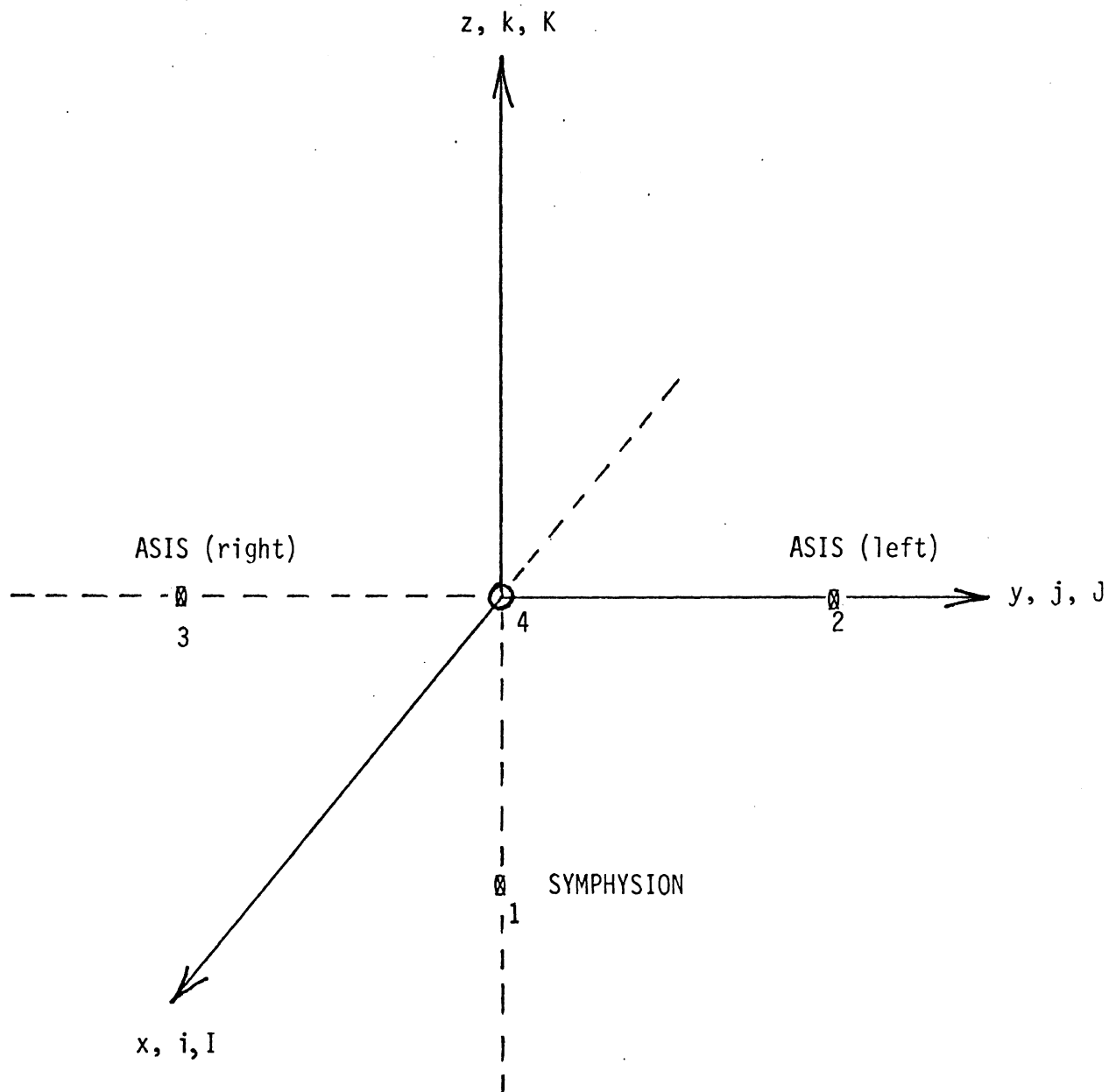
4.1. Errors in Definition of an Anatomically-Based Coordinate System Using Anthropometric Data.

by D. H. Robbins

4.1.1. Introduction

Given the spatial location of three non-collinear points on the human body, it is possible to construct a coordinate system which can be used to describe the motion of the body or body segments, provided that the points remain equidistant from one another and are rigidly fixed to that part of the anatomy in question. However, it is known that it is not possible to obtain the precise location in space of points on the body using common techniques of anthropometry. Therefore, it follows that some error is inherent in any coordinate system which is constructed from anthropometric data. The purpose of this discussion is to present formulas for defining the location of a coordinate system in space based on anthropometric data and to demonstrate the uncertainty of its location using estimated data from the human pelvis.

Figure 8 shows coordinate systems and data for the human pelvis. Location of the pelvis is defined by three points--left and right anterior superior iliac spines and symphysis (points 1, 2, and 3). An inertial coordinate system (I, J, K) is shown superimposed on a moving pelvic system defined by (i, j, k). Data in the x, y, z system for the three points are based on best estimates of professional anthropometrists. Potential error estimates for the points represents a consensus opinion. The fourth point (4), which is the origin of the moving pelvis coordinate system, is located by dropping a perpendicular from point 1 to a line connecting points 2 and 3. It is apparent that point 4 and the axes of this moving system will not coincide with the inertial system when



	x (cm)	y (cm)	z (cm)
Point 1	0 ± 2	0 ± 2	-14.28 ± 3
Point 2	0 ± 1	14 ± 5	0 ± 3
Point 3	0 ± 1	-14 ± 5	0 ± 3

Figure 8. Pelvic Data and Coordinate System

errors of measurement occur in the anthropometric data.

4.1.2. Analysis.

The direction of the coordinates in the moving system are given by:

$$i = \alpha_1 I + \alpha_2 J + \alpha_3 K$$

$$j = \beta_1 I + \beta_2 J + \beta_3 K$$

$$k = \gamma_1 I + \gamma_2 J + \gamma_3 K$$

Direction cosines for the y-axis will be

$$\beta_1 = [(x_2 - x_3) + (\delta x_2 - \delta x_3)]/d_{23}$$

$$\beta_2 = [(y_2 - y_3) + (\delta y_2 - \delta y_3)]/d_{23}$$

$$\beta_3 = [(z_2 - z_3) + (\delta z_2 - \delta z_3)]/d_{23}$$

where

$$d_{23} = \sqrt{[(x_2 - x_3) + (\delta x_2 - \delta x_3)]^2 + [(y_2 - y_3) + (\delta y_2 - \delta y_3)]^2 + [(z_2 - z_3) + (\delta z_2 - \delta z_3)]^2}$$

and δx_1 , δx_2 , and δx_3 are the errors inherent in the anthropometric data. The z-axis is defined by dropping a perpendicular from point 1 to the y-axis yielding

$$\gamma_1 = (x_1 + \delta x_1 - x_4)/d_{14}$$

$$\gamma_2 = (y_1 + \delta y_1 - y_4)/d_{14}$$

$$\gamma_3 = (-z_1 + \delta z_1 - z_4)/d_{14}$$

where

$$d_{14} = \sqrt{(x_1 + \delta x_1 - x_4)^2 + (y_1 + \delta y_1 - y_4)^2 + (z_1 + \delta z_1 - z_4)^2}$$

Because of orthogonality,

$$\beta_1 \gamma_1 + \beta_2 \gamma_2 + \beta_3 \gamma_3 = 0$$

The location of point 4 can be written

$$x_4 = x_2 + t(x_2 - x_3) + \delta x_2 + t(\delta x_2 - \delta x_3)$$

$$y_4 = y_2 + t(y_2 - y_3) + \delta y_2 + t(\delta y_2 - \delta y_3)$$

$$z_4 = z_2 + t(z_2 - z_3) + \delta z_2 + t(\delta z_2 - \delta z_3)$$

where t is defined as a proportionality factor along d_{23} . Substitution into the orthogonality condition and simplification yields

$$t = \frac{(x_1 + \delta x_1 - x_2 - \delta x_2)(x_2 + \delta x_2 - x_3 - \delta x_3)}{d_{23}^2} +$$

$$\frac{(y_1 + \delta y_1 - y_2 - \delta y_2)(y_2 + \delta y_2 - y_3 - \delta y_3)}{d_{23}^2} +$$

$$\frac{(-z_1 - \delta z_1 - z_2 - \delta z_2)(z_2 + \delta z_2 - z_3 - \delta z_3)}{d_{23}^2}$$

Direction cosines (α_1 , α_2 , and α_3) for the x-axis are determined from

$$h = ixj = (\beta_2\gamma_3 - \beta_3\gamma_2)I + (\beta_3\gamma_1 - \beta_1\gamma_3)J + (\beta_1\gamma_2 - \beta_2\gamma_1)K$$

Euler angles can now be defined to describe the orientation of the moving system with respect to the fixed system. The angles (ϕ , θ , and ψ) are associated with the (x, y, and z) axes respectively:

$$\theta = \sin^{-1}(-\alpha_3)$$

$$\phi = \tan^{-1}\left(\frac{\beta_3}{\gamma_3}\right)$$

$$\psi = \tan^{-1}\left(\frac{\alpha_2}{\alpha_1}\right)$$

4.1.3. Examples

The location of point 4 and the Euler angles associated with the moving coordinate system have been computed for several combinations of errors within the ranges given in Figure 8. The results are tabulated in Table 1.

TABLE 1. POTENTIAL COORDINATE SYSTEM LOCATIONS
USING ANTHROPOMETRIC DATA

Case	Given									Predicted					
	Point 1			Point 2			Point 3			Point 4					
	x	y	z	x	y	z	x	y	z	x	y	z	ψ	θ	ϕ
Skewed about z	0	0	-14.28	1	14	0	-1	-14	0	0	0	0	4.09°	0	0
Skewed about y	2	0	-11.28	-1	14	-3	-1	-14	-3	-1	0	-3	0	11.86°	0
Skewed about x	0	2	-11.28	0	14	3	0	-14	-3	0	4.22	-0.9	0	0	12.02°
Z-shift of data	0	0	-11.28	0	14	3	0	-14	3	0	0	3	0	0	0
Y-shift of data	0	2	-14.28	0	19	0	0	-9	0	0	2	0	0	0	0
X-shift of data	1	0	-14.28	1	14	0	1	-14	0	1	0	0	0	0	0
Typical (about 1/2 maximum error)	1	1	-12.75	-.5	17	-2	.75	-16	1.8	.16	-.5	.01	1.71°	3.97° - 6.58°	

*It should be noted that the origin and coordinate system locations do not reflect pelvic symmetry.

4.1.4. Conclusions.

Based on the analysis and on the examples, four conclusions have been drawn.

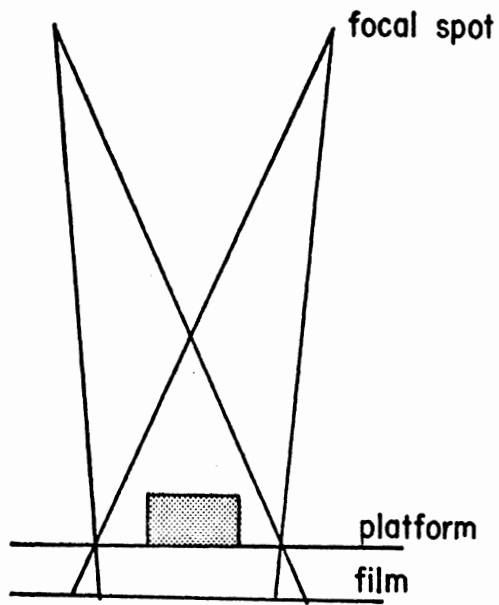
1. The location of a point in a coordinate system (e.g., joint centers and centers of gravity) can be no more accurate than the coordinate system itself.
2. The points which are the most accurately determined should be used in constructing coordinate systems subject to the fact that they must also be the farthest apart.
3. Using these equations, it is possible to study the effect of measurement errors on the ability to define anatomically-based coordinate systems.
4. Given pelvic data plus an estimate of its current range of accuracy using present measurement techniques, we predict errors could be as large as 12° in angular orientation of a coordinate axis and 3 cm. in translation. More typically, however, errors of $\frac{1}{2}$ cm. and 6° are to be expected on the pelvis.

4.2 Radiographic Methodology for Systems Anthropometry Measurement

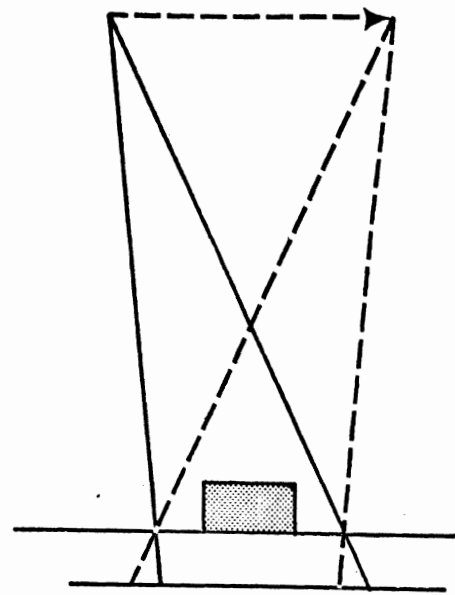
M. Bender

An important goal in the systems anthropometry program is accurate and repeatable quantitative specification of anatomical landmarks in a three-dimensional coordinate system. The distribution of these landmarks, or points, includes points on the skin surface and points on the skeletal structure within the body. This condition suggests use of radiographic techniques for the location of such points; the main problem is establishment of a coordinate axes system which permits accurate measurements in a convenient, economical, and straight-forward procedure. After consideration of several approaches involving a rigid cartesian framework in which an x-ray head and film cassette could be mounted and scaled for axes measurements, it was concluded that the problems and costs associated with fabricating, scaling, and performing measurements with such a device would be extensive. A more simple and straight-forward procedure was found in the technique of x-ray stereo photogrammetry, which offers the possibility of accurate location of points in space explicitly from measurements of corresponding images on a pair of x-ray radiographs.

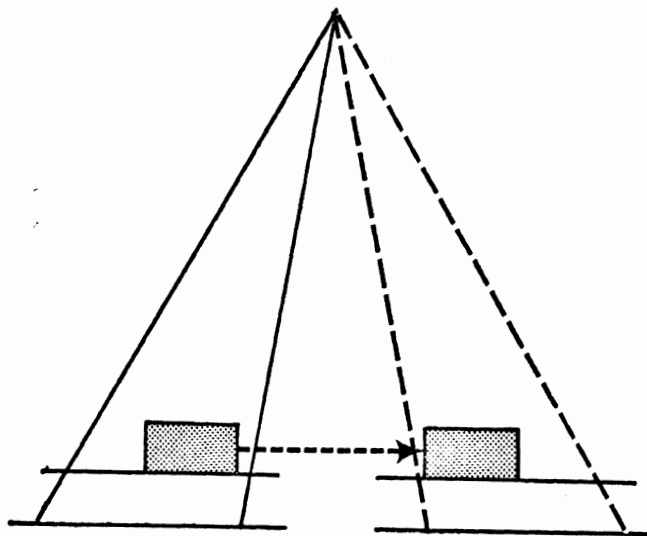
There are basically four configurations of x-ray tube focal spot, object platform, and film plane which can be used to produce stereo-radiographs (McNeil, 1966). These are shown in Figure 9, and are: a) two stationary tubes with stationary object and film, b) translation of one tube with stationary object and film, c) translation of object with one stationary tube, and d) rotation of object and film with one stationary tube. In practical terms, the first configuration, (a), and the third, (c), are not suitable for purposes of this program because of inavailability



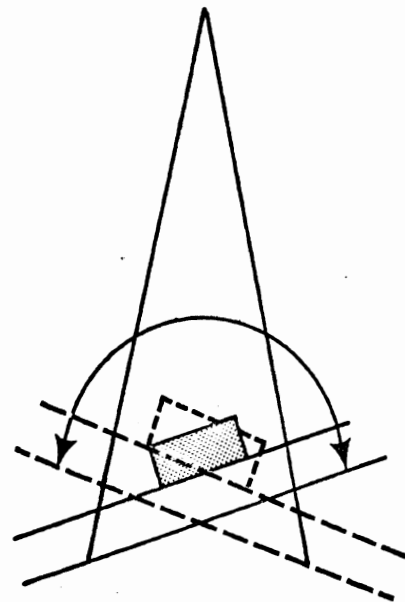
(a) Two Stationary Tubes with Stationary Object.



(b) Translation of one tube with Stationary object.



(c) Translation of Object with one Stationary Tube.



(d) Rotation of Object with one Stationary Tube.

Figure 9. Basic Configurations for Producing Stereoradiographs.

of two appropriately mounted x-ray tubes, and, in the latter, accurate translation of the object and film is not feasible. Configurations (b) and (d) are under consideration for use in this program, but (b) is better suited for use with cadavers than configuration (d) because of the necessity to avoid any possible displacement of a surface skin marker with respect to an internally designated landmark, between exposures in the production of a pair of stereoradiographs. The structure of the x-ray unit at HSRI is well-adapted to this configuration because the single tube displacement can be locked in each position vertically and horizontally and displacements can be conveniently calibrated, but it is essential that the line of tube displacement be parallel to the image plane.

4.2.1. Origin Calibration and Image Distance Calibration.

A 14-inch by 17-inch x-ray film cassette surface was provided with x-ray opaque thin wires at the edges of the cassette frame, at points 90° from each other, so that the images of these points could be connected on the developed image to form an x-y axis system in the image plane. The y-axis corresponds to the 17-inch dimension. In order to establish a reference coordinate system, two calibrations must be performed. These are 1) an origin calibration to position the focal spot of the x-ray tube vertically above the origin of the x-y axis system of the film, and 2) an image distance calibration to determine the perpendicular distance from the focal spot to the film, or image plane. These steps are required regardless of the configuration used to produce stereo radiographs. These steps were accomplished by construction and use of a calibration device, shown in the photograph of Figure 10.

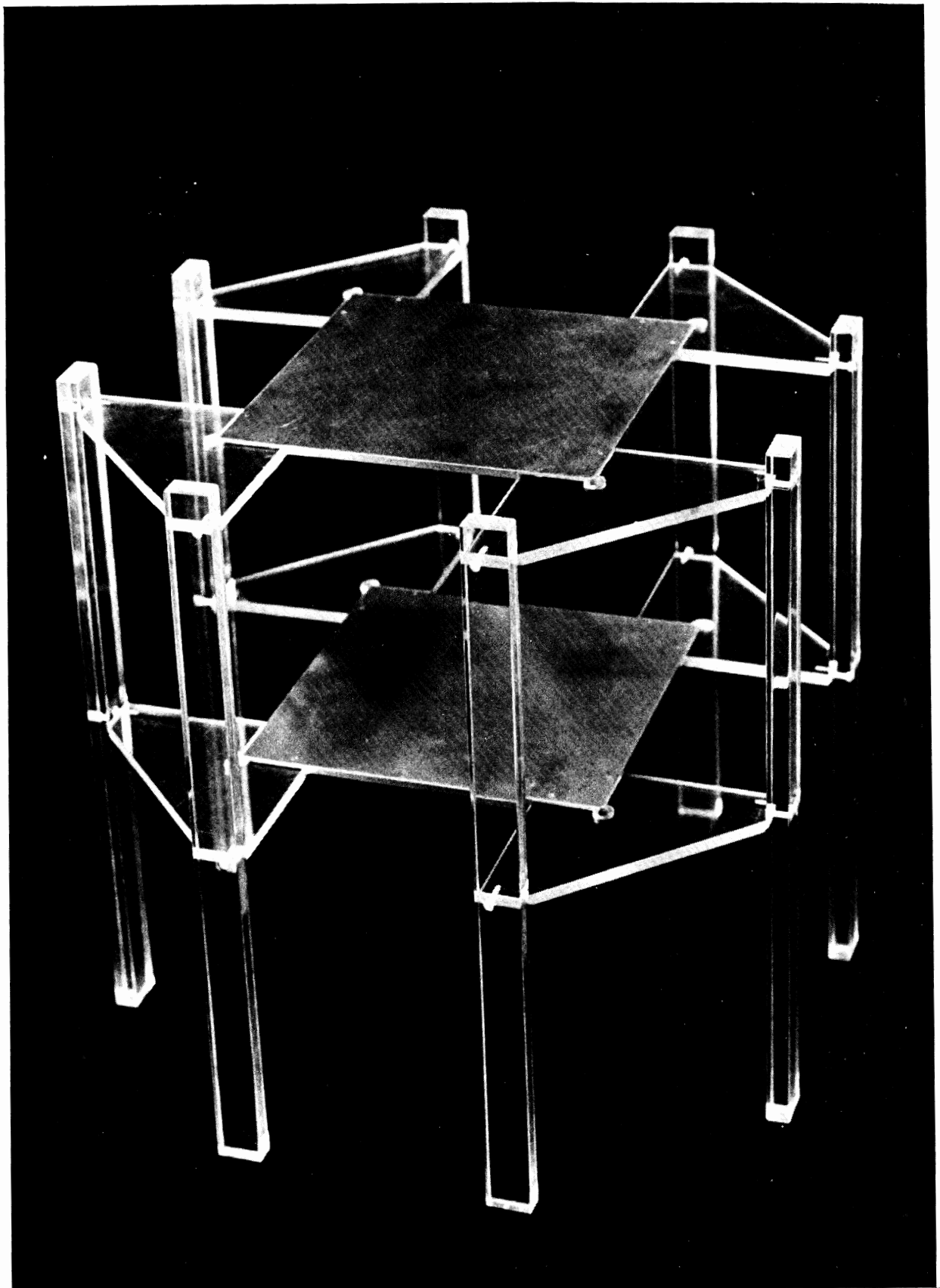


Figure 10

X-Ray Image Distance and Origin Calibration Device

Two 6-inch by 6-inch parallel planes of aluminum of 1/8-inch thickness are supported by eight rigid plexiglass legs. The surfaces of each plane contain a symmetrical array of four x-ray absorbing targets in the corners, and one in the center of the plane. Average distances between targets, from corner to corner along the edges of the square, are 5.008 ± 0.001 inches. The upper plane targets consist of 0.010-inch diameter by 0.010-inch depth cylinders, and the lower plane targets consist of 1/4-inch crosses, also of 0.010-inch width and 0.010-inch depth. Average distances of the upper surfaces of each plane from a flat granite table surface were found to be 10.024 ± 0.002 inches for the upper plane, and 5.012 ± 0.001 inches for the lower plane. The device can be disassembled to interchange the planes, if desired. The supporting legs are placed considerably outboard to the target-bearing planes so that x-ray images of the legs do not obscure the tiny images of the targets on the film. An x-ray image of the device is shown in Figure 11, where the x-y markers are connected to form coordinates in the image plane. An idea of the degree of orthogonality of the focal spot and center targets may be obtained by observing the proximity of the center targets. The focal spot was 45.83 inches above the film plane, determined by the calibration procedure described below.

The image distance and origin calibration procedure consists of first aligning as closely as visually possible the calibration device symmetrically with the four edge markers on the film loaded cassette which represent the x- and y-axes. The x-ray tube is adjusted so that the focal spot is approximately vertical over the origin of the x- and y-axes. Geometry of the image distance calibration set-up is shown in Figure 12.

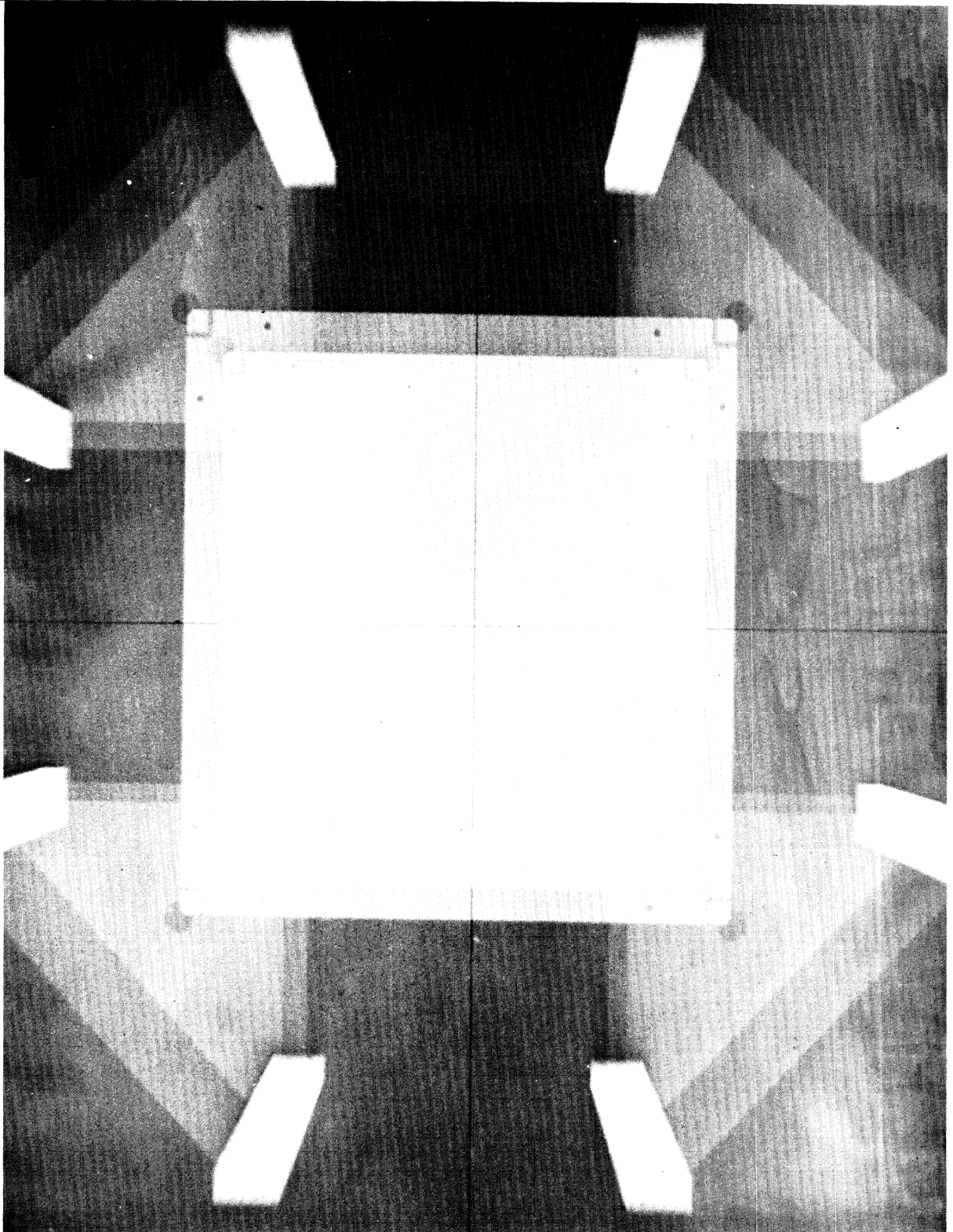


Figure 11

X-Ray Radiograph of Calibration Device

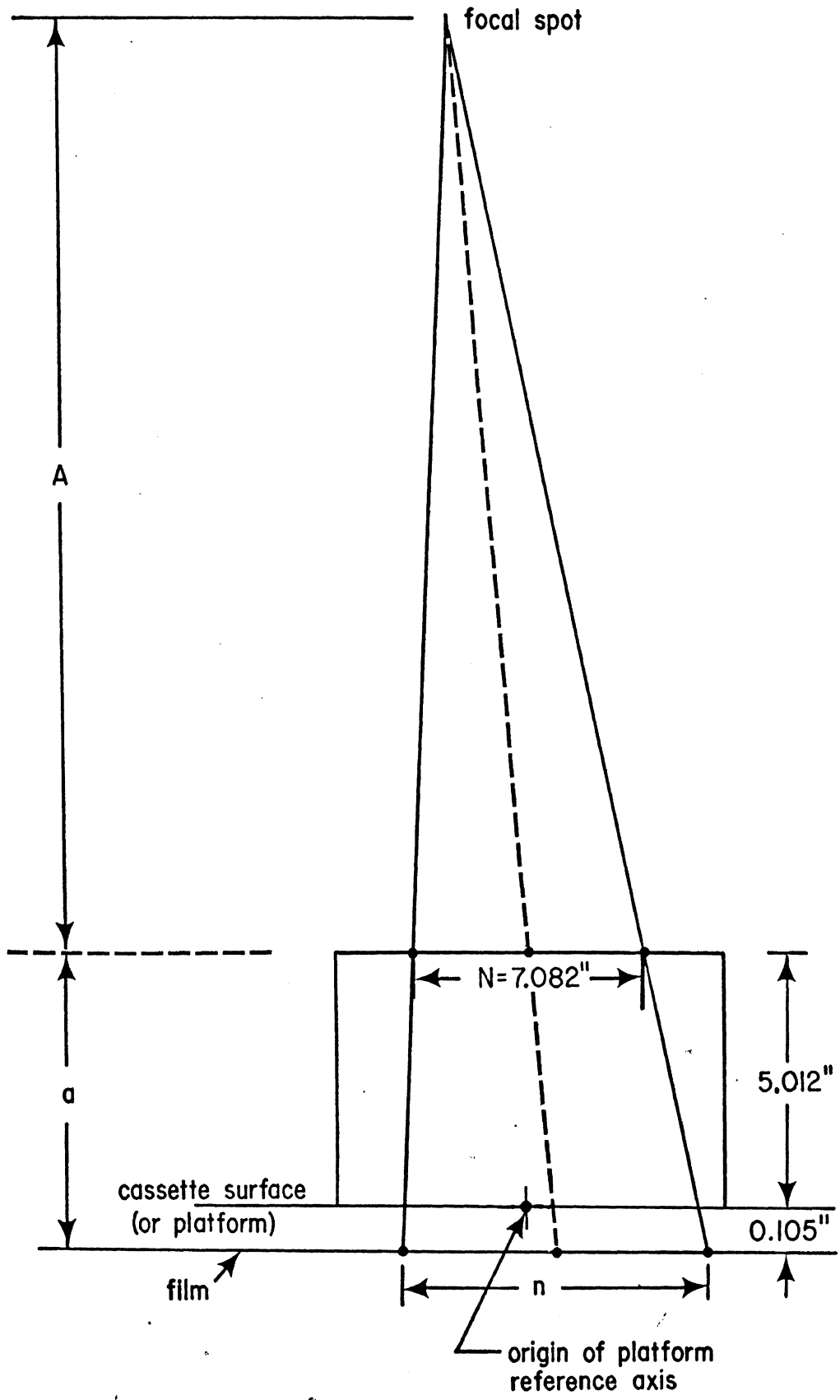


Figure 12. Image Distance Calibration Geometry.

Distances between the two sets of diametrically opposite cross target images were measured; an average value was 7.082 inches. The height of the upper surface of the lower plane of the calibration device from the cassette surface was 5.012 inches. An additional dimension, the distance of the film from the cassette surface, must be added to the device height because of the cassette structure which includes the phenolic surface thickness, an intensifying screen, and a layer of felt. An average of a distribution of this measurement was determined to be 0.105 inches.

Determination of the focal spot to image plane distance is obtained from:

$$A + a = na/(n-N),$$

where

$A + a$ is the image distance,

A is the distance from the focal spot to the plane of the cross targets,

a is a measured distance between the cross target plane and the film plane,

n is a measured distance between images of diametrically opposite cross target images on the film, and

N is a measured distance between the diametrically opposite cross targets on the calibration device.

A value for N obtained from measurement on the film was 7.972 inches. From the above given data and their relationship, an image distance of 45.83 inches was determined.

For the origin calibration, the x - and y -coordinates of the image

of the center cross target were measured on the film. The x- and y-coordinates of the focal spot from the vertical line through the origin are given by

$$X = - x A/a,$$

$$Y = - y A/a.$$

Geometry of the origin calibration is shown in Figure 13. Values obtained for x and y from the film were 0.055 inches and 0.183 inches, respectively, which in turn gives, for X and Y, values of -0.438 inches and -1.456 inches, respectively. In order to complete the origin calibration, it is required to translate either the x-ray tube focal spot or the cassette by the values for X and Y. It is more convenient to translate the cassette, and to do this with the order of accuracy of three or four significant figures, a cassette mounted on a lathe bed would be required.

4.2.2. Quantitative Stereoradiography. Use of stereoradiography for determination of the location of an object in the body with respect to a reference marker placed on the body has long been a common clinical procedure. Figure 14 shows the geometry for locating such points. In general, a single tube is shifted a known distance, B, often called the stereo base, and the differential parallax is measured. The elevation, h, of a point from a reference object plane is given by

$$h = (\Delta p) D / [(Bd/D) + \Delta p],$$

where h is the elevation of the point under consideration, above the plane,
B is the distance between focal spots, or stereo base,

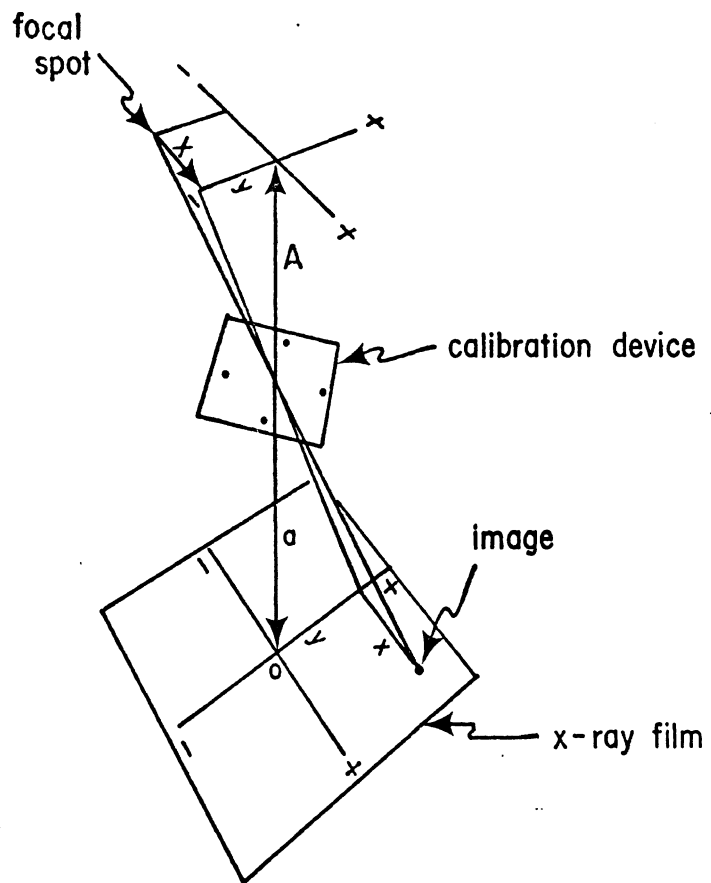


Figure 13. Origin Calibration Geometry.

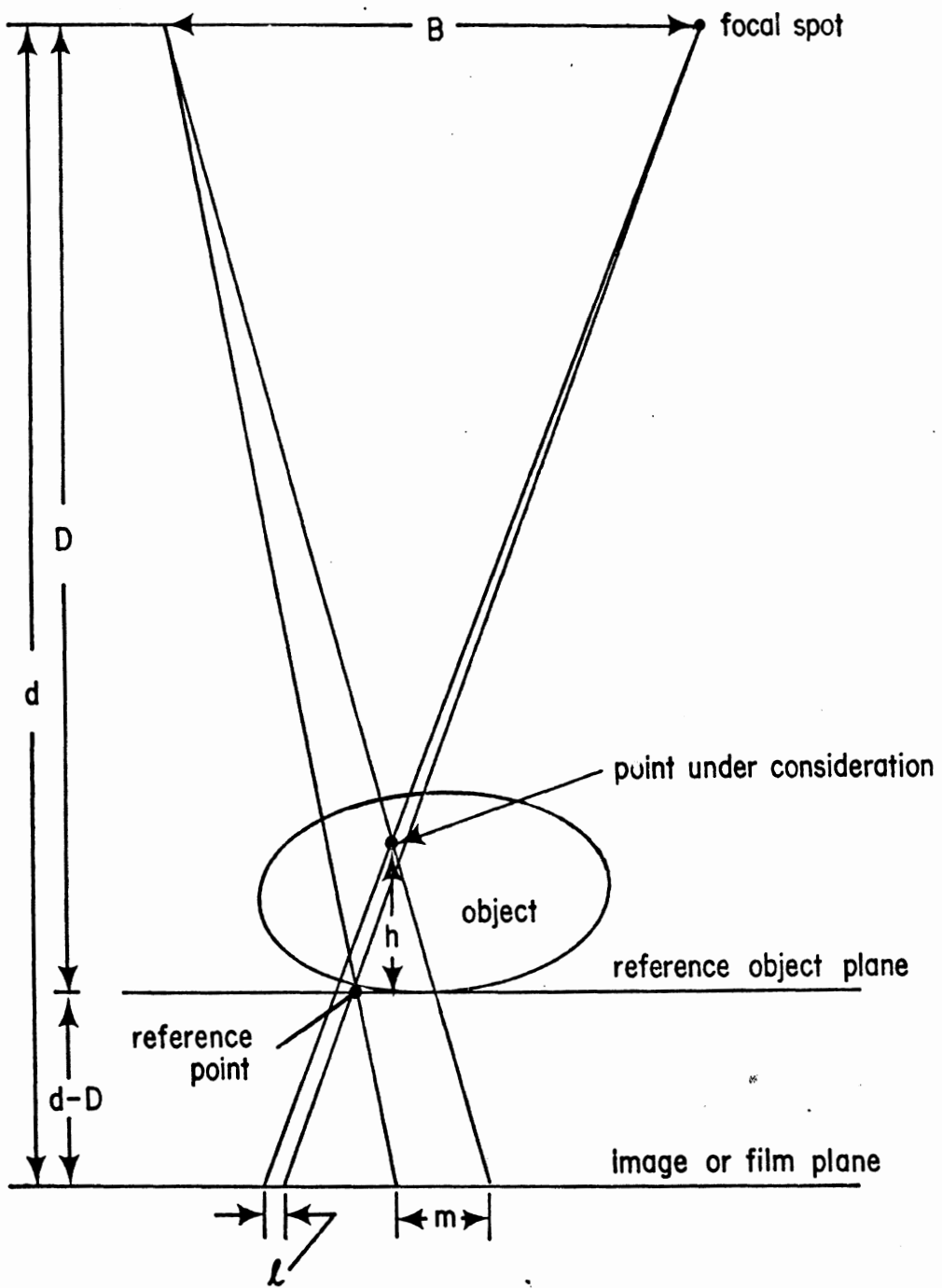


Figure 14. Stereoradiography Geometry for Determining Elevation of a Point from a Reference Point on a Surface.

D is the object distance, or distance from focal spot to reference object plane,

d is the image distance, or distance from focal spot to image plane, and

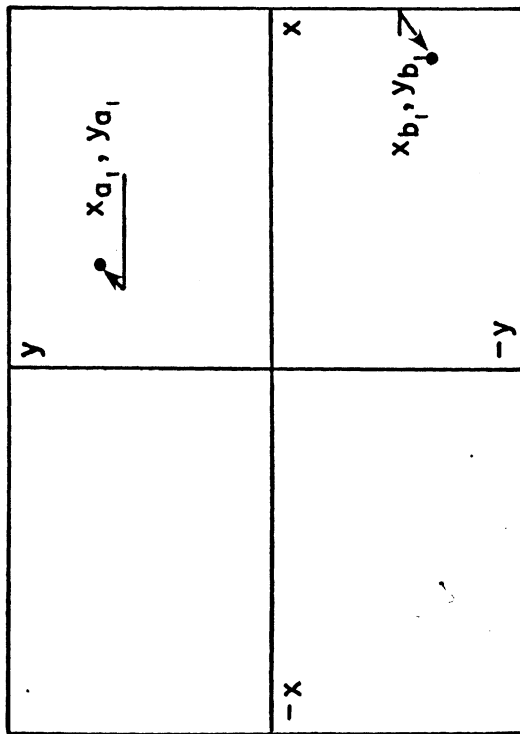
Δp is the differential parallax $(1 + m)$.

Since D is approximately equal to d, and Δp is relatively small compared with B, a very close approximation for h is

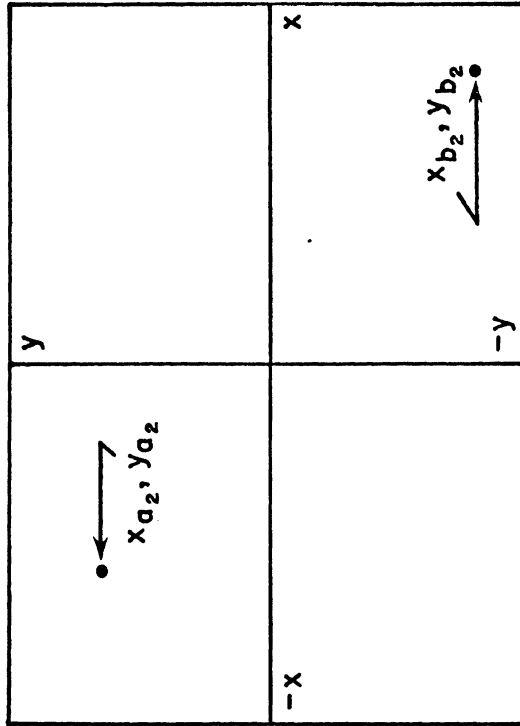
$$h = (\Delta p) D/B.$$

From this, the elevation difference is obtained by the product of the differential parallax and object distance--stereo base ratio. The preceding expression can be shown to be a very close approximation to the former by assuming some typical values and comparing the computations for h. Let B = 18 inches, D = 36 inches, so that a value for the object distance-base ratio, $K=D/B=2$, $d=36.2$ inches, and $p=0.50$ inches. The elevation, h, computed exactly is 0.992 inches. The approximation gives $h=1.000$ inch, an error of 0.008 inch for the assumed conditions.

The difference in elevation determination is only a one-dimensional solution. The procedure for obtaining three-dimensional coordinates of points in the radiation field is as follows. First, an image distance and origin calibration of an x- y marked cassette must be performed. Assume two points, A and B, are to be located in three-dimensional space. An x-ray stereopair is then obtained. Figure 15 is a graphical representation of the resulting stereopair of the points in space. The x and y axes on each exposure are drawn on the films connecting the images of the wire markers that are the X- and Y-axes on the reference platform,



Exposure No. 1



Exposure No. 2

Figure 15. Coordinates of Stereopair of Points A and B.

or cassette surface. The x and y coordinates of image points a and b are measured, and translated relative to x'- and y'- axes with origin at o, on exposure one and o₂ on exposure two, according to the following computations:

$$x'_{a1} = x_{a1} + o_1 t_1, y'_{a1} = y_{a1}$$

$$x'_{b1} = x_{b1} + o_1 t_1, y'_{b1} = y_{b1}$$

$$x'_{a2} = x_{a2} + o_2 t_2, y'_{a2} = y_{a2}$$

$$x'_{b2} = x_{b2} + o_2 t_2, y'_{b2} = y_{b2}$$

where $o_1 t_1 = -o_2 t_2 = d \tan \theta$ and $\theta = \tan^{-1} \left(\frac{B/2}{d-s} \right)$ as shown in Figure 16, which represents an equivalent composite of the stereopair. Point T is a reference marker indicating the origin of the X-, Y-axes of the platform plane. Point B is not shown so that the figure does not become unduly complex.

Coordinates of points A and B are then obtained as follows:

Point A	Point B
$p_a = x'_{a1} - x'_{a2}$	$p_b = x'_{b1} - x'_{b2}$
$K_a = B/p_a$	$K_b = B/p_b$
$X_a = x'_{a1} K_a$	$X_b = x'_{b1} K_b$
$Y_a = y'_{a1} K_a$	$Y_b = y'_{b1} K_b$
$Z_a = D - dK_a$	$Z_b = D - dK_b$

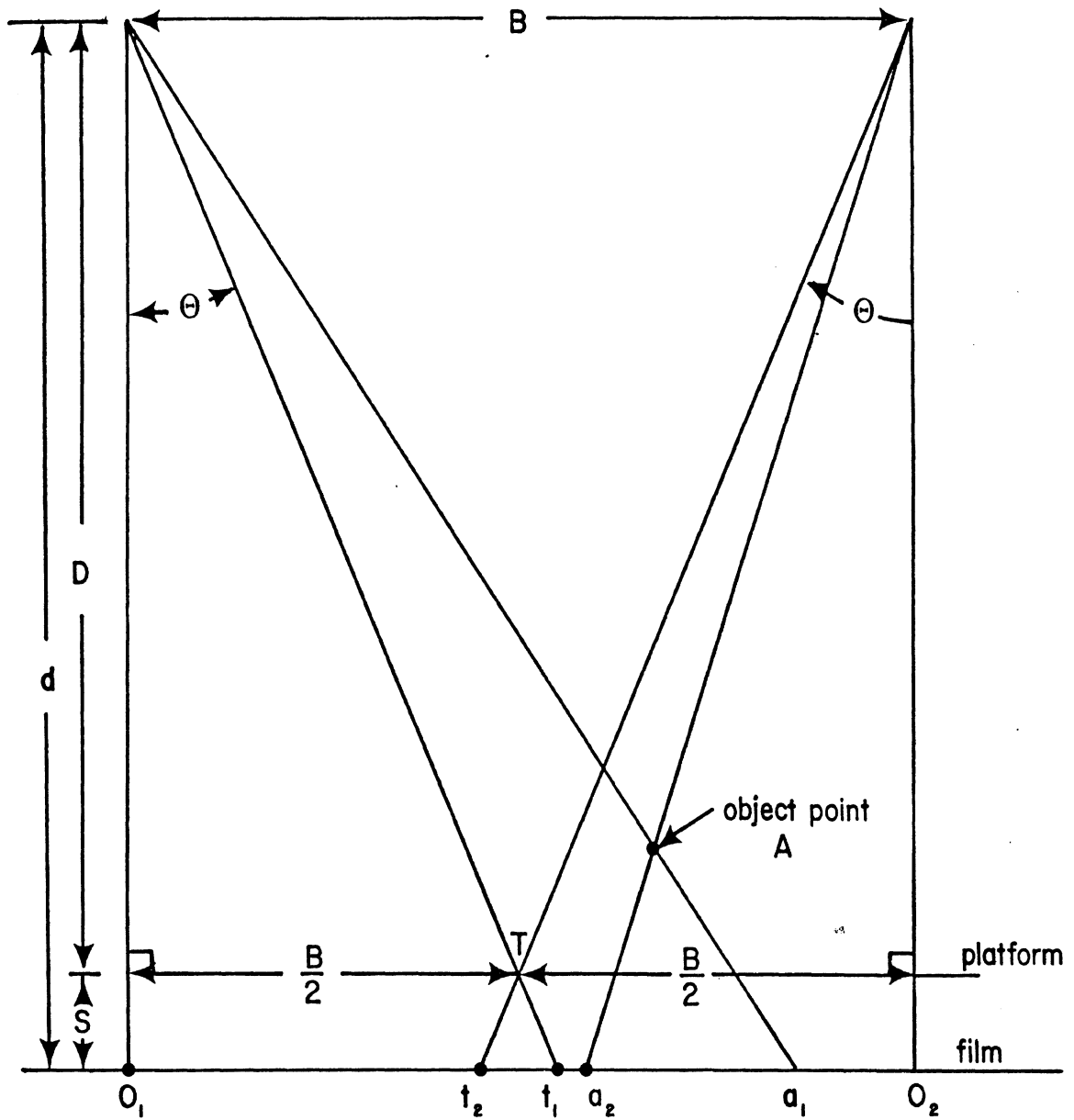


Figure 16. Equivalent Composite of the Stereopair.

4.2.3. Sources of Error. For purposes of the systems anthropometry measurements an ideal x-ray stereoradiographic system would consist of perfect parallelism between the reference plane of object and the film plane, and constant object distance or image distance between exposures. X-ray tube shift, or the stereo base dimension, can be measured quite accurately to orders of 0.5%, but if this displacement is on a slight incline, error in the anthropometry can occur. The calibration device described above will be used to determine the degree of parallelism to be taken into account. The structure of the cassette determines the degree of parallelism between the object reference plane and the image plane. The image plane is separated from the reference plane of the object by 0.105 ± 0.001 inch, due to thicknesses of various components of the cassette, which is an acceptable degree of parallelism, and over small regions of the cassette, several inches, the deviation is less.

Another possible source of error was thought to occur in changes of x-ray film dimensions as a result of the developing and drying process. This was investigated by placing on a substrate an array of 0.002 inch tungsten filament segments of lengths ranging from 3/8 inch down to 1/32 inch in a random manner. Distances between selected segments and segment lengths were measured repeatedly by seven observers, using a British Indicators, Ltd., metric caliper, which can read to ± 0.05 millimeter. The array of filaments was then radiographed in contact with film on two samples of 10 by 12 inches and 14 by 17 inches Eastman RP/L-14 x-ray films. The four film samples were subjected to two different developing temperatures, 16°C and 22°C , in pairs, to observe possible effects of change in film size and change in developing temperature. Comparison of measurements of the actual filaments with x-ray images

of the filaments was made. Overall deviation in the sets of measurements was found to be 0.003%, resulting in the conclusion that film dimension changes are insignificant.

Another type of error in the classification of errors is blunder, which is certainly to be avoided in the handling of data. It was thought that stereo pairs could be produced on single sheets of film in the interests of economy. A stereopair of the calibration device was taken on a single film, as shown in Figure 17. It is to be noted that the calibration device is a symmetric, well-designated structure, with ideally divergent x-ray absorbing material properties; the process of selecting appropriate points for corresponding exposures can give rise to confusion amongst various observers, so to reduce the probability of occurrence of blunder, separate films for exposures will be used.

A final consideration is the critical problem in the film measurement process: the identification of a point in the x-ray image. Very small spheres of 0.080 inch diameter were found to be projected as very small ellipses, and in addition, even if the center could be identified, that point would be in error with respect to the anatomical landmark it purports to designate. A more promising approach appears through use of fine tungsten metallic mesh cut in a square of 1/8 inch, placed in contact with an anatomical landmark so that the center of the square is in close contact with the landmark point. X-ray projections of these square meshes offer a better prospect of more accurate location, except in the case where the square is projected as a line. This point identification problem is under investigation.

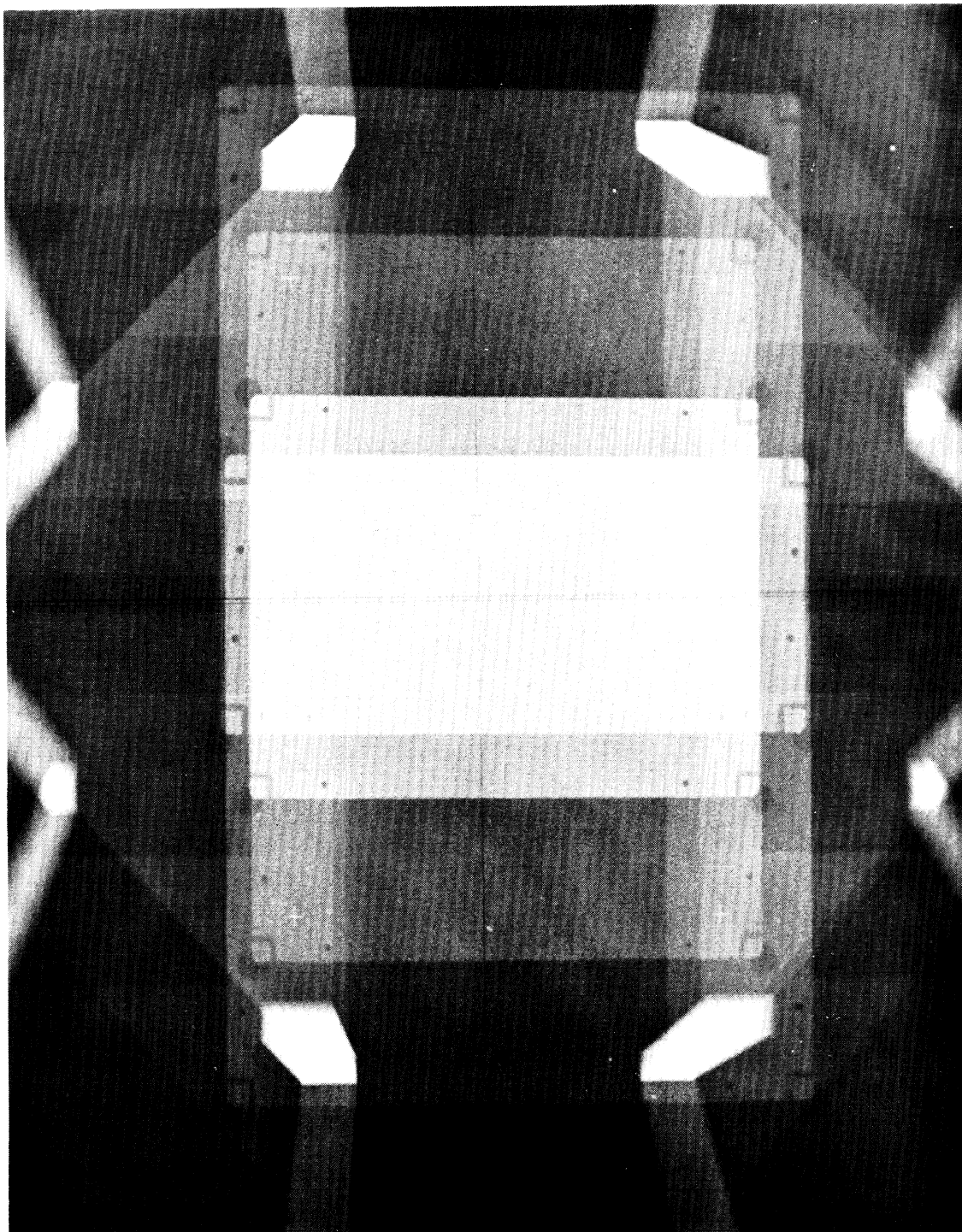


Figure 17

Stereopair of Calibration Device on a Single Film

4.3. Body Sizing Schemes for Systems Anthropometry

H. M. Reynolds and D. H. Golomb

Defining body size categories is an important procedure in the construction of an experimental design and in the analysis of data. Specifically, in constructing an experimental design, body sizing schemes may be used to stratify a population so that representative samples can be selected, and, in analyzing data, body sizing schemes provide a way of distinguishing between "large" and "small" individuals. This procedure has been applied in selecting pelves from the Hamann-Todd collection at the Cleveland Museum of Natural History (see Section 4.4).

Our work, thus far, in defining body size categories has not been conclusive. Our attempt has been to make these definitions based on a bivariate distribution of two standard anthropometric measurements. A fairly complicated procedure was devised as follows: a line is generated by least squares fitting of one variable versus the other. This line roughly divides the data into two equal segments. Orthogonal lines then may be drawn so that roughly $x\%$ of the data is to the left of the first, $y\%$ to the left of the second, etc. The least squares fit and the orthogonal lines define the boundaries of the sizing categories (See Figure 18).

This procedure is appealing because it defines the categories based on two variables with an adjustment for the linear relationships between the variables. If the two variables are correlated at a level very close to zero, the above procedure is equivalent to defining a standard rectangular grid--that is, each category is defined by one

variable being less than or greater than a fixed value, and by the other variable being between two fixed values, or greater than or less than a fixed value.

To illustrate how the adjustment works, the height and weight of males measured in the 1964 HES study, were used to define 10 sizing categories with our procedure and with the standard rectangular procedure. For this population, height and weight are significantly correlated at about .4. In the standard procedure, the sizing cell defined by data above the 95th percentile height and above the mean weight, contains 5% of the data. In the procedure with the adjustment, the corresponding cell contains 2.4% of the data. Likewise, the sizing cell defined by data above the 95th percentile height and below the 50th percentile weight, contains 0% of the data. Using our procedure, the corresponding cell contains 2.6% of the data.

The above example demonstrates how our body sizing schemes can distinguish between "heavy/tall" and "light/tall" individuals. However, the procedure is somewhat arbitrary. The least squares fit could be reversed, producing different size cell definitions. This was done and the newly defined adjustment worked equally well as in the above example.

We also experimented with using different pairs of variables. Weight is a skewed variable and is, thus, difficult to deal with statistically. Waist circumference, which is nearly normally distributed and highly correlated with weight, was used as a substitute. Pairing waist circumference with height, sizing cells were defined again from the 1964 HES male data. The average height in each cell was statistically

equal to the average height in the corresponding cells defined by pairing weight with height. Therefore, it appears that the skewness of weight does not effect the sizing procedure.

Preliminary work has indicated a degree of independence between mass distribution, as represented by body weight and circumferences, and linkage, as represented by stature, heights and bone lengths. Therefore, in selecting cadavers for our linkage study, a skeletal dimension/height bivariate should be used in determining the body size categories. Two measurements with low correlation should be chosen so that each measurement can represent orthogonal dimensions in the geometry of the body. These two measurements have not been chosen at this time.

4.4. Three-Dimensional Geometry of the Adult Pelvis

H. M. Reynolds

The Hamann-Todd skeletal collection at the Cleveland Museum of Natural History has been sampled according to a stratification designed to match the U. S. general population as closely as possible. The sample contains 144 females and 141 males divided into six sizing cells (Figure 18).

The sizing cells are defined by the relationship between height and weight in the 1960-62 Health Examination Survey data reported by Stoudt, Damon, McFarland, and Roberts (1965). We have the original data in the computer from which we constructed the sampling cells. In order to make the Hamann-Todd cadaver/skeleton collection comparable with the HES sample, 46.61 lbs. and 31.52 lbs. were added to the H-T male and female weights respectively. These constants are the difference between the average weights in the two samples. The results are compared in Table 2 where it can be observed by the percentage difference ($\Delta\%$) that the match is reasonable.

The first shipment of 30 male and 30 female pelvises has been delayed until the week of 1 February 1977. This delay will not affect our progress in studying joint kinematics but could delay anticipated results on landmark definitions and identification of "stable" skeletal landmarks relative to population differences.

The three-dimensional measurements will be made at the Civil Aeromedical Institute in Oklahoma City under the direction of Dr. Clyde C. Snow. The techniques were developed at CAMI and the landmarks were

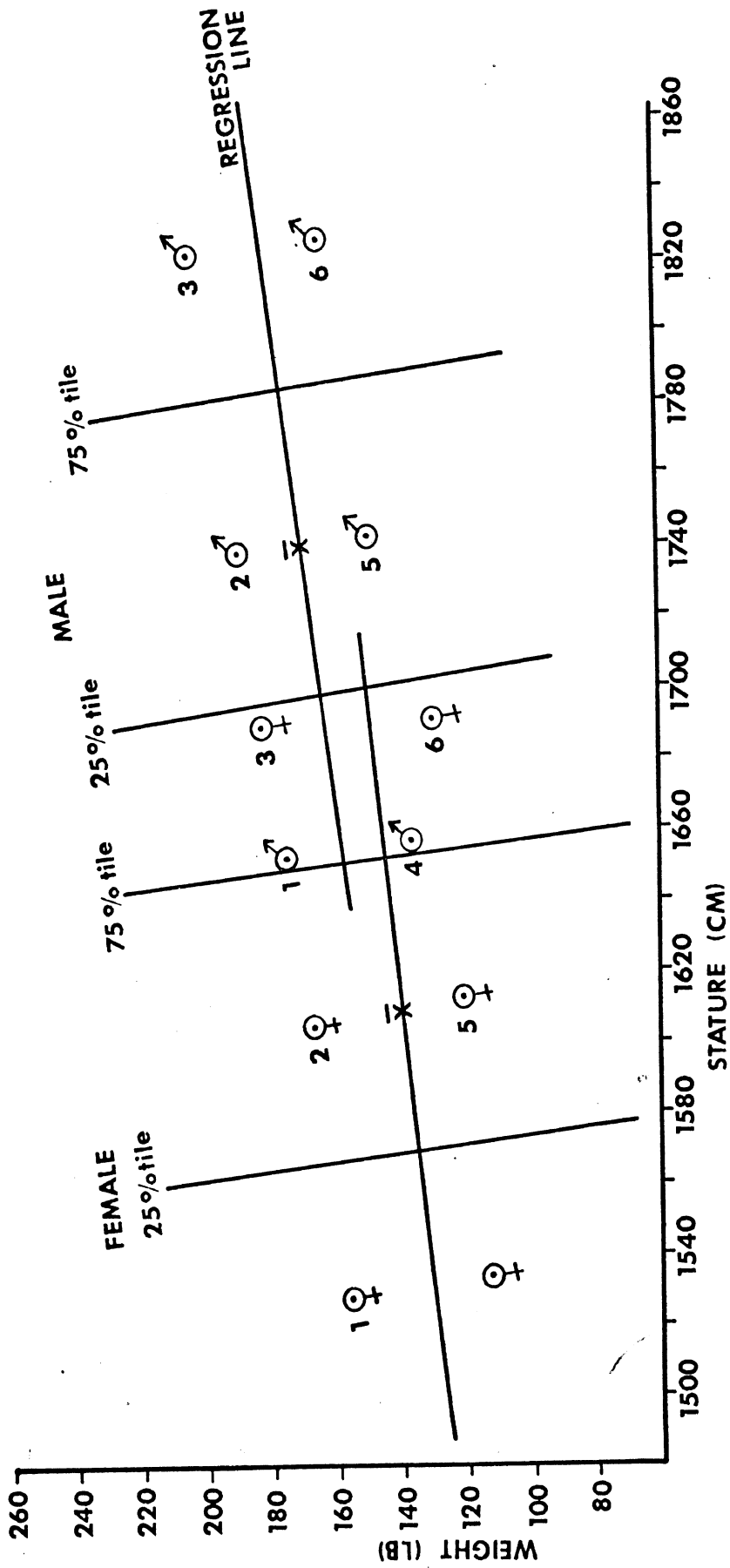


Figure 18. Sizing Cells for Male and Female Specimens from the Hamann-Todd Skeletal Collection.

Average HEIGHT (cm)

Sample Cell Number	MALE			FEMALE		
	HES	H-T	%	HES	H-T	%
1 \bar{x}	165.8	165.1	+0.4	153.4	153.8	-0.3
SD	36.45	35.80		31.99	26.38	
2 \bar{x}	165.3	163.8	+0.9	152.9	152.3	+0.4
SD	31.35	48.41		28.98	37.14	
3 \bar{x}	174.2	174.6	-0.2	161.3	161.3	0.0
SD	23.28	25.65		22.86	24.83	
4 \bar{x}	173.9	173.3	+0.3	160.6	160.7	-0.1
SD	24.28	24.41		22.47	23.23	
5 \bar{x}	182.7	182.7	0.0	169.0	170.0	-0.6
SD	33.86	37.50		29.44	38.13	
6 \bar{x}	182.2	181.9	+0.2	169.0	168.4	+0.4
SD	36.17	30.87		39.17	31.09	
\bar{x} %			0.33%			0.3%

Average WEIGHT (lb.)

Sample Cell Number	MALE			FEMALE		
	HES	H-T	%	HES	H-T	%
1 \bar{x}	137.5	139.3	-1.3	114.4	107.5	+6.0
SD	12.72	12.25		10.93	15.35	
2 \bar{x}	175.1	172.4	+1.5	156.9	157.1	-0.1
SD	18.97	15.06		23.24	22.91	
3 \bar{x}	149.6	149.9	-0.2	122.2	118.3	+3.2
SD	12.53	13.98		11.43	14.16	
4 \bar{x}	189.2	183.6	+3.0	166.9	160.7	+3.7
SD	18.59	16.56		26.54	13.84	
5 \bar{x}	164.6	164.2	+0.2	130.3	129.2	+0.8
SD	12.48	16.49		11.75	19.27	
6 \bar{x}	204.7	204.1	+0.3	181.8	171.5	+5.7
SD	19.66	18.94		31.70	25.08	
			1.08%			3.25%

Table 2. Comparison by Sampling Cells between Health Examination Survey and Hamann-Todd collection for males and females.

established through discussions between Dr. Snow and myself. In general, there will be 120 points measured on the pelvis which will define the shape of various parts of the pelvis as well as anatomical landmark locations. Detailed descriptions of all landmarks will be included in the final report for Phase II, but the following twelve landmarks will be located on the complete articulated pelvis.

- 1) Right Anterior Superior Iliac Spine
- 2) Left Anterior Superior Iliac Spine
- 3) Right Iliocristale
- 4) Left Iliocristale
- 5) Right Posterior Superior Iliac Spine
- 6) Left Posterior Superior Iliac Spine
- 7) Right Hip Point (Acetabular Centroid)
- 8) Left Hip Point (Acetabular Centroid)
- 9) Right Ischial Tuberosity
- 10) Left Ischial Tuberosity
- 11) Symphision
- 12) Promontory of Sacrum

Thus, the basic geometry of the pelvis can be described. The additional landmarks will only be measured on the articulated left innominate and sacrum. The total collection of data should provide the three-dimensional shape geometry relative to an anatomical axis system defined by landmarks on the totally articulated pelvis.

The analysis of these data will utilize many of the techniques described in Subsection 4.1 and 4.5. For example, these data will

provide base line information on the accuracy with which anatomical axes systems can be defined. All succeeding work on cadaveric and living subjects should be less accurate since the landmarks are obscured by tissue. In addition, variation in the location of principal landmarks will be summarized and described by the use of principal components analysis (See Subsection 4.5). Additional analytical techniques will be used, but these represent a cross-section of the application of our present efforts to future data collection and analysis in systems anthropometry.

The Hamann-Todd collection is unique in one major aspect of importance to the present investigation. Prior to the skeletalization of each cadaver, Dr. Todd and his associates took a series of anthropometric dimensions according to Martin (1928). A copy of the original data collection sheet with translation is presented in Figure 19. These data on each specimen in our sample have now been entered into the computer and the editing process has begun. These data for our sample will permit the examination of anthropometric data relative to skeletal geometry for the first time. Todd and his associates published a series of papers between 1923 and 1928 discussing the changes that occur in cadavers relative to anthropometric dimensions. These papers will need to be reviewed carefully in order to use these data. Correlations between skeletal geometry and anthropometry as well as a closer examination of the anthropometric characteristics of the individuals in our sample will result.

No. 3272		No. d. Phot.	Ort und Tag der Aufnahme: 2. 1. 38	Beobachter: H. T. C.
Eigennamen:			Väterliche Ascendenz:	
Stammesname:				
Geschlecht: M.		Wohnort:		
Alter: 58		Geburtsort:		
Soziale Stellung:		Religion:		
Ernährungszustand: sehr mager, mager, mittel, fett, sehr fett.			Kopf:	
Gesundheitszustand:			Stirn: niedrig, hoch; schmal, breit; gerade, mäßig fliehend, stark fliehend; flach, gewölbt; voll, keilförmig.	
Krankheiten (hereditäre?):			Schädel: ganz flach, leicht-, mittel-, stark gewölbt.	
Defekte: P. 4			Mitherrhaupt: steil, flach, gewölbt, stark ausladend.	
Hautfarbe:			Gesicht:	
No. der Hautfarbenstufen oder:			Gesicht: hoch, mäßig hoch, niedrig; elliptisch, oval, rund, eckig; (mit Stirn) schmal, mäßig breit, breit, sehr breit; nach unten-, nach oben zugespitzt; ganz flach, mäßig flach, vorgewölbt, vorspringend, Vogelgesicht.	
Stirne:			Wangenbeleggegend: stark-, mäßig vortretend; mäßig-, stark zurückliegend.	
Wange:			Augenspalte: gerade, schräg; eng-, mäßig-, weit geöffnet; spindelförmig, mandelförmig; Mongolenfalte, Epicanthus.	
Brustbeinregion:			Nase: Wurzel: schmal, mittel, breit; ganz flach, flach, mäßig hoch, hoch, sehr hoch.	
Bauch (über dem Nabel):			Rücken: schmal, mittel, breit; stark-, leicht konkav, gerade, leicht-, stark konvex, wellig, winklig gebogen.	
Schulterblattgegend:			Spitze: aufwärts-, vorwärts-, abwärts gerichtet.	
Oberarm Beugeseite:			Flügel: dick, dünn; hoch, niedrig; anliegend, mäßig gewölbt, gebüht; durchbohrt wie oft? rechts: links:	
Oberarm Streckseite:			Septum: lang, kurz; schmal, breit; nach hinten-, nach vorne keilförmig verjüngt, sanduhrförmig; nach unten vortretend, hochliegend; durchbohrt.	
Handteller:			Löcher: sehr schmal, schmal, längsoval, schrägoval, rundlich, queroval, breit, sehr breit; klein, groß.	
Innenfläche d. Oberschenkels:			Lochfläche: horizontal, nach vorn oben, nach hinten oben geneigt.	
Schleimhaut-Oberlippe:			Integumentallippen: Procheilie: sehr stark, stark, mäßig, leicht. Orthocheilie, Opisthocheilie.	
Schleimhaut-Unterlippe:			Sohleimhautlippen: dünn, mittel dick, wulstig; Lippenleiste; Oberrand: einfacher, zusammengesetzter Bogen.	
Hautcharakter: sammetartig, weich, rau; feucht, trocken, fettig.			Mundspalte: klein, mittel, groß.	
Irisfarbe:			Zähne: gerade, schräg; sehr groß, groß, mittel, klein, sehr klein.	
No. der Augenfarbenstufen oder: a. schwarzbraun. b. dunkelbraun. c. braun. d. hellbraun. e. grünlich. f. dunkelgrau. g. hellgrau. h. dunkelblau. i. blau. k. hellblau. l. albinotisch.			R. $\frac{m. m. m. p. p. e. i. i. i. e. p. p. m. m. m. l.}{m. m. m. p. p. e. i. i. i. e. p. p. m. m. m.}$ (Distansum und Tremas abzeichnen, fehlende Zähne durchstrich, bei Kranke ablesen, abweichend euternis untrische, abweichend veränderte euklammer.)	
Sklera: weiß, bläulich, gelblich. Konjunktiva: farblos, fleckig, im Bereich der geöffneten Lidspalte verfarbt.			Art der Verstümmelung: Orthodontie, Prodentie: mäßig, stark, Labiodontie, Psalidodontie, Stegodontie, Opisthodontie, Hiatodontie.	
Haarfarbe:			Farbe: bläulich, weiß, gelblich. Färbung:	
No. der Haarfarbenstufen oder:			Oberrand: anliegend, absteilend, zienkelobren. Halixrand: oben, hinten gestutzt, ungestutzt.	
Kopfhaar:			Darwin'sches Höckerchen rechts: No. 1, 2, 3, 4, 5, 6 links: No. 1, 2, 3, 4, 5, 6	
Barthaar:			Ohrläppchen: groß, klein; frei, angewachsen, fehlend.	
Körperhaar:			Durchbohrung im Läppchen r. 1 ; im Helixrand r. 1.	
Schamhaar:				
Haarform:				
Kopfhaar:				
Barthaar:				
Körperhaar:				
Schamhaar:				
Körperbehaarung: stark, mittel, schwach, sehr schwach, fehlend.				

Figure 19. Sample Hamann-Todd Data Collection Sheet and Translation from the German.

Figure 19 (cont.)

No.	1.	4.	5.	6.	7.	8.	9.	10.	11.	13.
Somatologisches Beobachtungsblatt nach R. MARTIN. Ausgabe 1913. Bezeichnung der zu verwendenden Instrumente: A = Anthropometer St = Stangenzirkel G = Gleitzirkel T = Tasterzirkel B = Bandmaß O = Ohrhöhenmaß W = Waage	Körpergröße	Höhe des oberen Brustbeinrandes über dem Boden	Höhe des Nabels u. d. B.	Höhe des oberen Symphysenrandes u. d. B.	Höhe der rechten Brustwarze u. d. B.	Höhe des rechten Akromion u. d. B. <i>R. 1751</i>	Höhe der rechten Ellenbogen-gelenk-fuge u. d. B.	Höhe des Griffelfortsatzes des rechten Radius u. d. B.	Höhe der rechten Mittelfinger-spitze u. d. B.	Höhe des rechten vorderen Darmbeinstachels u. d. B.
	1747 A	1739 A	1856 A	750 A	1307 A	1.1464 A	1115 A	803 A	675 A	700 A
	St	St	St o. G	X	X	X	X	St	St	B
	Länge des rechten Unterarmes	Länge der rechten Hand	Breite der rechten Hand	Ganze Beinlänge rechts	Beinlänge rechts ohne Fuß	Länge des rechten Oberschenkels	Länge des rechten Unterschenkels	Länge des rechten Fußes	Breite des rechten Fußes	Umfang der Brust bei ruhigem Atmen
	250 48.	176 49.	76 52.	880 912 53.	895 829 54.	510 777 55.	373 56.	229 58.	77 59.	770 61.
No.										
No.										
Die wichtigsten abnehmenden Maße sind durch ausgezogene, die wichtigsten zu berechnenden Dimensionen durch gebrochene Striche bezeichnet. Die Nummern beziehen sich auf die Somatometrische Technik in R. MARTINS Lehrbuch der Anthropologie. Ein X bedeutet: durch Berechnung festzustellen. Alle Zahlen sind in Millimeter in die leeren horizontalen Felder einzutragen.	1. Größe Länge des Kopfes	3. Größe Breite des Kopfes	4. Kleinste Stirnbreite	6. Jochbogenbreite	8. Unterkieferwinkelbreite	9. Breite zwischen den inneren Augenwinkeln	11. Breite der Augenlidspalte	12. Pupillendistanz	13. Breite der Nase	14. Breite der Mundspalte
	100 T	103 T	102 T	136 T	117 T	34 G	29 G	65 G	33 G	50 G
	B	B	B	X	X	X	X	X	X	X
	Horizontal-Umfang des Kopfes	Sagittaler Kopfbogen	Transversaler Kopfbogen	Längenbreiten-Index des Kopfes	Längenhöhen-Index des Kopfes	Breitenhöhen-Index des Kopfes	Transversaler Frontoparietal-Index	Physiognomischer Gesichtes-Index	Morphologischer Gesichtes-Index	Physiognomischer Obergesichts-Index
	100 45.	317 48.	347 49.	$\frac{3 \times 100}{1}$	$\frac{15 \times 100}{1}$	$\frac{15 \times 100}{3}$	$\frac{4 \times 100}{3}$	$\frac{17 \times 100}{6}$	$\frac{18 \times 100}{6}$	$\frac{19 \times 100}{6}$
No.										

Figure 19 (cont.)

14.	15.	16.	17.	23.	27.	35.	38.	40.	41.	45.	46.	47.
Höhe des rechten oberen Schultergelenks u. d. B.	Höhe der rechten Kniegelenkfuge u. d. B.	Höhe der rechten inneren Knöchelspitze u. d. B.	Spannweite der Arme	Stammhöhe (Körperhöhe im Sitzen)	Länge der vorderen Rumpfwand	Breite zwischen den Akromien	Breite zwischen den Brustwarzen	Größe Breite zwischen den Darmbeinkämmen (Beckenbreite)	Breite zwischen den vorderen oberen Darmbeinstacheln	Ganze Armlänge rechts	Armlänge rechts ohne Hand	Länge des rechten Oberarmes
187	403	77	1770	1791	513	332	157	512	228	787	573	350
A	A	A	A	A	X	St	St	St	St	X	X	St
B	B	B	B	B	B	B	B	B	W	X		
Umfang der Brust bei Inspiration	Umfang der Brust bei Expiration	Größter Umfang des rechten Oberarmes bei Streckung	Größter Umfang des rechten Oberarmes bei Beugung	Größter Umfang des rechten Unterarmes	Kleinster Umfang des rechten Unterarmes	Größter Umfang des rechten Oberschenkels	Größter Umfang des rechten Unterschenkels	Kleinster Umfang des rechten Unterschenkels	Körpergewicht	Index der Körperfälle		
61a.	61b.	65. 127	65(1)	66.	67.	68.	69.	70.	71.			
15.	16a.	17.	18.	19.	20.	21.	22.	25.	29.	30.	31.	32.
Ohrenhöhe des Kopfes	Ganze Kopfhöhe	Physiognomische Gesichtshöhe	Morphologische Gesichtshöhe	Physiognomische Obergesichtshöhe	Morphologische Obergesichtshöhe	Höhe der Nase	Länge des Nasenbodens	Höhe der Schleimhautlippen	Physiognomische Länge des Ohres	Physiognomische Breite des Ohres	Morphologische Länge des Ohres	Morphologische Breite des Ohres
150	220	183	122	74	70	52	23	12	67	37	38	43
u. O	St	St	G o. St	G o. St	G o. St	G o. St	G o. St	G	G	G	G	G
X	X	X	X	nach 9 rech	crystal -keiged trans	ant. prot.	ant. prot.	St. Conj.	ant.			
Höhenindex der Nase	Breitenindex der Nase	Physiognomischer Ohrindex	Morphologischer Ohrindex									
$\frac{3 \times 100}{21}$	$\frac{22 \times 100}{13}$	$\frac{30 \times 100}{29}$	$\frac{32 \times 100}{31}$	317	1066	264	217	207	138			

Figure 19 (cont.)

r.	L.	r.	L.		
Schärfre:		Farbensinn:		Hörschärfe:	
Pulsation:		Respiration:		Körpertemperatur:	
Druckkraft: r.	L.	r.	L.	Mittel: r.	L.

Körper:

Weibliche Brust: Pubertäre Form, Halbkugelform des Warzenhofes, primäre, sekundäre Mamma; Brustentwicklung No. schalenförmig, halbkugelig, konisch, zingeneuterförmig; üppig, voll, mäßig, klein; stehend, sich senkend, hängend.
 Warzenhof: Durchmesser transv.: vert.: Farbe No. Rand: scharf, verschwommen; Papille: groß, mittel, klein, vertieft.

Gestalt:

Beschneidung und andere Deformationen:

Hände:

Altenfalte:

Finger: dick, dünn; lang, kurz; verjüngt; hyperextendiert.

Verstümmelung:

Nägel: groß, klein; lang, kurz; schmal, breit; gewölbt, flach; sagittal gekrümmt, oval, rundlich, fächerförmig.

Waden: dick, dünn; lang, kurz; stramm, schlaff.

Füße: groß, klein; lang, kurz; schmal, breit; Fußgewölbe: hoch, mittel, niedrig, Plattfuß.

Längste Zehe: r. 1. 2. l. 1. 2. Große Zehe abstehend, anliegend, eingebogen.

Besondere Beobachtungen: (Tatauierung, Ziernarben, Hornhautnarben, geistige Fähigkeiten usw.)

Endeavour laster about: 50

Type: more eutomorph

... ..

... ..

... ..

... ..

... ..

... ..

(Verlag von Gustav Fischer in Jena.)

Figure 19 (cont.)

Photo No.	Place and date of acceptance	Observer
Given name	Place of residence	Paternal parentage
Surname		
Sex		
Age	Place of birth	Maternal parentage
Social class	religion	
Condition of nourishment: very thin, thin, average, obese, very obese		
Condition of health: forehead: low, high; narrow, broad; moderately, strongly;		
sicknesses (hereditary?) retreating; flat, domed; full, keel-shaped		
defects		
skincolor	# skincolor table or:	top of skull: quite flat; lightly-, moderately-, strongly domed.
forehead	a gray-black	back of skull: inclined, straight, domed, strongly projecting
cheeks	b black-brown	
sternal	c pure dk. brn	
abdomen	d reddish dk. bn.	Face:
scapular	. reddish bn.	entire face: high, moderately high, low; elliptical;
upper arm prox.	. pure bn.	(w/ fore- ovoid, round, angular; narrow, moderately broad.
dist.	lite brnish	head) broad, very broad; tapered toward bottom, -top;
palm	olive yellow	completely straight, moderately straight; forward-domed; jutting out, shaped like a bird.
mucosal upperlip	yellowish	cheek area: strongly-, moderately protruding, strongly mod-regressed.
lower lip	yellowish-wh.	orbits: straight, slanted; narrow, moderate, wide; spindle-shaped; inner-, outer-epicanthic fold.
med. prox.	reddish-wh	Nose: root: narrow, average, broad; very flat, flat, mod. high, high, very high
thigh	pale white	back: narrow, med., broad; markedly-, slightly concave, straight; markedly-, lightly convex, undulating, bent
skin appearance: velvety, smooth, rough; moist, dry, greasy		Zip: upward, forward, downward bent.
Iris color: # of eye color table or:		Alae: thick, thin; high, low; close, mod. swollen; inflated; perforated how many times? R L
a black-brown; dark brown, brn, light brn, greenish, dark-gray, light-gray, dark blu, blue, light blu, albinotic		Sentum: long, short; narrow, broad; constricted forward in keel shape; hour-glass shaped; projecting beneath;
Sclera: white, bluish, yellowish		foramina: very narrow; narrow, long-oval, trans oval, round, long oval, broad, very broad, small
Conjunctiva: colorless, mottled, colored in the area of the eyelid(?)		foraminal position: horizontal, sloped forward, sloped backward.
Haircolor: # haircolor table or:	a pure black f dk blnd	Integumental lip: protruded(?): very marked, marked, medium, slight; straight; in-turned(?)
head hair	b brown-black, bite blnd	Mucosal lip: thin, med., thick, swollen; edged(?); upper border: simple, bowed together.
facial hair	c dark brn	Mouth: small, medium, large.
body hair	d reddish br	Teeth: straight, sloping; very big, big, med., small, very small.
pubic hair	e. narrow waves	
	f. curly	
Body hair: heavy, medium, light, very light, absent		R; $\frac{m}{m} \frac{m}{m} \frac{m}{m}$ etc...
Ears: close-lying, standing-out, jug-shaped.		(Note diastema and tremata; cross out, lack in teeth; circle purposely removed teeth; check diseased t, bracket purposely mutilated t.)
Helix border: above, below, absent		Type of rutilation:
Darwin's point: right No 1...6		orthodontia, prodontia: medium, strong
left No 1...6		Labiodontia, Psalidontia, Stegodontia,
Earlobes: big, small, unattached, attached, absent		Opisthodontia, Hiatodontia.
Perforation in earlobes: r, l; in edge of ear: r, l.		Color: bluish, white, yellowish. Coloring material(?)

Figure 19 (cont.)

page 4

This is a translation of the instructions appearing at the top long edge of page 2:

The most important measurements are underlined; the most important calculated dimensions are indicated by a broken line. Numbers refer to the somatological techniques in Martin's Lehrbuch der Anthropologie. An 'X' means derive by calculation. All numbers are in mm. and are to be placed in the open spaces on the chart.

Somatological observation form according to R. Martin, 1913 edition.

Key to instruments to be used: A = anthropometer, G = spreading calipers; St = sliding calipers; T = calipers (refers to a small sliding calipers); B = tape; O = ear-height measuring instrument (we would use a sliding calipers); W = scales

Measurements in upper 2 columns of page 2:

1. Total body height
4. upper sternal ht. from floor
5. naval ht. above floor
6. upper pubic symphysis edge from floor
7. Rt. nipple ht. above floor
8. Rt. acromion ht above floor
9. Rt. elbow joint above floor
10. Rt. distal radius end above floor
11. Rt. middle fingertip above floor
13. Rt. iliac crest above floor
48. length of right lower arm
49. length right hand
52. breadth of right hand
53. total rt. leg length
54. rt. leg length minus foot
55. rt. thigh (upper leg) length
56. rt. lower leg length
58. lt. foot length
59. rt. foot breadth
60. chest circum., relaxed (i.e., ^{normal} not while taking a breath)

Measurements in lower 2 columns of p. 2.

1. head length
3. head breadth
4. min. forehead breadth
6. bizygomatic diam.
8. max. mandibular breadth
9. Min. interorbital breadth
11. orbit (or eyelid) breadth
12. interpupillary distance
13. nasal breadth
14. mouth breadth
45. cephalic circum.
48. sagittal arc
- X cephalic index
- X cephalic length-ht index (~~to be shown on the chart~~)
- X breadth-height index " " "
- X transversa frontoparietal index
- X physiognomic facial index (~~to be shown on the chart~~) (these are
- X morphological facial index " " " } facial ht. indic
- X upper face index

Upper 2 columns:

- 14. Ht. rt. greater trochanter(?) from floor
- 15. Ht. right knee joint from floor
- 16. Ht. rt. medial malleolus point (ankle) from floor
- 17. arm span
- 23. sitting ht.
- 27. Length of forward side of trunk (?)
- 35. bi-acromial breadth
- 38. breadth between nipples
- 40. bi-iliac crest breadth
- 41. breadth between superior lower iliac points (standard measurements-I forgot the terminology of the ilium)
- 45. Total rt. arm length
- 46. rt. arm length minus hand
- 47. rt upper arm length
- 61a. chest circumference, expanded (inhaling)
- 61b. chest circum, breath expired (exhaling)
- 65. largest circum right upper arm, extended
- 65(1) " " " " " contracted
- 66. " " " lower "
- 67. smallest " " " "
- 68. greatest " " upper leg
- 69. smallest " " lower "
- 70. smallest " " " "
- 71. body weight
- X2. index of body fullness

Lower 2 columns:

- 15. ht. of head to ear (apparently a standard measurement despite apparent vagueness)
- 16a. total head height
- 17. physiognomic facial ht.
- 18. morphological facial ht.
- 19. physiognomic upper face ht.
- 20. morphological upper face ht.
- 21. nasal ht.
- 22. nasal length (i.e., of floor of interior nose)
- 25. ht. of mucosal lip
- 29. physiognomic ear length
- 30. " " breadth
- 31. morphological " length
- 32. " " breadth
- X nasal index
- X breadth-depth index of nose
- X physiognomic ear index
- X morphological ear index

r	l		r	l		
visual acuity	color sense	hearing	pulse	respiration	temp.	
Pressing strength; r, l. etc.				Means (Instrument)	r l	

Body observations:

Female breast: infantile form; hemispherical ^{corona} corona; primary, secondary mammae; breastdevelopment No.:

bowl-shaped, hemispherical, conical, ??; very full, full, medium, small;

standing up, ^{sitting} sitting, hanging ^{pseudoluces} pseudoluces

Coronas: transverse diameter; vertical diameter; Color No. border: sharp, indistinct. ^{retracted} nipples: large, medium, small, ^{retracted} retracted.

Genitalia:
circumcision and other deformations

Hands:

^{Simon crease:}
~~"Apo-fold"??~~

Fingers: thick, thin, long, short, tapered; hyperextended.

Nails: big, small, long, short; narrow, broad; domed, flat; sagittally bent; oval, round, fan-shaped

Calfs: thick, thin, long, short; tense, flabby.

Feet: big, small; long, short, narrow, broad; arch: high, medium, low, flat feet
Longest toe: r l, 2; lt:l, 2. Great toe separate, close-lying, bowed.

Special Observations: (tattooing, ornamental scars; epidermal scars; mental abilities, etc.)

** "Ziegeneckerförmig" literally means "shape like a goat's udder"
(if you really are interested).

4.5. Statistical and Probabilistic Properties of Three-Dimensional Anthropometric Data.

D. H. Golomb

In this section, a discussion is presented of the general population-related causes of variation of 3-dimensional coordinates of landmarks on the human body. These variations are due to the size and shape of individuals, but they are also related to the position and posture of the individual. The variations in posture are perhaps the most difficult to model because two individuals of the same size and shape could have significantly different locations of many landmarks on the body measured in 3-dimensional space.

4.5.1. Discussion of a Linkage Model.

An investigation into the three-dimensional location of skeletal landmarks on the torso was conducted at the University of Michigan (Snyder, et al., 1972). Two models--sitting and standing positions--were constructed to predict the spatial relationship between the landmarks. Each model is fairly general in scope, in that landmarks may be predicted for a wide range of seated and standing positions. Positions, in the model, are defined by the three-dimensional coordinates of the right elbow with the spine of L5, as the origin. In addition to the elbow coordinates, the other independent variables are the following standard anthropometric measurements: stature, sitting height, weight, chest circumference, biacromial breadth and humeral length.

An unexpected trend has been observed in the sitting position model of surface landmarks. It would be expected that the equations predicting

x-coordinates (values along the anterior/posterior axis) have high loadings from chest circumference or weight; likewise, the equations predicting y-coordinates (values along the lateral axis) have high loadings from biacromial breadth, and humeral length; and, the equations predicting z-coordinates (values along the vertical axis) have high loadings from stature and sitting height. These hypothesized relationships do hold for all the equations predicting z-coordinates and for the x and z coordinates in the lower back. In the equations along the upper spine and for acromion and suprasternale, the elbow coordinates play a dominate role. Specifically, the x-coordinate of the elbow has the highest loading for x predictions; the y-coordinate for y predictions; and, the z-coordinate for z predictions.

Further analysis is necessary to understand the significance of this trend. First, the equations predicting x, y, and z of the upper regions do not imply that standard anthropometry is unrelated to the location of these points since the elbow coordinates are a function of standard anthropometry. The implication is that a simple polynomial relationship (in this model, cubic regressions were derived) may not be sufficient to explain the locations of points on the upper torso. In fact, the weakness of this relationship is further emphasized when it is noted that the elbow, whose position can be relatively independent of torso configuration, is the sole predictor of these points.

The above discussion raises several questions. First, what is the relationship between standard anthropometry and landmarks on the body in three-dimensional space? Second, are the positions of landmarks along the same axis highly correlated? Thus, even though there is substantial variation in the posture of individuals for a given position (e.g., seated with arms at the side), can three-dimensional locations

of the body be statistically predicted with reasonable accuracy?
Furthermore, can the paths of landmark positions be predicted on a moving body?

4.5.2. Analysis of Stewardess Data.

In order to investigate the relationships observed in the Snyder, et al. investigation, three-dimensional positions of 13 landmarks collected on 280 airline stewardess trainees were examined. These data were collected by Herbert Reynolds as part of an anthropometric project for the Federal Aviation Administration but they have not been previously published. All the three-dimensional data were taken for one position - namely, a normal seated position with the subject's hands at her sides (see Figure 20). The analysis below is, thus, limited to describing variation in one particular, fixed position. It should also be mentioned that these data represent a highly selected sample of the general female population. The subjects were hired by the airline only if they met a stringent height-weight table. Thus, in general, the sample does not contain overweight and/or excessively short or tall individuals.

The first step in the analysis identified the standard measurements that have a linear relationship with three-dimensional coordinate data (Tables 3-5). As in the Snyder et al. (1972) link study model, stature and sitting height are highly correlated with z-coordinate data, especially those landmarks on the upper part of the body--vertex, right and left acromions, etc. Likewise, almost none of the standard measurements correlate well with the upper body landmarks in the x- and



Figure 20

Photograph of Measurement Device used in 3-D Stewardess Study

CORRELATION MATRIX	CASES READ= 268				
	VERTEX Z	SITTING EYE Z	NECK-SHOULDER Z	RT. ACROMION Z	SUPRABERNAL E Z
BODY WEIGHT	0.639	0.503	0.634	0.623	0.597
STATURE	0.741	0.660	0.711	0.650	0.625
SUPRATERNALE HEIGHT	0.692	0.637	0.679	0.637	0.647
SITTING HEIGHT	0.607	0.642	0.644	0.755	0.781
EYE HEIGHT SITTING	0.810	0.700	0.823	0.811	0.736
ACROMIALE HEIGHT	0.506	0.510	0.613	0.597	0.572
THIGH CIRCUMFERENCE	0.331	0.307	0.316	0.360	0.330
HIP CIRCUMFERENCE	0.579	0.536	0.590	0.542	0.546
WAIST CIRCUMFERENCE	0.319	0.296	0.340	0.301	0.294
INSP CHEST CIRCUMFERENCE	0.350	0.314	0.364	0.400	0.340
SHOULDER CIRCUMFERENCE	0.355	0.350	0.370	0.339	0.330
NECK CIRCUMFERENCE	0.347	0.283	0.341	0.351	0.256
BUTTOCKS DEPTH	0.345	0.332	0.377	0.350	0.353
WAIST DEPTH	0.223	0.221	0.260	0.242	0.204
CHEST DEPTH	0.171	0.154	0.170	0.185	0.180
BIACROMIAL BREADTH	0.294	0.294	0.310	0.171	0.193
CHEST BREADTH	0.190	0.151	0.193	0.246	0.166
WAIST BREADTH	0.185	0.180	0.227	0.235	0.184
ILIOCRISTALE BREADTH	0.406	0.442	0.405	0.454	0.411
IliosPINALE BREADTH	0.270	0.266	0.316	0.251	0.216
BITROCHANTERIC BREADTH	0.547	0.516	0.530	0.486	0.484
HIP BREADTH STANDING	0.541	0.529	0.542	0.467	0.409
SHOULDER BREADTH	0.180	0.170	0.201	0.210	0.144
HEAD LENGTH	0.179	0.185	0.160	0.166	0.162
HEAD BREADTH	0.143	0.157	0.147	0.154	0.151

Table 3. Correlations of Z-Coordinate of Landmarks with Standard Anthropometry.

Table 3. (Cont.)

CORRELATION MATRIX

CASES READ = 200

	LT. ACROMION Z	ILIOCRISTALE Z	ASIS Z	TROCHANTERIO N Z	THIGH CL. Z
BODY WEIGHT	0.594	0.599	0.674	0.275	0.576
STATURE	0.656	0.574	0.593	0.264	0.300
SUPRASTERNALE HEIGHT	0.637	0.589	0.612	0.222	0.409
SITTING HEIGHT	0.757	0.430	0.555	0.277	0.339
EYE HEIGHT SITTING	0.667	0.460	0.510	0.252	0.345
ACROMIALE HEIGHT	0.630	0.216	0.234	0.284	0.281
THIGH CIRCUMFERENCE	0.300	0.347	0.464	0.277	0.563
HIP CIRCUMFERENCE	0.530	0.525	0.610	0.290	0.501
WAIST CIRCUMFERENCE	0.357	0.433	0.460	0.106	0.323
INSP CHEST CIRCUMFERENCE	0.369	0.320	0.399	0.087	0.281
SHOULDER CIRCUMFERENCE	0.364	0.439	0.436	0.107	0.319
NECK CIRCUMFERENCE	0.323	0.271	0.290	0.005	0.243
BUTTOCKS DEPTH	0.359	0.404	0.407	0.206	0.437
WAIST DEPTH	0.204	0.205	0.287	0.047	0.234
CHEST DEPTH	0.169	0.296	0.309	-0.027	0.243
BIACROMIAL BREADTH	0.156	0.243	0.299	0.100	0.143
CHEST BREADTH	0.256	0.191	0.234	0.059	0.189
WAIST BREADTH	0.236	0.311	0.319	0.131	0.264
ILIOCRISTALE BREADTH	0.451	0.214	0.211	0.136	0.231
ILIOSPINALE BREADTH	0.246	0.113	0.033	0.000	0.120
THIGH CL. Z	0.256	0.269	0.407	0.306	1.000
BITROCHANTERIC BREADTH	0.479	0.397	0.440	0.265	0.326
HIP BREADTH STANDING	0.450	0.431	0.512	0.105	0.389
SHOULDER BREADTH	0.161	0.167	0.205	0.073	0.260
HEAD LENGTH	0.209	0.133	0.082	0.021	0.109
HEAD BREADTH	0.173	0.172	0.065	-0.000	0.134

	CORRELATION MATRIX				CASES READ = 260			
	VERTEX X	SITTING EYE X	NECK-SHOULDER R X	RT. ACROMION X	SUPRASTERNAL E X			
BODY WEIGHT	0.136	0.159	0.140	0.152	0.220			
STATURE	0.133	0.100	0.163	0.146	0.190			
SUPRASTERNALE HEIGHT	0.088	0.137	0.119	0.136	0.159			
SITTING HEIGHT	0.100	0.132	0.091	0.111	0.115			
EYE HEIGHT SITTING	0.103	0.211	0.118	0.020	0.148			
ACROMIALE HEIGHT	0.160	0.147	0.078	0.017	0.107			
THIGH CIRCUMFERENCE	0.071	0.069	0.037	0.087	0.117			
HIP CIRCUMFERENCE	0.071	0.107	0.081	0.095	0.144			
WAIST CIRCUMFERENCE	0.057	0.102	0.089	0.081	0.123			
INSP CHEST CIRCUMFERENCE	0.112	0.103	0.080	0.041	0.140			
SHOULDER CIRCUMFERENCE	0.070	0.079	0.096	0.201	0.103			
NECK CIRCUMFERENCE	0.166	0.166	0.160	0.123	0.176			
BUTTOCKS DEPTH	0.076	0.116	0.103	0.093	0.157			
WAIST DEPTH	0.049	0.051	0.062	0.071	0.070			
CHEST DEPTH	0.096	0.110	0.133	0.140	0.316			
BIACROMIAL BREADTH	0.050	0.035	0.030	0.135	0.013			
CHEST BREADTH	0.013	0.066	-0.015	-0.025	0.002			
WAIST BREADTH	0.032	0.074	0.047	0.110	0.020			
ILIOCRISTALE BREADTH	0.064	0.095	0.047	0.054	0.045			
ILIOSPINALE BREADTH	0.070	0.059	0.073	0.059	0.046			
BITROCHANTERIC BREADTH	0.089	0.099	0.076	0.064	0.113			
HIP BREADTH STANDING	0.066	0.066	0.058	0.084	0.129			
SHOULDER BREADTH	0.020	0.048	0.044	0.065	0.071			
HEAD LENGTH	-0.043	-0.053	-0.047	-0.046	-0.094			
HEAD BREADTH	-0.019	-0.006	-0.024	0.029	-0.035			

Table 4. Correlations of X-Coordinate of Landmarks with Standard Anthropometry.

Table 4. (Cont.)

CORRELATION MATRIX

CASES READ= 200

	LT. ACROMION X	ILIOCRISTALE X	ASIS X	TROCHANTERIO N X	THIGH CL. X
BODY HEIGHT	0.181	-0.057	0.134	0.181	0.265
STATURE	0.183	-0.066	0.116	0.233	0.258
SUPRASTERNALE HEIGHT	0.157	-0.037	0.130	0.234	0.274
SITTING HEIGHT	0.101	-0.074	0.225	0.181	0.237
EYE HEIGHT SITTING	0.038	-0.048	0.240	0.176	0.243
ACROMIALE HEIGHT	0.077	0.049	0.212	0.110	0.169
THIGH CIRCUMFERENCE	0.095	-0.004	0.030	0.084	0.213
HIP CIRCUMFERENCE	0.147	-0.072	0.083	0.169	0.232
WAIST CIRCUMFERENCE	0.111	-0.031	0.082	0.177	0.134
INSP CHEST CIRCUMFERENCE	0.065	0.012	0.060	0.171	0.128
SHOULDER CIRCUMFERENCE	0.105	-0.023	0.049	0.082	0.098
NECK CIRCUMFERENCE	0.167	0.003	0.065	0.177	0.129
BUTTOCKS DEPTH	0.128	0.056	0.107	0.126	0.156
WAIST DEPTH	0.074	0.118	0.184	0.192	0.209
CHEST DEPTH	0.113	0.072	0.064	0.081	0.017
BIACROMIAL BREADTH	0.110	-0.040	0.001	0.102	0.126
CHEST BREADTH	0.030	0.029	-0.007	0.065	-0.054
WAIST BREADTH	0.145	-0.059	-0.009	0.126	0.024
ILIOCRISTALE BREADTH	0.108	-0.039	0.185	0.199	0.130
ILIOSPINALE BREADTH	0.125	-0.035	0.022	0.096	0.066
BITROCHANTERIC BREADTH	0.086	-0.102	0.037	0.057	0.174
HIP BREADTH STANDING	0.135	-0.121	0.098	0.131	0.191
SHOULDER BREADTH	0.081	-0.068	0.005	0.144	0.165
HEAD LENGTH	-0.012	-0.020	0.053	0.033	0.086
HEAD BREADTH	0.071	0.094	0.050	0.014	-0.037

CORRELATION MATRIX

CASES READ= 280

	VERTEX Y	SITTING EYE Y	NECK-SHOULDER Y	RT. ACROMION Y	SUPRASTERNAL E Y
BODY HEIGHT	-0.120	-0.102	-0.043	-0.292	-0.136
STATURE	-0.108	-0.102	0.006	-0.292	-0.098
SUPRASTERNALE HEIGHT	-0.110	-0.100	0.006	-0.265	-0.099
SITTING HEIGHT	-0.082	-0.061	0.067	-0.214	-0.057
EYE HEIGHT SITTING	-0.154	-0.136	-0.028	-0.156	-0.067
ACROMIALE HEIGHT	-0.056	-0.028	0.044	0.019	-0.002
THIGH CIRCUMFERENCE	-0.079	-0.053	-0.056	-0.164	-0.110
HIP CIRCUMFERENCE	-0.103	-0.026	-0.012	-0.249	-0.084
WAIST CIRCUMFERENCE	-0.153	-0.076	0.040	-0.177	-0.055
INSP CHEST CIRCUMFERENCE	-0.001	-0.034	-0.011	-0.170	-0.102
SHOULDER CIRCUMFERENCE	-0.096	-0.076	-0.004	-0.320	-0.113
NECK CIRCUMFERENCE	0.017	0.010	0.177	-0.059	0.020
BUTTOCKS DEPTH	-0.139	-0.077	-0.077	-0.161	-0.108
WAIST DEPTH	-0.074	-0.028	0.052	-0.079	0.029
CHEST DEPTH	-0.055	-0.077	-0.073	-0.110	-0.150
BIACROMIAL BREADTH	-0.062	-0.055	-0.011	-0.519	-0.053
CHEST BREADTH	-0.072	-0.056	0.013	-0.124	-0.055
WAIST BREADTH	-0.102	-0.001	0.051	-0.126	-0.037
ILIOCRISTALE BREADTH	-0.035	0.014	0.089	-0.109	0.001
ILIOSPINALE BREADTH	-0.021	0.070	0.032	-0.099	-0.023
THIGH CL. Y.	0.047	0.107	0.122	0.005	0.145
BITROCHANTERIC BREADTH	-0.025	-0.004	0.059	-0.163	-0.012
HIP BREADTH STANDING	-0.069	-0.043	-0.006	-0.230	-0.059
SHOULDER BREADTH	-0.059	-0.033	-0.008	-0.214	-0.005
HEAD LENGTH	-0.003	0.037	0.018	-0.005	-0.005
HEAD BREADTH	-0.049	0.066	0.020	-0.008	-0.060

Table 5. Correlations of Y-Coordinate of Landmarks with Standard Anthropometry.

Table 5. (Cont.)

CORRELATION MATRIX

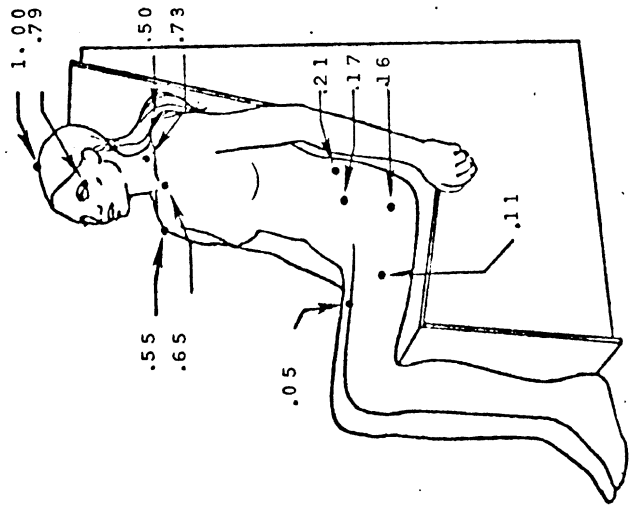
CASES READ= 260

	LT. ACROMION Y	ILIOCRISTALE Y	ASIS Y	TROCHANTERIO N Y	THIGH CL. Y.
BODY WEIGHT	0.157	0.316	0.170	0.534	0.132
STATURE	0.226	0.323	0.282	0.417	0.102
SUPRASTERNALE HEIGHT	0.214	0.290	0.241	0.421	0.096
SITTING HEIGHT	0.196	0.367	0.240	0.393	0.142
EYE HEIGHT SITTING	0.061	0.369	0.216	0.326	0.096
ACROMIALE HEIGHT	-0.005	0.264	0.147	0.195	0.039
THIGH CIRCUMFERENCE	0.036	0.117	0.024	0.456	0.104
HIP CIRCUMFERENCE	0.165	0.309	0.205	0.627	0.214
WAIST CIRCUMFERENCE	0.109	0.365	0.163	0.202	0.125
INSP CHEST CIRCUMFERENCE	0.112	0.222	0.052	0.170	0.061
SHOULDER CIRCUMFERENCE	0.212	0.227	0.156	0.292	0.107
NECK CIRCUMFERENCE	0.112	0.262	0.227	0.123	0.029
BUTTOCKS DEPTH	0.014	0.061	0.001	0.372	0.053
WAIST DEPTH	0.123	0.192	0.116	0.205	0.100
CHEST DEPTH	-0.090	0.002	0.054	0.146	0.011
BIACROMIAL BREADTH	0.475	0.121	0.166	0.300	0.227
CHEST BREADTH	0.065	0.190	0.045	0.104	-0.060
WAIST BREADTH	0.120	0.329	0.102	0.269	0.155
ILIOCRISTALE BREADTH	0.135	0.521	0.546	0.305	0.077
ILIOSPINALE BREADTH	0.079	0.365	0.567	0.206	0.130
TROCHANTERIC BREADTH	0.190	0.335	0.302	0.419	0.130
HIP BREADTH STANDING	0.200	0.309	0.230	0.613	0.293
SHOULDER BREADTH	0.102	0.158	0.062	0.242	0.352
HEAD LENGTH	0.027	0.159	0.101	0.014	-0.039
HEAD BREADTH	0.020	0.134	0.136	0.022	-0.079

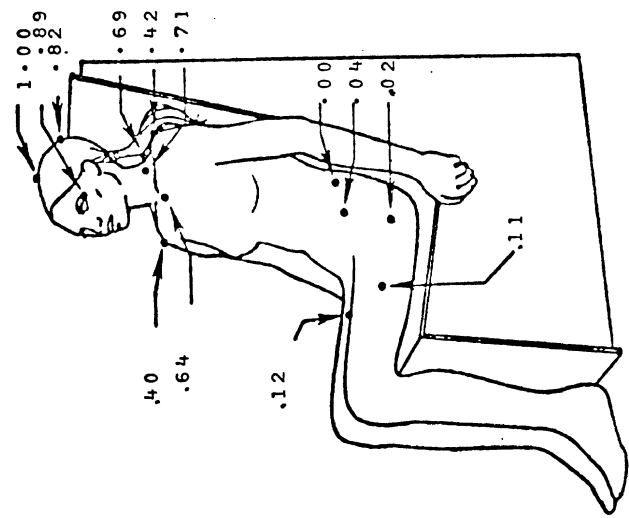
y-axes. For vertex, this is not unreasonable for this seated position. For example, the correlation of stature with vertex x is .13 and stature with vertex y is -.11. For the lateral dimension of sitting eye (ectocanthus), some correlation with head breadth was expected but is nonexistent. The value calculated is .05, which is not significantly different from zero. The x-coordinate of suprasternale has a correlation with weight at .22 and chest depth at .33, which are also weaker than expected. Even the y-coordinates of the right and left acromions are correlated at a surprisingly low level with weight and biacromial breadth. The correlations of the right and left acromions with weight are -.29 and .16, respectively, and with biacromial breadth are -.53 and .48. We explain this by the seemingly extensive variations in posture among individual which appears to weaken the relationship of standard anthropometric data to coordinate data. In addition, the relationships may not be linear and, thus, may have to be described by more complex, multivariate statistics.

The coordinate data describing landmarks on the pelvis should be independent of the subject's posture. However, none of the coordinate points measured have a strong simple, linear relationship with standard anthropometry. It is possible that pelvic dimensions are poorly related to body size, but further investigation of this will be delayed until the Hamann-Todd collection pelvic measurements have been completed.

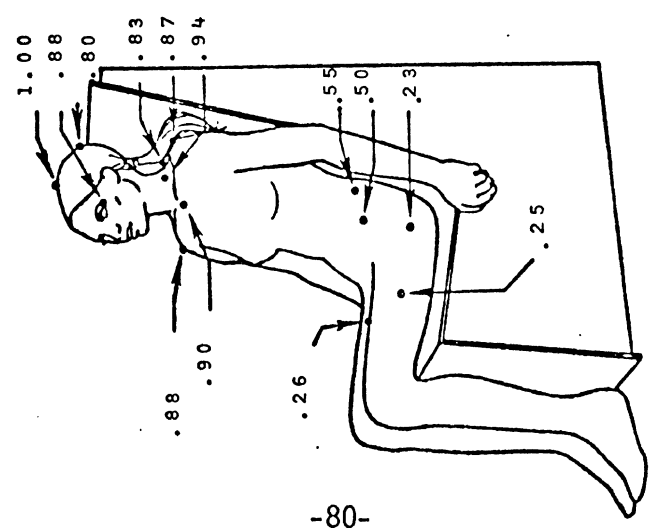
Correlations between the coordinate points show similar relationships to those found in the Snyder model (See correlations - Table 6 and Figure 21). The z-coordinates are highly related with each other



Y-Coordinate Correlations of Landmarks with Vertex Y



X-Coordinate Correlations of Landmarks with Vertex X



Z-Coordinate Correlations of Landmarks with Vertex Z

Figure 21. Correlations of Landmarks with Vertex.

CORRELATION MATRIX	CASES READ = 200				
	VERTEX Z	SITTING EYE Z	NECK-SHOULDER R Z	RT. ACROMION Z	SUPRASTERNAL E Z
VERTEX Z	1.000	0.879	0.942	0.876	0.897
SITTING EYE Z	0.879	1.000	0.852	0.781	0.865
NECK-SHOULDER Z	0.942	0.852	1.000	0.863	0.883
RT. ACROMION Z	0.876	0.781	0.863	1.000	0.876
SUPRASTERNAL Z	0.897	0.865	0.883	0.876	1.000
LT. ACROMION Z	0.868	0.774	0.907	0.887	0.838
ILIOCRISTALE Z	0.553	0.516	0.561	0.556	0.559
ASIS Z	0.504	0.499	0.489	0.473	0.469
TROCHANTERION Z	0.226	0.165	0.186	0.219	0.184
THIGH B. Z	0.252	0.236	0.249	0.272	0.218
THIGH CL. Z	0.262	0.271	0.265	0.252	0.242
OPISTHOCRANION Z	0.797	0.527	0.767	0.681	0.624
CERVICALE Z	0.834	0.715	0.843	0.747	0.762

Table 6. Landmark Coordinate Correlations.

Table 6. (Cont.)

CORRELATION MATRIX

CASES READ = 200

	LT. ACROMION Z	ILIOCRISTALE Z	ASIS Z	TROCHANTERIO N Z	THIGH B. Z
VERTEX Z	0.868	0.553	0.504	0.226	0.252
SITTING EYE Z	0.774	0.516	0.499	0.165	0.236
NECK-SHOULDER Z	0.907	0.561	0.489	0.186	0.249
RT. ACROMION Z	0.887	0.556	0.473	0.219	0.272
SUPRASTERNALE Z	0.838	0.559	0.469	0.184	0.218
LT. ACROMION Z	1.000	0.569	0.452	0.205	0.243
ILIOCRISTALE Z	0.569	1.000	0.613	0.171	0.191
ASIS Z	0.452	0.613	1.000	0.308	0.338
TROCHANTERION Z	0.205	0.171	0.308	1.000	0.615
THIGH B. Z	0.243	0.191	0.338	0.615	1.000
THIGH CL. Z	0.256	0.269	0.487	0.346	0.478
OPISTHOCRANION Z	0.706	0.374	0.356	0.223	0.258
CERVICALE Z	0.756	0.511	0.436	0.173	0.222

Table 6. (Cont.)

CORRELATION MATRIX	THIGH CL. Z	OPISTHOGRANI ON Z	CERVICALE Z
VERTEX Z	0.262	0.797	0.834
SITTING EYE Z	0.271	0.527	0.715
NECK-SHOULDER Z	0.265	0.747	0.843
RT. ACROMION Z	0.252	0.661	0.747
SUPR-ASTERNALE Z	0.242	0.624	0.762
LT. ACROMION Z	0.256	0.706	0.756
ILIOCRISTALE Z	0.269	0.374	0.511
ASIS Z	0.487	0.356	0.436
TROCHANTERION Z	0.346	0.223	0.173
THIGH B. Z	0.470	0.250	0.222
THIGH CL. Z	1.000	0.239	0.201
OPISTHOGRANION Z	0.239	1.000	0.755
CERVICALE Z	0.201	0.755	1.000

CASES READ= 280

Table 6. (Cont.)

CORRELATION MATRIX	CASES READ= 200					
	VERTEX X	SITTING EYE X	NECK-SHOULDER R X	RT. ACROMION X	SUPRASTERNAL Z X	
VERTEX X	1.000	0.878	0.714	0.403	0.642	
SITTING EYE X	0.878	1.000	0.762	0.431	0.663	
NECK-SHOULDER X	0.714	0.762	1.000	0.574	0.840	
RT. ACROMION X	0.403	0.431	0.574	1.000	0.515	
SUPRASTERNAL X	0.642	0.663	0.840	0.515	1.000	
LT. ACROMION X	0.422	0.485	0.611	0.710	0.585	
ILIOCRISTALE X	0.001	0.010	-0.027	-0.017	0.016	
ASIS X	0.035	0.034	0.019	0.024	0.032	
TROCHANTERION X	0.024	0.015	0.022	0.078	0.110	
THIGH B. X	0.107	0.076	0.106	0.119	0.150	
THIGH CL. X	0.110	0.085	0.109	0.117	0.150	
OPISTHOCRANION X	0.816	0.899	0.748	0.445	0.654	
CERVICALE X	0.691	0.727	0.616	0.494	0.808	

Table 6. (Cont.)
CORRELATION MATRIX

CASES READ= 200

	LT. ACROMION X	ILIOCRISTALE X	ASIS X	TROCHANTERIO N X	THIGH B. X
VERTEX X	0.422	0.001	0.035	0.024	0.107
SITTING EYE X	0.085	0.010	0.034	0.015	0.076
NECK-SHOULDER X	0.611	-0.027	0.019	0.022	0.106
RT. ACROMION X	0.710	-0.017	0.024	0.070	0.119
SUPRATERNALE X	0.585	0.016	0.032	0.110	0.150
LT. ACROMION X	1.000	0.057	0.016	0.016	0.037
ILIOCRISTALE X	0.057	1.000	0.435	0.326	0.139
ASIS X	0.016	0.435	1.000	0.339	0.174
TROCHANTERION X	0.016	0.326	0.339	1.000	0.604
THIGH B. X	0.037	0.139	0.174	0.604	1.000
THIGH CL. X	0.039	0.154	0.172	0.600	0.993
OPISTHOCRANION X	0.495	-0.025	0.055	0.012	0.115
CERVICALE X	0.527	-0.046	0.025	0.059	0.100

Table 6. (Cont.)

CORRELATION MATRIX

CASES READ= 280

	THIGH CL. X	OPISTHOCRANI ON X	CERVICALE X
VERTEX X	0.110	0.816	0.691
SITTING EYE X	0.085	0.899	0.727
NECK-SHOULDER X	0.109	0.748	0.816
RT. ACROMION X	0.117	0.445	0.494
SUPRASTERNALE X	0.150	0.654	0.808
LT. ACROMION X	0.039	0.495	0.527
ILIOCRISTALE X	0.154	-0.025	-0.046
ASIS X	0.172	0.055	0.025
TROCHANTERION X	0.608	0.012	0.059
THIGH B. X	0.993	0.115	0.148
THIGH CL. X	1.000	0.120	0.144
OPISTHOCRANION X	0.120	1.000	0.784
CERVICALE X	0.144	0.784	1.000

Table 6. (Cont.)

CORRELATION MATRIX

CASES READ= 200

	VERTEX Y	SITTING EYE Y	NECK-SHOULDER R Y	RT. ACROMION Y	SUPRASTERNAL E Y
VERTEX Y	1.000	0.769	0.726	0.548	0.646
SITTING EYE Y	0.789	1.000	0.692	0.502	0.612
NECK-SHOULDER Y	0.726	0.692	1.000	0.684	0.865
RT. ACROMION Y	0.548	0.502	0.684	1.000	0.749
SUPRASTERNAL Y	0.646	0.612	0.865	0.749	1.000
LT. ACROMION Y	0.499	0.475	0.724	0.283	0.743
ILIOCRISTALE Y	0.208	0.237	0.414	0.202	0.360
ASIS Y	0.174	0.215	0.282	0.101	0.241
TROCHANTERION Y	0.163	0.196	0.242	0.020	0.190
THIGH B. Y	0.106	0.154	0.102	0.007	0.149
THIGH CL. Y.	0.047	0.107	0.122	0.005	0.145

TABLE 6
CORRELATION MATRIX

CASES READ= 200

	LT. ACROMION Y	ILIOCRISTALE Y	ASIS Y	TROCHANTERION N Y	THIGH B. Y	THIGH CL. Y.
VERTEX Y	0.499	0.200	0.174	0.163	0.106	0.047
SITTING EYE Y	0.475	0.237	0.215	0.196	0.154	0.107
NECK-SHOULDER Y	0.724	0.414	0.282	0.242	0.182	0.122
RT. ACROMION Y	0.203	0.202	0.101	0.020	0.007	0.005
SUPRASTERNAL Y	0.743	0.360	0.241	0.190	0.149	0.145
LT. ACROMION Y	1.000	0.410	0.296	0.350	0.278	0.224
ILIOCRISTALE Y	0.410	1.000	0.715	0.586	0.476	0.300
ASIS Y	0.296	0.715	1.000	0.449	0.362	0.261
TROCHANTERION Y	0.350	0.586	0.449	1.000	0.881	0.519
THIGH B. Y	0.278	0.476	0.362	0.881	1.000	0.500
THIGH CL. Y.	0.224	0.300	0.261	0.519	0.500	1.000

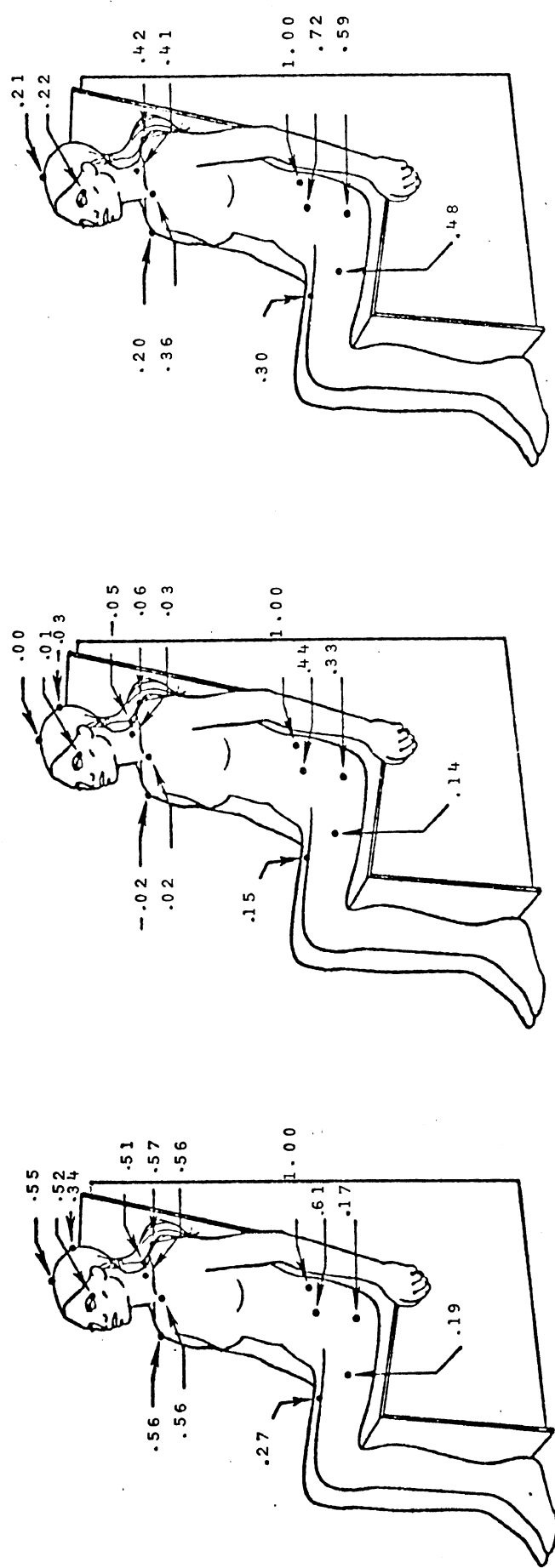
as are the x- and y-coordinates. The correlations of the landmark coordinates on or near the pelvis are similarly, but much less strongly correlated. (See Figure 22).

However, this analysis indicates nothing of the pattern of the variation - for example, in what axis is the most variation? To study this problem, a probability distribution needs to be fitted to the coordinate data for each landmark. The logical choice is a trinormal distribution whose three dimensions correspond to the x, y, and z coordinates. Scatter plots of the coordinate data visually justify the use of this distribution.

Variation is easily studied in the trinormal distribution by examining the covariance matrix and the axes of the smallest volume, confidence ellipsoids of the distribution. The covariance matrices show that the greatest variation is in the z axis for points measured in the upper torso, and in the x axis for points measured on the head and lower portions of the body. (See Table 7). The least variance is in the y axis (with the exception of the anterior superior iliac spine).

The principal axis of the confidence ellipsoid gives that line along which the greatest variation in the portion of the point occurs. (See Table 8). This analysis is sometimes called principal components analysis. This line most frequently lies in the xz-plane for points in the upper body. The axis of least variation follows the y axis with negligible components in the z and x directions.

The graphs of Figure 23, are a projection of the ellipsoid axes onto the xz plane. The origin of each graph is at the mean x-coordinate



Z-Coordinate Correlations

X-Coordinate Correlations

Y-Coordinate Correlations

of Landmarks with Iliocristale Z

of Landmarks with Iliocristale X

of Landmarks with Iliocristale Y

Figure 22. Correlations of Landmarks with Iliocristale.

Table 7. Covariance Matrices of Landmarks

	VERTEX Z	VERTEX X	VERTEX Y
VERTEX Z	0.7779E 05	0.1017E 05	-1883.
VERTEX X	0.1017E 05	0.9049E 05	-3586.
VERTEX Y	-1883.	-3586.	0.1443E 05

	SITTING EYE Z	SITTING EYE X	SITTING EYE Y
SITTING EYE Z	0.7731E 05	-0.1350E 05	216.5
SITTING EYE X	-0.1350E 05	0.1012E 06	-6909.
SITTING EYE Y	216.5	-6909.	0.1399E 05

	NECK-SHOULDE R Z	NECK-SHOULDE R X	NECK-SHOULDE R Y
NECK-SHOULDER Z	0.5930E 05	3739.	-789.1
NECK-SHOULDER X	3739.	0.2845E 05	-2753.
NECK-SHOULDER Y	-789.1	-2753.	0.1310E 05

	RT. ACROMION Z	RT. ACROMION X	RT. ACROMION Y
RT. ACROMION Z	0.5879E 05	-5619.	-2560.
RT. ACROMION X	-5619.	0.3385E 05	-1586.
RT. ACROMION Y	-2560.	-1586.	0.1630E 05

Table 7. (Cont.)

	SUPRASTERNAL E Z	SUPRASTERNAL E X	SUPRASTERNAL E Y
SUPRASTERNALE Z	0,4969E 05	-3981.	-1155.
SUPRASTERNALE X	-3981.	0,1638E 05	-1776.
SUPRASTERNALE Y	-1155.	-1776.	0,1027E 05
	LT. ACROMION Z	LT. ACROMION X	LT. ACROMION Y
LT. ACROMION Z	0,6176E 05	-208.5	-946.9
LT. ACROMION X	-208.5	0,3427E 05	-1996.
LT. ACROMION Y	-946.9	-1996.	0,1629E 05
	ILIOCRISTALE Z	ILIOCRISTALE X	ILIOCRISTALE Y
ILIOCRISTALE Z	0,1477E 05	93.17	1779.
ILIOCRISTALE X	93.17	0,1145E 05	-75.94
ILIOCRISTALE Y	1779.	-75.94	9724.
	ASIS Z	ASIS X	ASIS Y
ASIS Z	9152.	132.4	-132.1
ASIS X	132.4	0,1055E 05	-219.1
ASIS Y	-132.1	-219.1	0,1320E 05

Table 7. (Cont.)

	TROCHANTERIO N Z	TROCHANTERIO N X	TROCHANTERIO N Y
TROCHANTERION Z	8908.	2870.	1682.
TROCHANTERION X	2870.	0.3420E 05	5635.
TROCHANTERION Y	1682.	5635.	0.1160E 05

	THIGH B. Z	THIGH B. X	THIGH B. Y
THIGH B. Z	2563.	5416.	441.1
THIGH B. X	5416.	0.3026E 05	1614.
THIGH B. Y	441.1	1614.	0.1277E 05

	THIGH CL. Z	THIGH CL. X	THIGH CL. Y.
THIGH CL. Z	0.1047E 05	8629.	39.46
THIGH CL. X	8629.	0.2961E 05	-105.1
THIGH CL. Y.	39.46	-105.1	0.1297E 05

Table 8. Principal Components Analysis of Three-Dimensional Stewardess Data.

Axes:	Vertex			Sitting Eye (Ectocanthus)		
	Direction	Cosines		Direction Cosines		
	1	2	3	1	2	3
Z	.485	.874	.023	.405	.914	.013
X	.873	-.485	.044	-.912	.403	.081
Y	-.049	.002	.999	.068	-.045	.997
Explained Variance:	96338.	72189.	14222.	107700.	71336.	13427.
%Variance:	52.7	92.2	100.0	56.0	93.0	100.0

Axes:	Neck-Shoulder			Right Acromion		
	Direction Cosines			Direction Cosines		
	1	2	3	1	2	3
X	.992	.234	.002	-.977	.200	.074
Y	.121	-.978	.171	.206	.972	.111
Z	-.024	.169	.985	.050	-.124	.991
Explained Variance:	59774.	28455.	12609.	60091.	32901.	15929.
%Variance:	59.3	87.5	100.0	55.2	85.4	100.0

Axes:	Suprasternale			Left Acromion		
	Direction Cosines			Direction Cosines		
	1	2	3	1	2	3
X	-.993	.104	.056	-.999	.004	.021
Y	.116	.951	.287	.006	.994	.109
Z	.024	-.29	.956	.021	-.109	.994
Explained Variance:	50178.	16486.	9669.9	61776.	34487.	16044.
%Variance	65.7	87.3	100.0	55.0	85.7	100.0

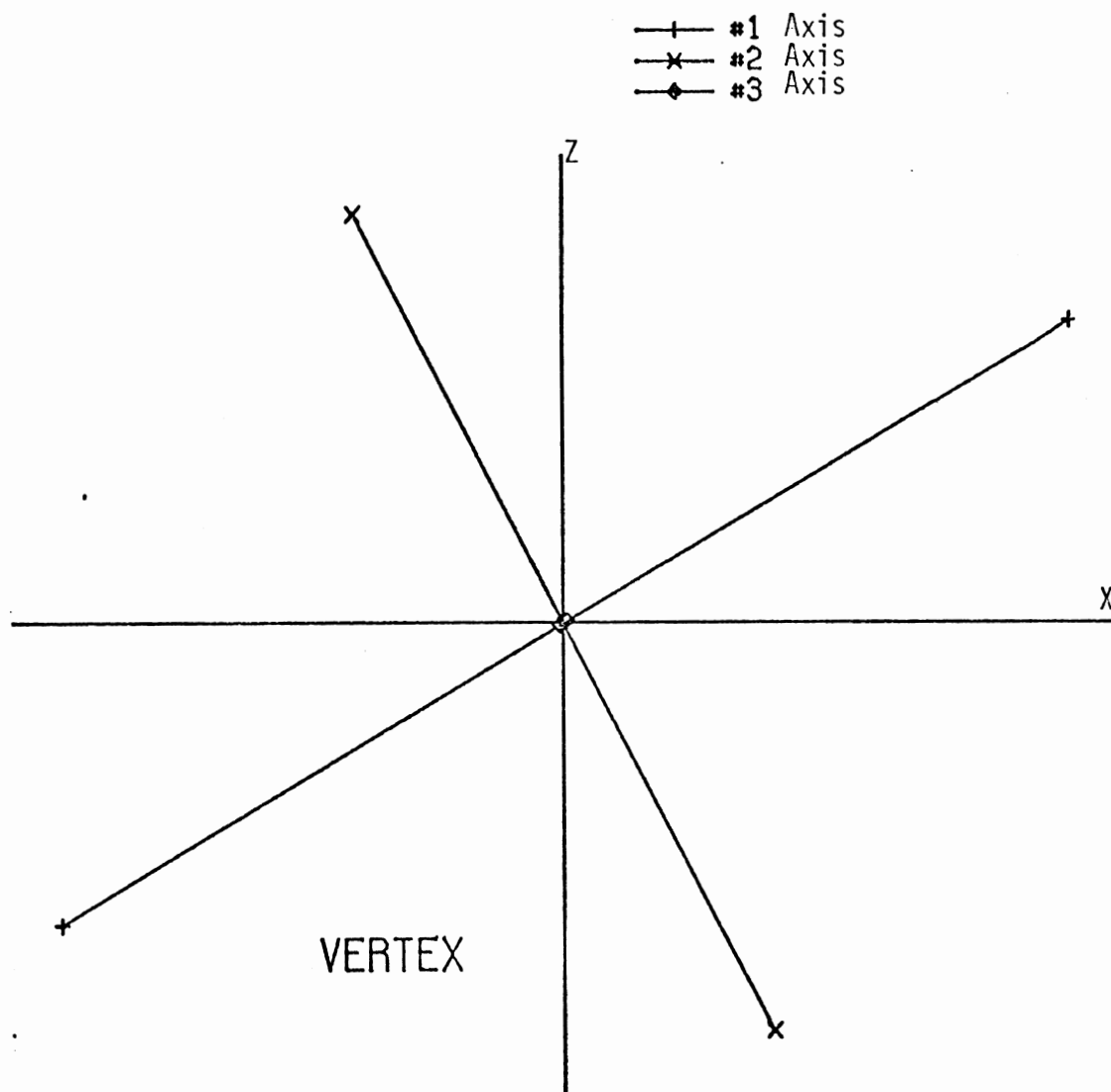
Table 8. (Cont.)

Iliocristale				Anterior Superior Iliac Spine			
Direction Cosines				Direction Cosines			
Axes:	1	2	3	1	2	3	
X	.948	.011	-.317	.035	.098	.995	
Y	.00	.994	.035	.082	.992	-.101	
Z	.317	-.033	.948	-.996	.085	.027	
Explained Variance:	15273.	11461.	9144.	13303.	10557.	9052.1	
%Variance:	42.6	74.5	100.0	40.4	72.5	100.0	

Trochanterion				Thigh Breadth			
Direction Cosines				Direction Cosines			
Axes:	1	2	3	1	2	3	
X	.117	.406	-.907	.185	.005	-.983	
Y	.966	-.260	.009	.979	.090	.185	
Z	.232	.876	.422	.089	-.996	.012	
Explained Variance:	35896.	10700.	8097.6	31432.	12610.	1539.5	
%Variance	65.6	85.2	100.0	69.0	96.6	100.0	

Thigh Clearance			
Direction Cosines			
Axes:	1	2	3
X	.359	.014	-.933
Y	.933	-.001	.359
Z	-.004	.999	.013
Explained Variance:	32919.	12960.	7152.9
%Variance	62.1	86.5	100.0

Figure 23. Projection of Least Volume Ellipsoid Axes
Scaled to Explained Variance, On To XZ Plane



Note: Axis 1 is the axis of greatest variation and axis 3 is the axis of least variation.

Figure 23. (Cont.)

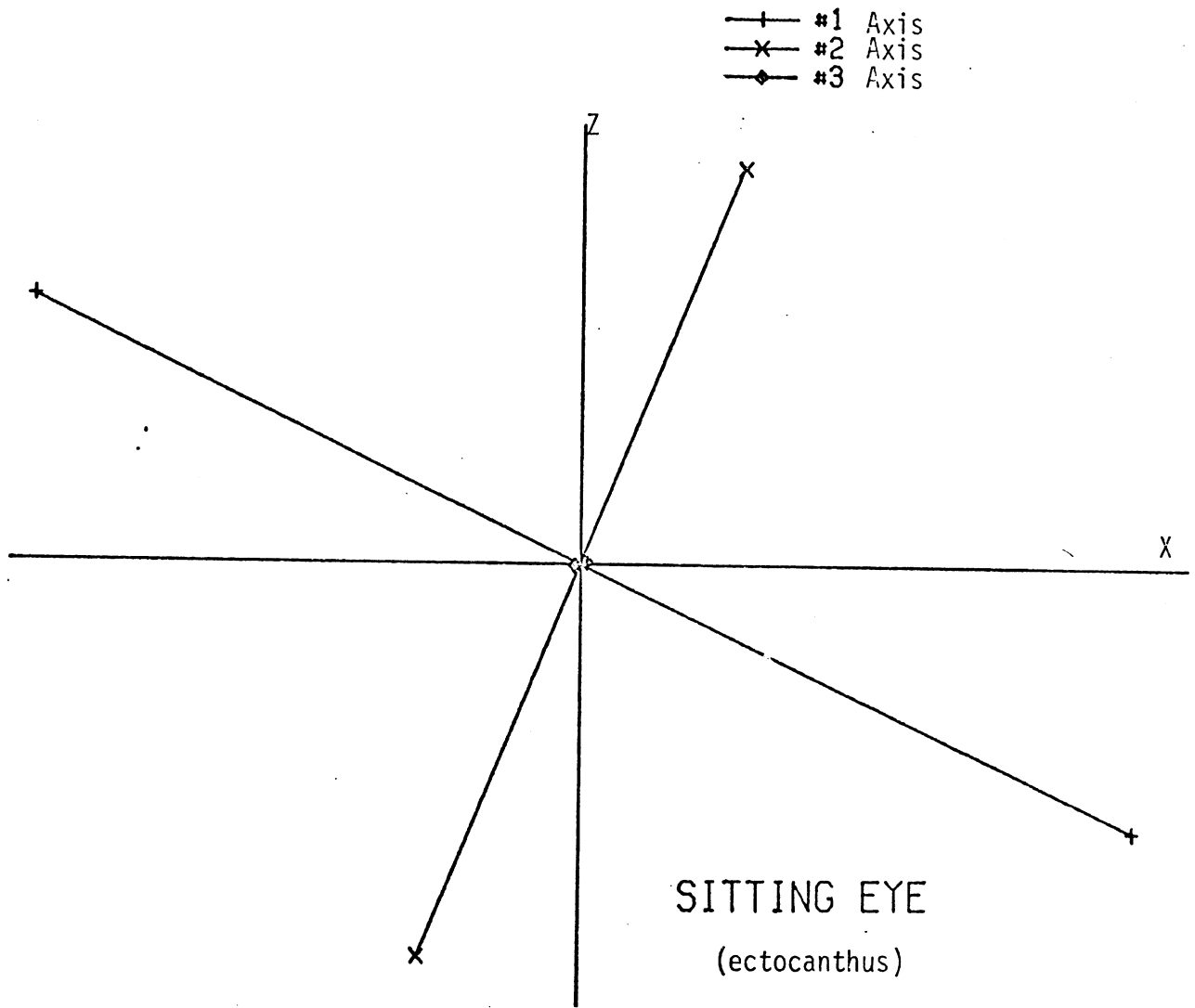


Figure 23. (Cont.)

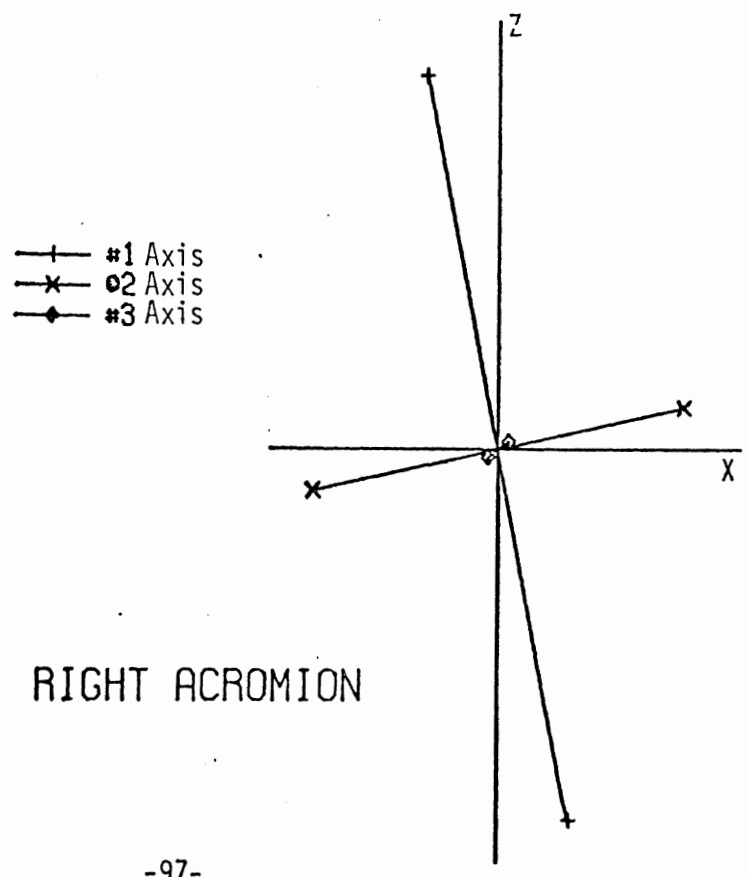
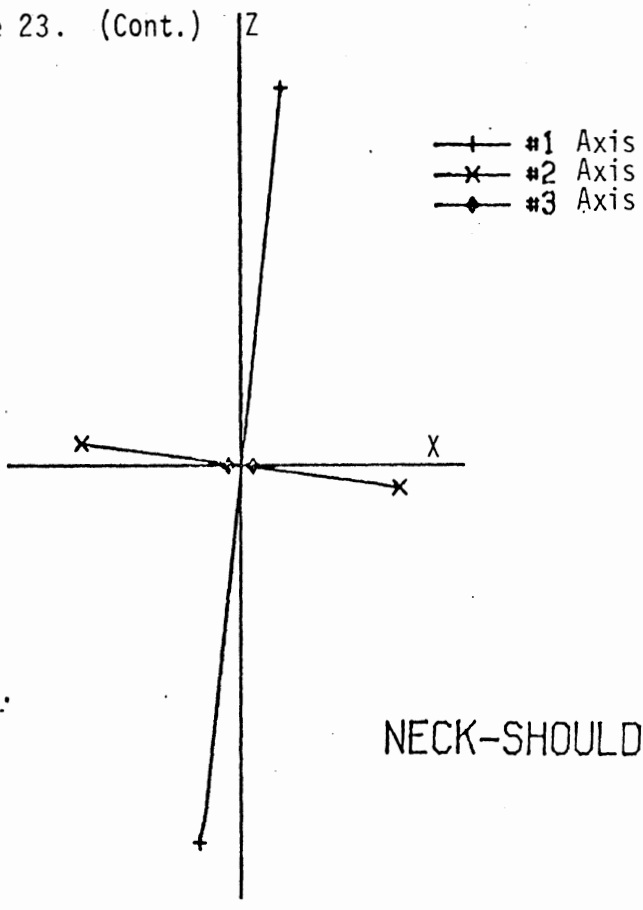
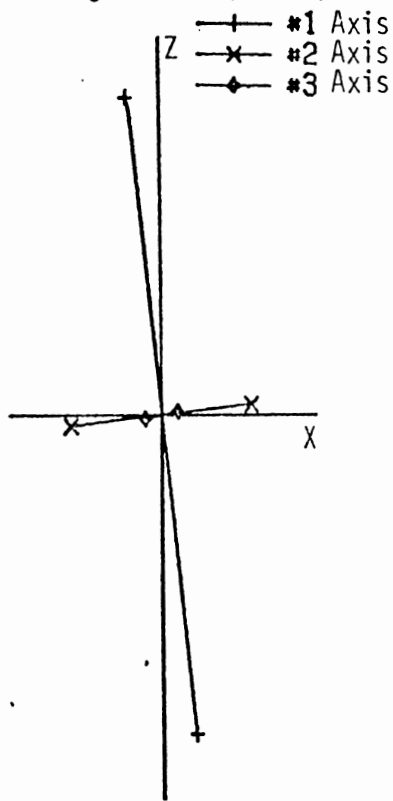
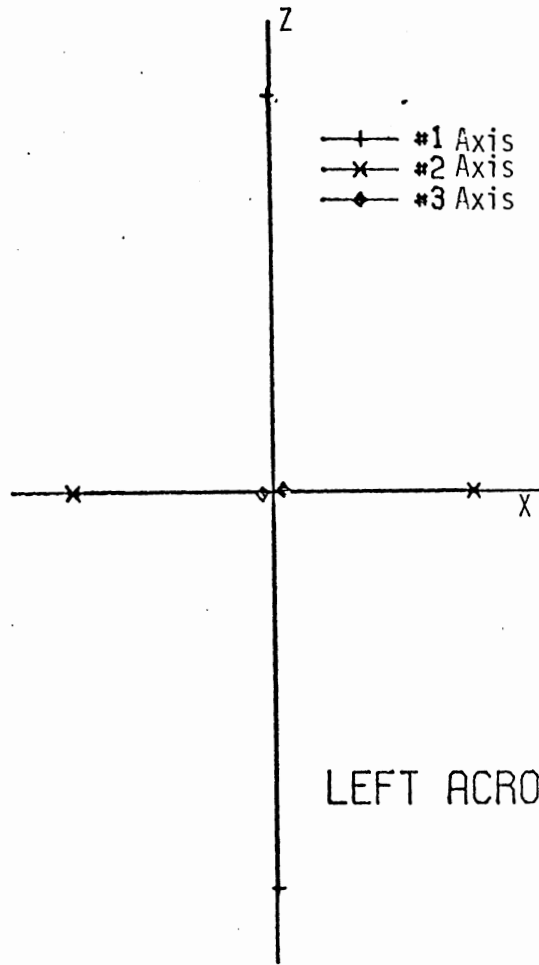


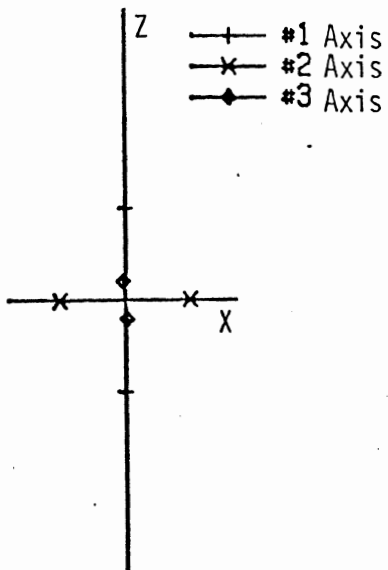
Figure 23. (Cont.)



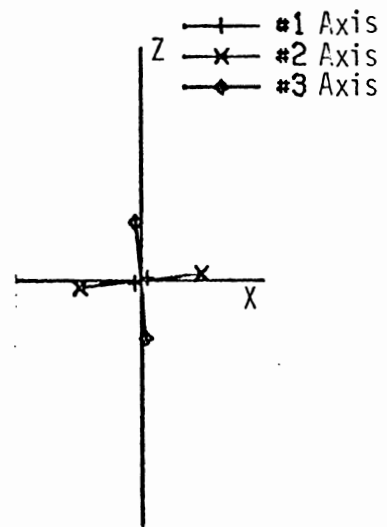
SUPRASTERNALE



LEFT ACROMION

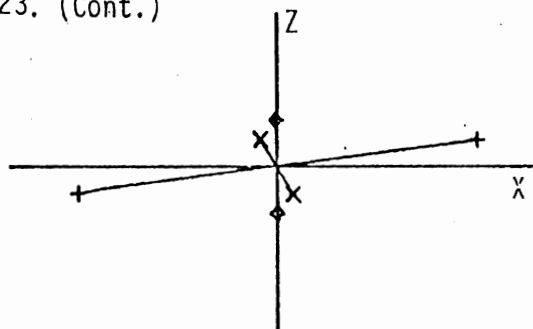


ILIOCRISTALE



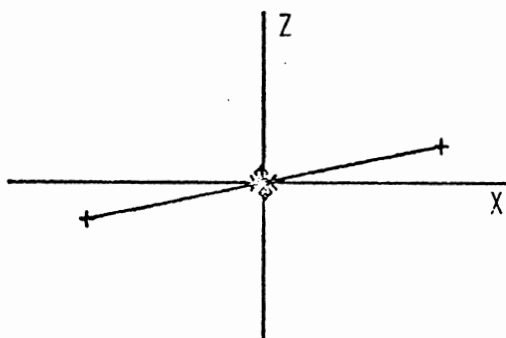
ANTERIOR SUPERIOR
ILIAC SPINE

Figure 23. (Cont.)



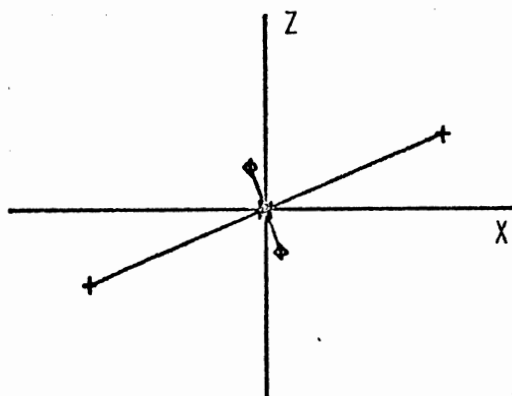
- +— #1 Axis
- x— #2 Axis
- ◆— #3 Axis

TROCHANTERION



- +— #1 Axis
- x— #2 Axis
- ◆— #3 Axis

THIGH BREADTH



- +— #1 Axis
- x— #2 Axis
- ◆— #3 Axis

THIGH CLEARANCE

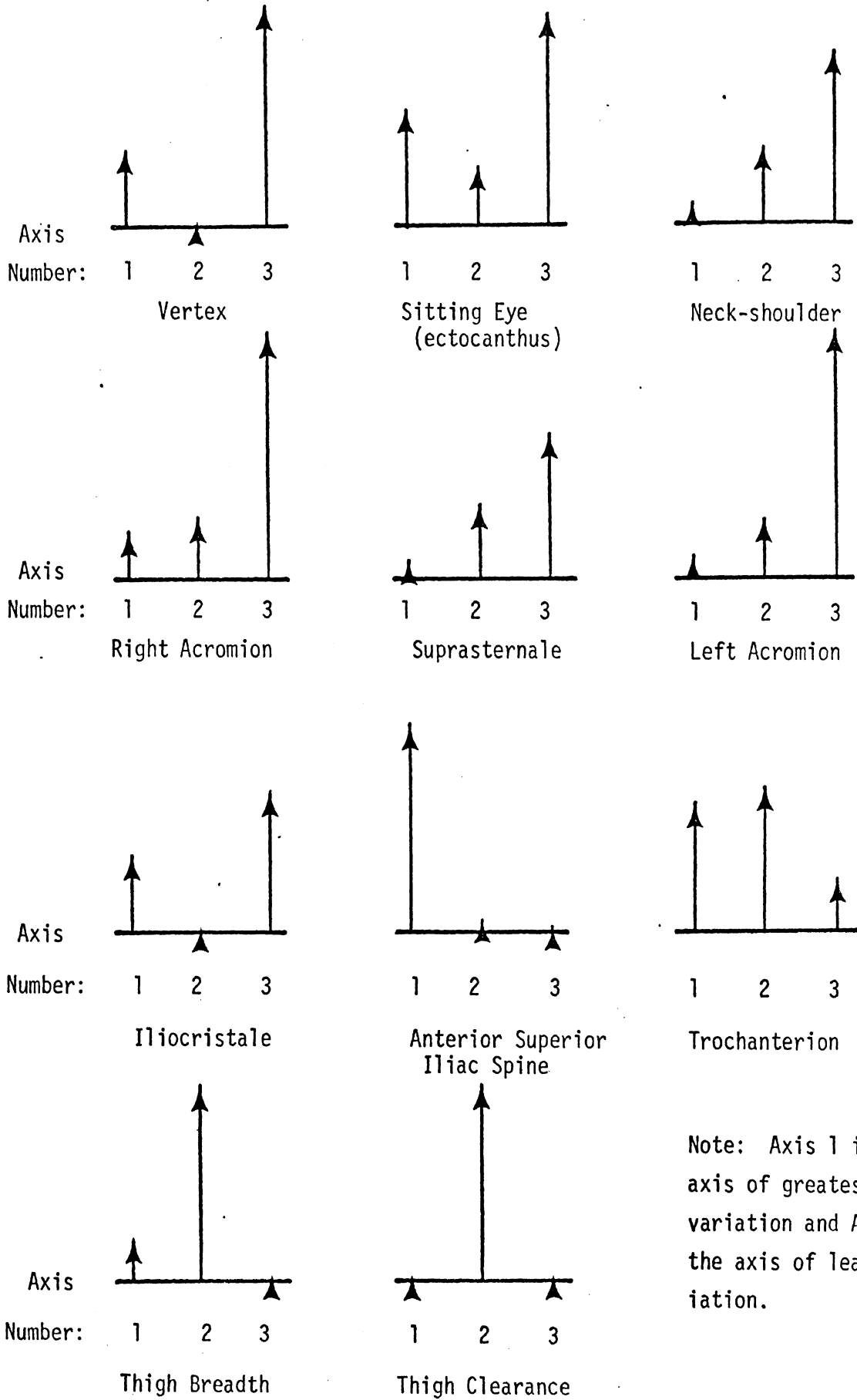
and y-coordinate of the landmark position. The length of an axis is drawn proportionately to the amount of variance along that axis. These graphs indicate the variations of the position of the landmarks in the xy plane. The graphs are scaled the same, and, thus, they may be compared.

The graphs of Figure 24, compare the y-component of variance along the three principal axes. These graphs represent the magnitude of variance projected onto the perpendicular y-axis. These graphs are proportional but are not of the same scale as those of Figure 23. However, the graphs of Figures 23 and 24 can be used to represent the three-dimensional anthropometric data.

The analysis of the different sources of variation points out some very interesting characteristics of the flight attendant trainees and perhaps, the general population. The high x and xz components of variation indicate that in a normal seated position, individuals have a tendency to bend forward. The smaller y components and non-existent yz and yx components indicate that individuals do sit fairly straight in the frontal plane--that is, they do not lean to one side or the other or sit twisted. These results support the observation that individuals, for any position, can bend forward at the waist with relative ease and only with great difficulty can they bend the same distance to the side or twist any large angle to the side. This large variation of the body in the x direction will, therefore, cause some difficulties in modeling from empirical data sources.

Unlike the upper part of the body, the pelvis is fairly fixed in a seated position. Therefore, the coordinate data of landmarks on the

Figure 24. Y-Component of Variance Along the Axes of the Least Volume Ellipsoid



pelvis should indicate more of the variability in the size and shape of the bone than in the variability in seated positions. The confidence ellipsoids for ilioacristale and anterior superior iliac spine are nearly spherical in shape indicating a fair degree of independence of the x, y, and z coordinates. This property will be analyzed further on the Hamann-Todd collection.

4.6. Geometric Model Estimates of Inertial Properties of Body Segments.

B. Bowman

The inertial properties of each body segment must be described in order to complete the anthropomechnaical model of the body. The limbs, in particular, appear to be suitable candidates for rigid geometric body analogies such as cylinders and frusta of cones (elliptical or circular). As a result a portion of the Phase I effort was directed towards several small tasks associated with these models.

4.6.1. Analytical Determination of the Inertial Properties of a Cored Frustum of a Right Elliptical Cone. During Phase I, the following problems were solved:

A. Analytical determination of the moment of inertia about the longitudinal principal axis of cored frustum of a right elliptical cone.

- a. The eccentricities of the upper and lower outside cross sections must be equal;
- b. The interior core is in the shape of the frustum of a right elliptical cone with equal eccentricities of the upper and lower cross sections;
- c. The interior core may be a density different from that of the outer section.
- d. Eccentricities of the inner and outer cross sections need not be equal;
- e. Principal axes of elliptical cross sections may not be skewed with respect to each other.

B. Analytical determination of moments of inertia about the lateral principal axes of the aforescribed frustum.

C. Analytical determination of the mass and the location of the center of mass of the cored frustum.

Formulae for the evaluation of these inertial properties and others are given in the following sections. The analytical quantities used in the formulæ are defined in Table 9 and illustrated in Figure 25 .

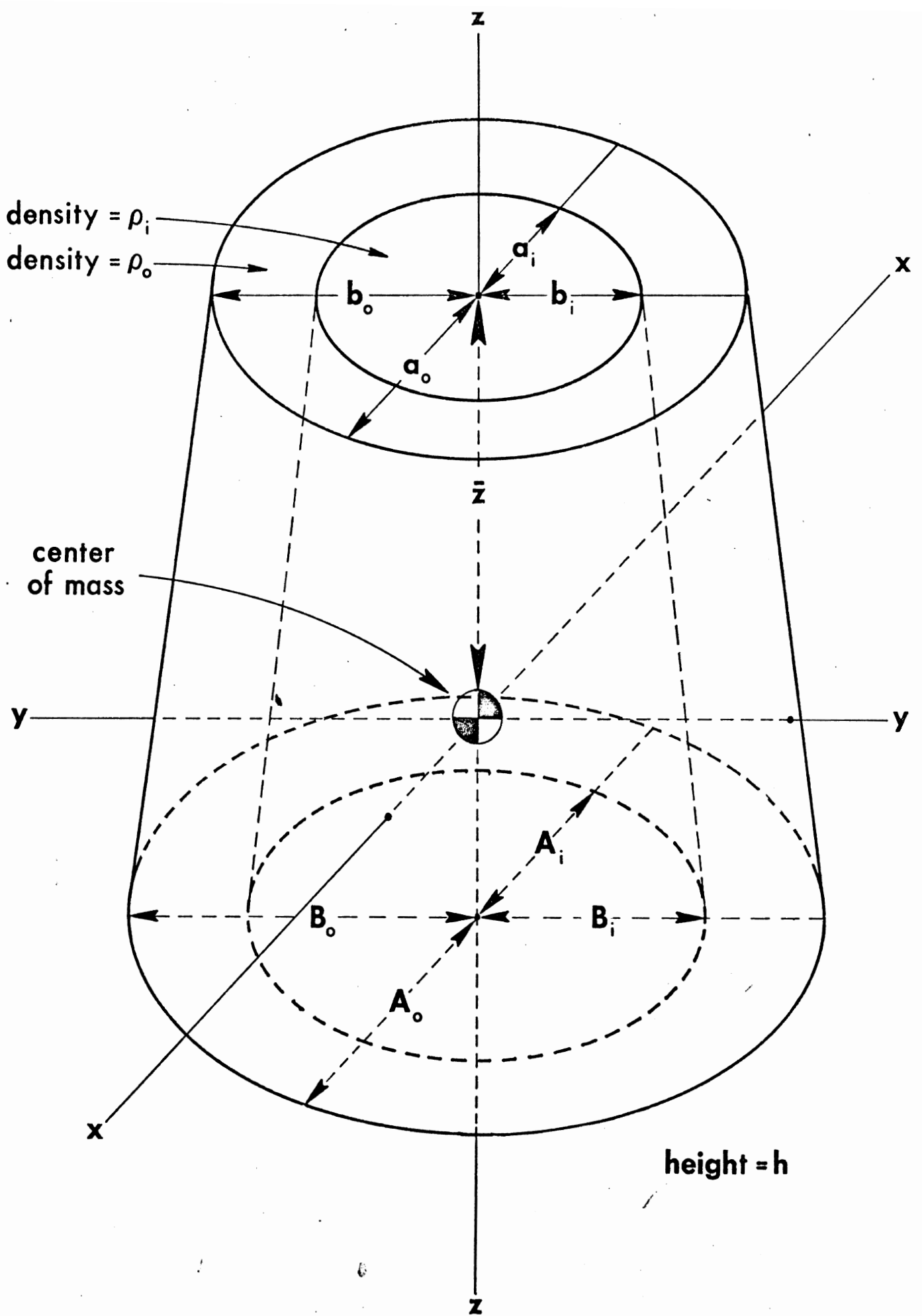


Figure 25. A Cored Frustum of a Right Elliptical Cone

Table 9. TABLE OF INERTIAL PROPERTY PARAMETERS

PARAMETERS	DEFINITIONS
h	Height of cored frustum of a right elliptical cone
"i"	A subscript indicating the inner frustum, or core
"o"	A subscript indicating the outer shell of the cored frustum
a_i, b_i	Ellipse x- and y- semi-axis dimensions of the "top" of the core
a_o, b_o	Ellipse x- and y- semi-axis dimensions of the "top" of the outer shell
A_i, B_i	Ellipse x- and y- semi-axis dimensions of the "base" of the core
A_o, B_o	Ellipse x- and y- semi-axis dimensions of the "base" of the outer shell
c_i, c_o, C_i, C_o	The core and outer shell circumferences at the top and base of the cored frustum
γ_i	A proportionality constant relating the semi-axes of all cross section of the core. e.g., $\frac{b_i}{a_i} = \frac{B_i}{A_i} = \gamma_i$
γ_o	A proportionality constant relating the semi-axes of all cross sections of the outer shell. e.g., $\frac{b_o}{a_o} = \frac{B_o}{A_o} = \gamma_o$

PARAMETERS	DEFINITIONS
V_i, V_o, V	The volumes of the core, outer shell, and composite cored frustum
ρ_i, ρ_o, ρ	The mass densities of the core, outer shell, and composite cored frustum
M_i, M_o, M	The masses of the core, outer shell, and composite cored frustum
W_i, W_o, W	The weight of the core, outer shell, and composite cored frustum
I_x, I_y, I_z	The mass moments of inertial of the composite cored frustum about the principle ases x-x, y-y, z-z.
\bar{z}	Distance from the "top" of the frustum which locates the center of mass of the composite cored frustum on the longitudinal axis

4.6.1.1. Definition of a Mathematical Operator.

It is convenient for the purpose of presenting formulae for the inertial properties of the cored frustum of a right elliptical cone to use a special mathematical notation. In the formulae which appear in the following sections the symbol " Σ " is a linear, algebraic operator defined as follows:

Where f is any function of parameters that must be subscripted either "i" (inner frustum, or core) or "o" (outer shell of the cored frustum). *

$$\Sigma f \equiv \rho_o f_o - (\rho_o - \rho_i) f_i, \quad 1.$$

where f_i and f_o are evaluations of f for "i" parameters and "o" - parameters, respectively.

As an example, consider the simple expression

$$J_2 = \sum \frac{\gamma h}{3} (a^2 + aA + A^2) .$$

Since A , a , and γ are parameters which require subscripts (see Table 9), this relation is evaluated by the definition in Equation 1 as

$$J_2 = \frac{h}{3} [\rho_o \gamma_o (A_o^2 + A_o a_o + a_o^2) - (\rho_o - \rho_i) \gamma_i (A_i^2 + A_i a_i + a_i^2)]$$

4.6.1.2. Constants.

All basic inertial properties of a cored frustum of a right elliptical cone of given dimensions can be expressed in terms of five constant functions, J_1 , J_2 , J_3 , J_4 , and J_5 where:

$$J_1 = \sum \frac{\gamma h^2}{12} (a^2 + 2aA + 3A^2) \quad 2.$$

* These parameters are γ , a , A , b , B , c , and C .

$$J_2 = \sum \frac{\gamma h}{3} (a^2 + aA + A^2) \quad 3.$$

$$J_3 = \sum \frac{h(1 + 2\gamma^2 + 5\gamma^4)}{160} (a^4 + a^3A + a^2A^2 + aA^3 + A^4) \quad 4.$$

$$J_4 = \sum \frac{h^3(1 + \gamma^2)}{60} (a^2 + 3aA + 6A^2) \quad 5.$$

$$J_5 = \sum \frac{h(5 + 2\gamma^2 + \gamma^4)}{160} (a^4 + a^3A + a^2A^2 + aA^3 + A^4) \quad 6.$$

Here, \sum is the linear operator defined in the preceding section, and γ designates the ratios

$$\gamma_i = \frac{b_i}{a_i} = \frac{B_i}{A_i} \quad 7.$$

and

$$\gamma_o = \frac{b_o}{a_o} = \frac{B_o}{A_o} \quad 8.$$

4.6.1.3. Mass Properties.

The total mass of the cored frustum is

$$M = \pi J_2 \quad 9.$$

The mass of the core is

$$M_i = \frac{\pi \gamma_i \rho_i h}{3} (a_i^2 + a_i A_i + A_i^2) \quad 10.$$

The mass of the outer shell is

$$M_o = M - M_i \quad 11.$$

The center of mass lies on the longitudinal principal axis at a distance of \bar{z} from the "top" of the cored frustum, the end with semi-axis dimensions a_o and b_o :

$$\bar{z} = J_1/J_2 \quad . \quad 12.$$

The distance from the "base" is $h - \bar{z}$.

The volumes of the core and outer shell, respectively, are

$$V_i = M_i/\rho_i \quad 13.$$

and

$$V_o = M_o/\rho_o \quad 14.$$

The total volume of the cored frustum is:

$$V = V_i + V_o \quad 15.$$

and its average density is

$$\rho = M/V \quad 16.$$

4.6.1.4. Moments of Inertia.

The mass moments of inertia of the cored frustum about the principal axes are given in Equations 17), 18), and 19). The axis $x-x$ in Figure 25 is in the direction of the "a" and "A" ellipse axes, and $y-y$ is in the direction of the "b" and "B" axes. The axis $z-z$ is the longitudinal axis of the cored frustum. The principal axes are mutually orthogonal and intersect at the center of mass.

$$I_x = \pi(J_3 + J_4 - J_1^2/J_2) \quad 17.$$

$$I_y = \pi(J_4 + J_5 - J_1^2 / J_2)$$

$$I_z = \pi(J_3 + J_5)$$

4.6.1.5. Use of the Formulae. The relations given in Equations 1) through 19) may be used to calculate all basic inertial properties of any circular or elliptical, cored or uncored, right cylinder, cone, or frustum. There are only two restrictions: 1) The core and outer shell must be homogeneous with respect to mass distribution, i.e., the mass densities ρ_i and ρ_o must be constants. 2) Eccentricities of cross sections of both the core and the outer shell must be invariant with respect to longitudinal position, although eccentricities of the inner and outer cross sections need not be equal.

4.6.2. Computer Evaluation of Inertial Properties.

A task which will be completed near the beginning of Phase II is the development of a computer program which will evaluate the analytical expressions for inertial properties presented in the foregoing sections. This program will accept as input: 1) the height of the cored frustum; 2) a pair of weights or weight densities or a density - weight pair for core and/or outer shell and/or total frustum; and 3) the two semi-axis lengths or, optionally, one semi-axis length and the circumference for each of the four elliptical cross sections which describe the core and outer shell of the composite frustum at its "top" and "base".

Example output from a preliminary version of the computer program is shown in Table 10.

Table 10. CALF--ESTIMATED INPUT DATA

DATA CARDS:
 -36.700 5.050 -18.700 2.976 -19.400 3.400 -18.700 2.976 38.100
 1065.98 1423.93 00000000
 001

ELLIPTICAL CROSS-SECTION DIMENSIONS FROM INPUT DATA (CM) :
 CROSS SECTION X-SEMI-AXIS (A) Y-SEMI-AXIS (B) CIRCUMFERENCE
 FRUSTRUM TOP 6.58 5.05 36.70
 CORE TOP 2.98 2.98 18.70
 FRUSTRUM BASE 2.76 3.40 19.40
 CORE BASE 2.98 2.98 18.70

FRUSTRUM HEIGHT (CM) : 38.10

OPTION #3 FOR B/A-RATIO ADJUSTMENT

OUTER AND INNER RATIOS WEIGHTED BY BASE AND TOP CROSS SECTION AREAS
 B/A(O) : 0.86969 B/A(I) : 1.00000

ADJUSTED ELLIPTICAL CROSS-SECTION DIMENSIONS (CM) :
 CROSS SECTION X-SEMI-AXIS (A) Y-SEMI-AXIS (B) CIRCUMFERENCE
 FRUSTRUM TOP 6.25 5.43 36.74
 CORE TOP 2.98 2.98 18.70
 FRUSTRUM BASE 3.25 2.83 19.14
 CORE BASE 2.98 2.98 18.70

MOMENTS OF INERTIA (GM*CM**2) -- IX: 362619. IY: 366875. IZ: 32695.

LOCATION OF CENTER OF MASS: ON LONGITUDINAL AXIS, 22.43 CM FROM BASE AND
 15.67 CM FROM TOP

	OUTER SHELL OF FRUSTRUM	INNER CORE OF FRUSTRUM	TOTAL FRUSTRUM
WEIGHT (GM*CM/SEC**2) :	1457410.	1509684.	2967095.
WEIGHT DENSITY (GM/SEC**2/CM**2) :	1066.0	1423.9	1222.3
MASS (GM) :	1486.1	1539.5	3025.6
MASS DENSITY (GM/CM**3) :	1.0870	1.4520	1.2464
VOLUME (CM**3) :	1367.	1060.	2427.

4.7. Measurement of Striated Muscle Density

J. Freeman

A methodology for determination of the density of unpreserved human striated muscle tissue has been developed at HSRI. The density of human striated muscle will be used in formulae developed in Phase I of this project, describing the inertial properties of cored frusta of right elliptical cones. Using these formulae, modeling of body segments with two different homogenous volumes will be possible. Thus, a segment, such as the thigh, may be modeled with soft and hard tissue densities representative of the body muscle and bone densities. The density of human bone tissue has been documented in both the fresh and preserved conditions (Blanton and Biggs, 1968). However, human muscle density has been best documented only on preserved specimens (Clauser, et al., 1969). This study has been undertaken, therefore, to provide a determination of the density of unpreserved human striated muscle.

4.7.1. Procedure. This investigation will proceed in two parts: an initial data gathering phase, and, once 12-15 cadavers have been sampled, a data analysis phase. The work done with each cadaver during the data collection phase will itself be composed of two parts: an initial Anthropometric and Roentgenographic examination of the cadaver, and within the following 24 hours, a determination of the density of muscle tissue sampled from the cadaver. Sample sites have been chosen in the upper and lower extremities as well as the torso. Muscle tissue taken from the extremities during the initial examination will be excised in the shape of a roughly one to two inch cylinder from the belly of each muscle chosen. Samples from muscles in the torso will be taken, if possible, at sites where large continuous amounts of muscle are found without encroaching fascia or other connective tissues. Small slivers of tissue will later be removed from these large tissue samples for the actual determination of muscle density.

The initial examination of the cadaver will yield information through several approaches (refer to figure 26 sample cadaver examination sheet showing measurements expected to be taken). Anthropometric measurements will be made of the cadaver overall as well as measurements which can be related more directly to those parts of the body from which samples will be taken. In addition, skinfold measurements and measurements of fat thickness above the sample sites will be taken. The maximum circumference of the muscle, where appropriate, will also be recorded. This information, together with data on bone, muscle and fat breadth obtained from x-ray studies should enhance our understanding of the relationship of muscle density to size.

SUBJECT NO. _____ DATE / /

SUBJECT NO. _____ DATE / /

AGE _____
SEX _____
RACE _____
HGT. _____
WGT. _____
GENERAL BODY CONDITION: _____
CAUSE OF DEATH: _____
DATE OF DEATH / /

FOREARM (Brachioradialis)
1. Anthropometry
Radiale-Styilion 1. _____
Olecronon-Styilion 1. _____
Forearm Circumference _____
Wrist Circumference _____
2. X-ray
Bone Breadth I _____
Muscle Breadth Ant. _____
Post. _____
Fat Breadth Ant. _____
Post. _____
3. Skinfold
Brachioradialis _____
4. Fat Thickness
Brachioradialis _____
5. Muscle Circumference
Brachioradialis _____

UPPER ARM (Biceps brachii, Triceps brachii - long head)

THIGH (Rectus femoris, Biceps femoris - long head)
1. Anthropometry
Trochanterior-Femoral condyle _____
Mid-Thigh Circumference _____
Knee Breadth _____
2. X-Ray
Bone Breadth _____
Muscle Breadth Ant. _____
Post. _____
Fat Breadth Ant. _____
Post. _____

1. Anthropometry
Acromion-Radiale 1. _____
Arm Circumference _____
Elbow Breadth _____
2. X-Ray
Bone Breadth _____
Muscle Breadth Ant. _____
Post. _____
Fat Breadth Ant. _____
Post. _____
3. Skinfold
Biceps brachii _____
Triceps brachii _____
4. Fat Thickness
Biceps brachii _____
Triceps brachii _____
5. Muscle Circumference
Biceps brachii _____
Triceps brachii _____

SUBJECT NO. _____ DATE / /

SUBJECT NO. _____ DATE / /

THIGH (cont.)

NECK (Trapezius)
1. Anthropometry
Neck Circumference _____
Neck Breadth _____
2. Skinfold
Trapezius _____
3. Fat Thickness _____

3. Skinfold
Rectus femoris _____
Biceps femoris _____
4. Fat Thickness
Rectus femoris _____
Biceps femoris _____
5. Muscle Circumference
Rectus femoris _____
Biceps femoris _____
SHANK (Gastrocnemius - medial head)
1. Anthropometry
Tibiale-Styilion 1. _____
Fibiale-Styilion 1. _____
Max. Calf Circumference _____
Ankle Breadth _____
2. X-Ray
Bone Breadth I _____
Muscle Breadth Ant. _____
Post. _____
Fat Breadth Ant. _____
Post. _____
3. Skinfold
Gastrocnemius _____
4. Fat Thickness
Gastrocnemius _____
5. Muscle Circumference
Gastrocnemius _____

BACK (Latissimus dorsi)
AXILLA (Pectoralis major)
1. Anthropometry
Chest Circumference _____
Chest Breadth _____
Chest Depth _____
2. Skinfold
Latissimus dorsi _____
Pectoralis major _____
3. Fat Thickness
Latissimus dorsi _____
Pectoralis major _____

Figure 26. Sample Cadaver Examination Sheet.

Muscles from which samples will be taken have been chosen for their size as well as ease of identification. Where possible samples will be taken from the right side of the body. Those muscles chosen for sampling in the extremities include: Biceps brachii and Triceps brachii (long head) in the arm; Brachioradialis in the forearm; Rectus femoris and Biceps femoris (long head) in the thigh; and the medial head of the Gastrocnemius in the shank. The neck, back and axilla will be sampled in the trunk as represented by the Trapezius, Latissimus dorsi and Pectoralis major muscles, respectively.

Muscle density measurements will be made on three slivers of tissue from each of the nine muscles dissected from each cadaver. Each sliver will be dissected from its muscle sample to cause as little distortion in the tissue as possible. The sliver will be immediately weighed on a double-pan, analytical balance and then immersed in a 25 ml. pycnometer filled with distilled water. Care will have been taken to assure that the muscle tissue, Pycnometer and room are approximately in thermal equilibrium as fluctuations in temperature can effect the accuracy of the resultant density determination. The Pycnometer will be quickly immersed in a 50 watt ultrasonic bath to remove any air bubbles adhering to the tissue or the inner surface of the Pycnometer. The Pycnometer will then be sealed, and at the end of a two minute stabilization period, the Pycnometer will be weighed. Following Figure 27, which shows the data sheet and calculations to be used in the density determination procedure, (the format of which was kindly volunteered by Clauser, McConville and Young), we can see that if the weights of the empty and water-filled Pycnometer are already known, and if the ambient temperature

Date / /

Card _____

Subject number _____

Tissue sample _____ Sample Site _____

1. Wt. of sample _____ Water temp. _____
2. Wt. of bottle..... _____
3. Wt. of bottle plus water..... _____
4. Wt. of bottle, water and sample _____
5. Wt. of water..... _____ (3-2)
6. Wt. of water and sample..... _____ (4-2)
7. Wt. of water less Wt. of Sample _____ (6-1)
8. Wt. of water less water not displ _____ (5-7)
9. Displaced vol. (8)*(temp.correc.) _____

intl. _____

10. $D = \frac{\text{mass}(1)}{\text{vol.}(9)}$

11. Dry sample Wt..... _____

12. % H₂O (100-(11/1))..... _____

Figure 27. Sample Data and Calculation Sheet used in Tissue Density Determination Process.

is known, the density of the muscle tissue may be calculated. A determination of the percent of water in muscle tissue will then also be performed as shown in the bottom of the form in Figure 27.

4.7.2. Discussion. In any micro-analytical research such as this, much consideration must be given to the discovery of sources of error and their possible solutions. Below are listed potential sources of error in this research and the procedures which have been devised to reduce or quantify them.

- air bubbles -

Air bubbles in the Pycnometer could cause an error in volume determination. Therefore, prior to sealing, the Pycnometer is immersed to its neck in an ultrasonic bath removing air bubbles from the sides of the vessel or tissue.

- Evaporation of water from the Pycnometer -

Initially very noticeable as an instability in serial weight readings, has been controlled by thoroughly drying the outside of the Pycnometer, sealing the ground glass joints with stop-cock grease and allowing a two minute stabilization period after sealing before the weight of the Pycnometer is measured.

- Evaporation of water from tissues -

Evaporation of water from tissue samples is a serious problem that could cause distortion of tissues and changes in density. Sealing tissue samples in air-tight bags immediately after removal from the cadaver and a reduction of open-air time to an absolute minimum should reduce water loss from tissues and the resultant error.

Similarly, the total elapsed time between tissue removal and density measurement will be kept to a minimum so that tissues will not need to be frozen or preserved - which could possibly cause tissue distortion or water loss.

- Temperature Fluctuations -

The density of the muscle tissue as well as that of water will change with temperature. Therefore, all density measurements will be carried out at a standard room temperature. (21-22°C).

- Tissue Distortion -

Since large muscle samples must first be removed from the cadaver and then slivers made from these samples, the possibility of mechanical distortion of the tissue is high. However, careful manual dissection appears at this time to be the least destructive technique for producing small muscle samples for the Pycnometer. This is a problem area which, at this time appears not to have an ideal solution.

4.7.3. Summary.

The data collected in this study, based upon the examinations of 12-15 cadavers and over three hundred density determinations, will enable a confident statement of the density of unpreserved human striated muscle and may allow further understanding of the relationship between anthropometrical measurements and the physical structure of the human body.

6.0. Summary, Conclusions and Recommendations.

Phase I has developed a measurement technique and examined some three-dimensional anthropometric data for analyzing variation in a sample of subjects fixed in space and time. Stereoradiography appears to provide an accurate measurement technique for the three-dimensional location of surface and skeletal landmarks. Some problems may be encountered, however, in the use of this measurement system to investigate the joint kinematics relative to those landmarks if the linkage geometry is rate dependent. Stereoradiography and the method of principal components analysis are equally well-suited for three-dimensional anthropometry of fixed subjects. Some three-dimensional anthropometric data have been summarized through principal components analysis which defines the shape of the three-dimensional data by magnitude (variance) and direction (direction cosines).

Phase II is investigating the measurement and analytical requirements of anthropometry of a three-dimensional body moving in space and time. Phase II will use data from a limited sample for development of anthropometric hypotheses about the population as dynamic systems. The human linkage system, one of the least quantified components of systems anthropometry will be investigated. This investigation will begin with the lumbar/pelvic/femur linkage system. Additional research on other areas of the human linkage system will be required. In particular, we recommend that the present effort continue into an examination of the spinal column and shoulder linkage system. The results of Phase II will need to be substantiated in a larger sample, but more importantly, the spinal column must be examined with respect to its interdependence with the lumbar/pelvic/femur system. We feel that significant progress towards a systems anthro-

pometry can be obtained by additional research on the human torso.

In conclusion, the role that systems anthropometry can take in handling real-world design problems that require human interface appears to be significantly larger than a comparable position for traditional anthropometry. Anthropometry, in general, has long been considered a useful, but limited, research tool. One of its criticisms has centered on the highly personal manner in which the measurements have been selected and made. Landmarks have been identified by training and experience, and dimensions have been measured relative to an often poorly defined series of external and internal planes. Systems anthropometry as a three-dimensional mensuration technique uses well-defined axis systems, and any desirable geometry may be specified within the three-dimensional array of landmarks. The definition and identification of landmarks as well as population differences in the location of these landmarks will remain as sources of variation in systems anthropometry that must be statistically analyzed. The practicality of the new anthropometric techniques of systems anthropometry must, however, be demonstrated.

6.0 Bibliography

1. Andriacchi, Thomas, Albert Schultz, Ted Belytschko, and Jorge Galente 1974, "A Model for Studies of Mechanical Interactions Between the Human Spine and Rib Cage." J. Biomechanics 7: 497-507.
2. Ayoub, M. M., S. Deivanayagam, and K. W. Kennedy 1976, Paths of Movement for Selected Body Segments During Typical Pilot Tasks. AMRL-TR-75-111, Wright-Patterson AFB, Ohio.
3. Bakke, S. N. 1931, Röntgenologische Beobachtungen über die Bewegungen der Wirbelsäule. Acta Radiol. Suppl. 13. 75pp.
4. Blanton, P. L. and N. L. Biggs 1968, "Density of Fresh and Embalmed Human Compact and Cancellous Bone." Amer. J. Phys. Anthropol. 29(1): 39-44.
5. Chandler, R. F., C. E. Clauser, J. T. McConville, H. M. Reynolds, and J. W. Young 1975, Investigation of Inertial Properties of the Human Body. Final Report DOT HS-801 430, National Highway Traffic Safety Administration, Washington, D. C.
6. Churchill, E. and J. T. McConville 1976, Sampling and Data Gathering Strategies for Future USAF Anthropometry. AMRL-TR-74-102, Wright-Patterson AFB, Ohio.
7. Clauser, E. C., J. T. McConville, and J. W. Young 1969, Weight, Volume, and Center of Mass of Segments of the Human Body. AMRL-TR-69-70, Wright-Patterson AFB, Ohio.
8. Dempster, Wilfred Taylor 1955a, "The Anthropometry of Body Action." Ann. N. Y. Acad. Sci., 63(4): 559-585.
9. Dempster, Wilfred Taylor 1955b, Space Requirements of the Seated Operator: Geometrical, Kinematic, and Mechanical Aspects of the Body with Special Reference to the Limbs. WADC-TR-55-159, Wright-Patterson AFB, Ohio.
10. Dempster, W. T., L. A. Skerr, and J. G. Priest 1964, "Conversion Scales for Estimating Humeral and Femoral Lengths and the Lengths of Functional Segments in the Limbs of American Caucasoid Males." Human Biology 36(3): 246-262.
11. Hanavan, Ernest P. 1964, A Mathematical Model of the Human Body. AMRL-TR-64-102, Wright-Patterson AFB, Ohio.
12. Lanier, R. 1939, "The Presacral Vertebrae of American White and Negro Males." Amer. J. Phys. Anthropol. 25(3): 341-420.
13. Martin, R. 1928, Lehrbuch der Anthropologie. G. Fischer, Jena.
14. McNeil, G. T. 1966, "X-Ray Stereo Photogrammetry." Photo. Eng. 32:

15. Schultz, Albert B. and Jorge O. Galente 1970, "A Mathematical Model for the Study of the Mechanics of the Human Vertebral Column." J. Biomechanics 3: 405-416.
16. Snyder, R. G., D. B. Chaffin, and R. K. Schutz 1972, Link System of the Human Torso. AMRL-TR-71-68, Wright-Patterson AFB, Ohio.
17. Stoudt, Howard W., Albert Damon, Ross McFarland, and Jean Roberts 1965, Weight, Height, and Selected Body Dimensions of Adults. NCHS, Series 11, No. 8, U. S. Dept. of Health, Education, and Welfare, Washington, D.C.
18. Thomas, Daniel 1976, Personal communication.
19. Thornton, William 1976, Personal communication.